Lawrence Berkeley Laboratory
UNIVERSITY OF CALIFORNIA

Materials & Molecular Research Division

STUDIES OF SURFACES USING OPTICAL SECOND-HARMONIC GENERATION

H.W.K. Tom
(Ph.D. Thesis)

April 1984

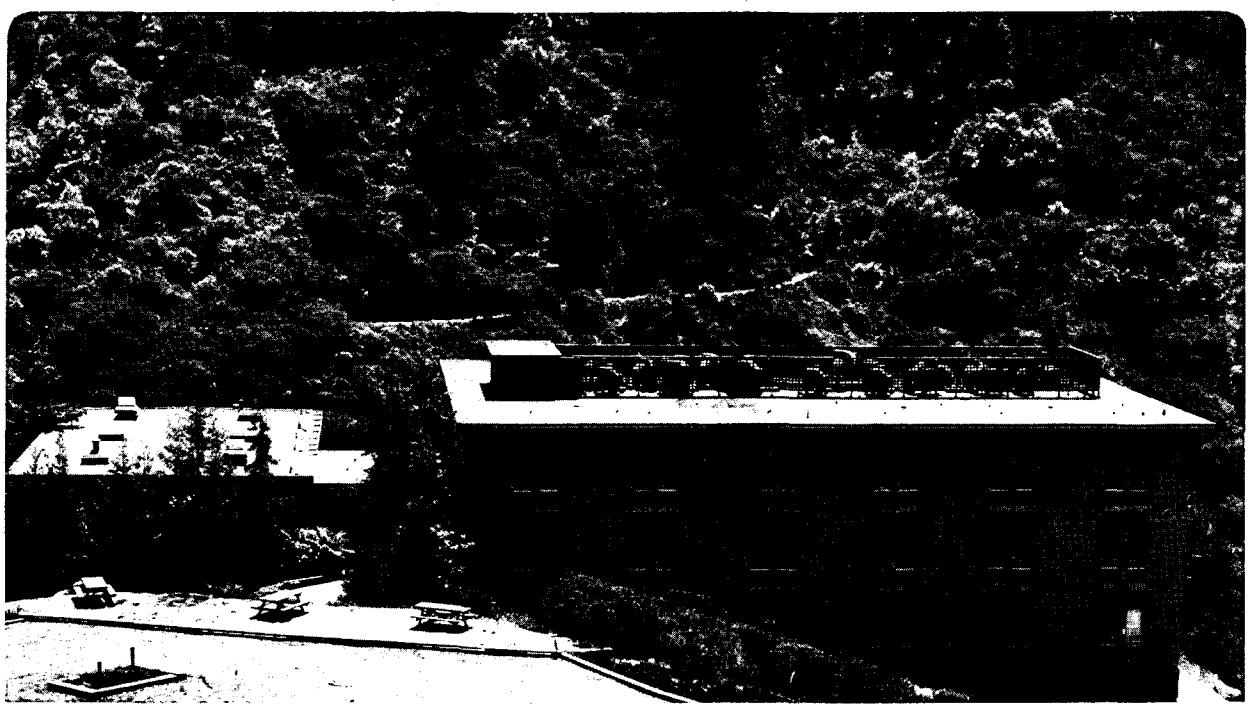

Prepared for the U.S. Department of Energy under Contract DE-AC03-76SF00098

DISCLAIMER

LBL-17820

STUDIES OF SURFACES

USING OPTICAL SECOND-HARMONIC GENERATION

Harry W. K. Tom

Department of Physics
University of California
Berkeley, California 94720

and

Materials and Molecular Research Division
Lawrence Berkeley Laboratory
Berkeley, California 94720

April 1984

Ph. D. Thesis

This work is partially supported by the Director, Office of Energy Research, Office of Basic Energy Sciences, Materials Sciences Division of the U.S. Department of Energy under Contract Number DE-AC03-76SF00098.

STUDIES OF SURFACE USING OPTICAL SECOND-HARMONIC GENERATION

Harry W. K. Tom

Abstract

The experiments reported in this thesis demonstrate the use of second-harmonic generation (SHG) and sum-frequency generation (SFG) in reflection from surfaces to study various surface properties. The experiments firmly establish SHG as a viable new surface probe that complements existing surface probes in ultrahigh vacuum environments and is in many ways unique for studying interfaces between dense media.

Surface structural symmetry can be revealed through the anisotropy in the SH signal from the surface as the sample is rotated about its normal. The form of this anisotropy is derived in theory and verified with an experiment on the Si(100) and (111) surfaces. The absence of an anisotropic contribution to the SH signal from the surface layer of the (100) face enabled the first measurement of the dipole-forbidden contribution to the SH from the underlying centrosymmetric Si bulk.

The SHG and SFG signals from molecules adsorbed on noninteracting substrates have a direct relationship to the number, average orientation, and spectroscopic properties of the molecules. The SH intensity was used to measure the isotherm for adsorption of p-nitrobenzoic acid from ethanolic solution to fused silica. The polarization of the SH field was used to measure the average tilt angle of PNBA to be ~ 38° when adsorbed at the ethanol/silica interface and to be ~ 70° at the air/silica interface. Preliminary results show that SFG combining a

visible frequency and an infrared frequency can be used to obtain vibrational spectra of adsorbates on silica.

Experiments performed on a strongly-interacting well-characterized Rh(111) surface in ultrahigh vacuum establish the sensitivity of the SH probe in corroboration with other surface probes. For the first time, the SH coverage-dependence was fit by theory in a quantitative way for the case of O-atom adsorption. The sensitivity of SH to adsorption at different sites was established for CO on top- and bridge-sites. SHG was shown to be surface specific in that the SHG from alkali metal surfaces originates from the first two monolayers. SH sensitivity to the adsorption of catalytically-important hydrocarbons and to chemical processes such as benzene dehydrogenation was also demonstrated.

Acknowledgments

In the last few hours before submitting this last of "partial fulfillments," I am sitting before the green screen of the IBM PC with a Cheshire cat grin thinking about all the people who have helped me to this stage in my life. For the record:

I wish first to thank my advisor, Professor Yuen Ron Shen for his support and guidance during the last four years. His ability to construct clear physical pictures and to explain them concisely has set a standard to which I will always aspire. His willingness to promote me professionally through mentioning me at or sending me to conferences has been most generous. He has always been available to talk to me. His letting me work with Tony Heinz on the orientation of molecules at surfaces led to the long string of extraordinarily clean and elegant experiments (if I do say so myself) reported in this thesis. Through his interest and enthusiasm for my work, he has driven me to do my personal best in the lab. An advisor can do little more for a student.

I wish also to thank the Hughes Aircraft Corporation that has supported me on a Howard Hughes Doctoral Fellowship these last 5 years. In addition to financial support, the Research Lab in Malibu, CA hosted me for three summers during which I gained a lot of practical lab experience working with H. Wang, R. C. Lind, and R. K. Jain. The beach wasn't so bad either.

It has been my good fortune to work closely with several students in the Shen group. The first was Chenson K. Chen with whom I did my first published experiment on the surface-enhanced Raman effect and from whose organization of the laboratory I profited throughout my years at

Berkeley. He taught me everything I know about getting 50 nm Ag films to peel off glass in electrochemical solution.

The second collaborator was Tony F. Heinz who more than anyone else has helped shape the way I look at myself professionally. I gratefully acknowledge Tony's help on all the work reported in this thesis. Tony's insight to physics and to life in general was both informative and inspirational. Our collaboration was extremely stimulating, productive, mutually beneficial and above all enjoyable. Tony, always quick with an idea and le mot juste, taught me how to avoid nuisances numerous and ideas irrelevant (at least he tried!).

I thank Ralph H. Page, my third collaborator, for exposing me to the work of fancy IR lasers and working in crowded rooms with molecular beam machines. While doing the preliminary experiment on sum-frequency generation together we had ample opportunity to show just who the "Night-Time Hero" was. Our "Potato-Eater" contest awaits the return of Dr. Heinz.

I was extremely lucky to have Xiang-Dong Zhu as my assistant on the ultrahigh vacuum experiments reported in Ch. VI. Due to my excellent "training" (actually more to his intelligence) we have since collaborated on projects as equal partners. Working with him has been pure joy, largely because he and I are kindred spirits. His inquisitiveness has always kept me honest and awake, even after 48 hours and too much coffee. His excitement at getting things working has been only second to my own. His energy definitely exceeds my own--although I caught him sleeping once or twice. If I ever become a professor, it will be because working with X. D. has been the most rewarding experience one could ask for in the lab. Besides he makes a mean Szechuan eggplant.

In addition, I would like to acknowledge the whole group for making the lab an enjoyable place to live. A special thanks goes to Steve Durbin for his good humor and readiness to explain anything from soup recipes to where to find the missing Fabry Perot mounts.

Rita Jones, our group secretary, has over the years been my friend and confidant. She and I also co-chaired the Shen Group Hot Tub Committee. Her ability to mediate between the third floor and first basement are an asset worth every salary increase MMRD has to offer. She has also been a complete angel for typing this thesis down to the wire. Even though she can't fix cars, she gets an A in my book.

More than anyone else, this thesis has been shared with Alesia Leung, my girlfriend for the last 3 and a half years. She has endured each success, failure, collapse, late arrival, and vacation excess with patience, understanding, and backrubs. She has been by far the best thing about my life in Berkeley. My only regret is that I'll never take her to the Mena House.

I also wish to thank my many friends in the Physics Department especially Glenn Held, Roger Tobin, Andy Skumanich....(I mention them here in the off chance they will be famous one day.) and my roomates: Randal Streck with whom I have shared 2 years at Harvard, a year abroad, my first year in Berkeley and the backyard at 2037 Lincoln, and Edie LaFalce Testa in whose living room I stayed for a year and from whom I inherited that pleasure resort of Gourmet Alley, 2037A Lincoln.

Most importantly, I thank my parents and sister Tiffany who taught me to find humor and happiness wherever I happen to be: whether that is drilling holes in steel plates or cleaning refrigerators with Tony, picking broken flashlamps out of the Quanta Ray with X. D., finding

leaks in chambers on New Year's Day, eating BBQ ribs at the vegetarian commune, baking out masking tape without a fan, cooking crepes for Chenson, seeing the first surface SFG signals with Ralph, handing YRS the results of a four day Silicon experiment, writing down the words for "We Got the Beat" for X. D. at 4 AM, bicycling to Chenonceaux or snorkeling at Molokini Island with Alesia.

Lastly, I thank selected industrial laboratories for offering me a job before this thesis was completed. It's nice to know, "Ah shall neva go hungry again."

TABLE OF CONTENTS

		PAGE
I.	Introduction	1
	References	6
II.	Second-Order Optical Processes at Surfaces	
	A. Radiation from the Surface of a Nonlinear Medium	7
	B. Second-Order Nonlinear Source Polarization for Centrosymmetric Media	10
	C. $\chi^{(2)}$ for Molecular Adsorbates on Surfaces	17
	D. Previous Experimental Work	21
	References	27
	Figure Captions	31
	Figures	32
III.	Experimental Setup for Detection and Analysis of SHG from Centrosymmetric Media	
	A. Basic Experimental Setup	33
	B. Optional Measurements: Laser Reference Channel, Calibration, SH Phase Measurement	36
	References	42
	Figure Captions	44
	Figures	45
IV.	Use of Second-Harmonic Generation to Probe Structural Symmetry of Cubic Media: Investigation of Silicon (100) and (111)	
	A. Theoretical Considerations	48
	B. Experimental Results and Discussion	53
	C. Comments on Previous SHG Investigations of Crystalline Si	57

PAGE

D. Conclusions 59

References 61

Tables 63

Figure Captions 66

Figures 67

V. Use of Second-Order Optical Processes to Probe Molecules Adsorbed to Noninteracting Substrates 72

A. Average Orientation of PNBA on Air/Silica and Ethanol/Silica Interfaces 73

B. Isotherm of p-Nitrobenzoic Acid (PNBA) Adsorption from Ethanolic Solution to Fused Silica 82

C. Vibrational Spectra of Hydrocarbons on Fused Silica: Preliminary Results 86

D. Extension to Molecules on Metal Substrates 90

References 92

Figure Captions 95

Figures 96

VI. Second-Harmonic Generation Studies of Surface Prepared in Ultrahigh Vacuum: Adsorbates on Rh(111) 102

A. Experimental 103

B. O_2 and CO on Rh(111) 104

C. Alkali Metals on Rh(111) 107

D. O_2 and CO on Alkali-Metal-Covered Rh(111) 113

E. Benzene and Pyridine on Rh(111) 117

F. Summary 122

References 123

PAGE

Figure Captions 126

Figures 128

VII. Conclusion 140

Appendix I: Anisotropic Bulk Term of the SH Polarization for the (100) and (111) Surfaces of Cubic Media 142

I. INTRODUCTION

Recently there has been a great deal of interest in surface phenomena ranging from the fundamental interest in two-dimensional physics, surface diffusion, and surface chemistry to the more applied interest in interfaces used in catalysis, crystal growth and in the semiconductor electronics industry. To understand the physics and chemistry of surface phenomena it is first necessary to characterize it -- to observe the composition, electronic properties and structure of the surface in question. To this end, several techniques[1] using either massive particle scattering or optical scattering have been developed. In vacuum environments, one may use the probes that employ particle scattering which have excellent surface specificity due to the short penetration depth of the particles (~ 20 Å in solids). To probe the more practical case of an interface between two dense media, however, one must employ optical techniques. Because optical penetration depths are typically hundreds of Angstroms, linear optical scattering lacks specificity for the few atomic layers at the surface and requires special care in the detection scheme.[2] This thesis is concerned with the use of second-order nonlinear optical probes, principally second-harmonic generation (SHG) but also sum-frequency generation (SFG), which like linear optical probes, may be used at interfaces between dense media, but which, like particle scattering, may be inherently specific to interfaces on the order of 10 Å thick. Unlike linear optical probes, however, no sophisticated detection scheme is required for SHG.

Previous workers have established the sensitivity of SHG in reflection from surfaces to detect submonolayer adsorbate coverages,[3] obtain

electronic spectra[4] and measure average orientation.[4] One series of experiments[5] reported here refine the SHG techniques for measuring adsorbate coverage by subtracting out the SH contribution from the substrate and for obtaining adsorbate orientation by measuring a moment of the tilt angle in a single highly accurate polarization measurement. The other experiments reported in this thesis extend the use of SHG and SFG to observe surface structural symmetry,[6] detect differences in adsorption at different sites,[7] and obtain vibrational spectra of adsorbates on surfaces. A series of experiments performed in ultrahigh vacuum[7] firmly establish SHG as a viable new surface probe by corroborating SHG studies with other surface probes.

A general discussion of SHG from the interface of two centrosymmetric media is presented in Ch. II. SHG and SFG are surface specific because these processes are electric-dipole forbidden in the centrosymmetric bulk media and are therefore suppressed with respect to the dipole-allowed processes in the necessarily asymmetric surface region. The form of the surface and bulk nonlinear polarizations are discussed and it is shown that for SHG from isotropic media, the surface and bulk contributions to the radiation cannot be distinguished experimentally. However, for anisotropic media, certain components of the nonlinear susceptibility tensors can be measured and the relative contributions of the bulk and surface can be obtained. The first measurements of this kind[6] are reported in Ch. IV. For silicon covered with a native oxide layer, the SH contributions of the surface and bulk are of the same order of magnitude.

The use of SHG to reveal surface structural symmetry is discussed in Ch. IV. The form for the anisotropy of the SH intensity as a surface is

rotated about its normal is derived in theory and verified with an experiment on the Si(100) and Si(111) faces. The results are consistent with the two surfaces having 4m and 3m symmetries, respectively, and for the bulk having cubic symmetry. The SH rotational anisotropy has already been used to monitor the surface crystalline order of Si during a subpicosecond time-scale melting experiment by C. V. Shank et al.[8]

For dilute layers of molecules weakly adsorbed to noninteracting substrates (such as insulators), the nonlinearity of the molecular layer can be taken to be proportional to the coverage and to the nonlinear polarizability of the adsorbates averaged over orientations in the layer. In Ch. V, section A, the SH field polarization is used to measure the tilt angle of p-nitrobenzoic acid (PNBA) to be ~ 38° from the normal adsorbed at the ethanol/silica interface and 70° at the air/silica interface.[5] In section B, the SH intensity is used to obtain the isotherm of adsorption of PNBA from ethanolic solution onto fused silica from which a free energy of adsorption, ΔG, of 8 kcal/mole is deduced.[5]

Vibrational spectra of molecules on surfaces can be obtained by sum-frequency generation (SFG) with a fixed visible frequency laser and a tunable infrared laser source near resonance with a vibrational transition. A brief discussion of the theory and preliminary results of an experiment using SFG to measure the C-H stretch (~ 3000 cm^{-1}) of adsorbates on silica are presented in Ch. V, section C. As the SF nonlinearity is expected to be higher for molecules at semiconductor and metal surfaces the laser fluences used for this experiment on a silica substrate (6 and 60 mj/10 ns pulse of IR and visible laser power on a 3 mm^2 spot) set an upper limit to the fluences necessary for future SFG measurements.

Experimental details common to the work in Chs. IV and VI are presented in Ch. III with special notes on the calibration of SH intensities and on an interference technique to obtain the relative phase of the SH field. The latter was essential in determining the nonlinear susceptibility tensor elements for the Si surfaces in Ch. IV and also in isolating the SH of the molecular layer from that of the substrate for the analysis of coverage and orientation in Ch. V.

Previous work involving SHG as a surface probe in electrochemical or atmospheric environments has been limited in its reliability due to possible contaminants on the surface. The series of experiments in Ch. VI were performed in ultrahigh vacuum (UHV) on an atomically-clean and well-characterized Rh(111) surface. The SHG results not only corroborate well with the established UHV probes but also showed that SHG was sensitive to the adsorbates of interest to surface scientists. In these studies the SH intensity was monitored continuously during relatively rapid adsorption and thermal desorption processes when other UHV techniques could not be used.

A SHG study of CO and O_2 adsorption on Rh(111) is presented in Ch. VI, section B. Similarities in the SH behavior suggest that for excitation at 1.06 μm and 532 nm, the surface nonlinearity is dominated by the free-electrons of the metal surface which are damped when acceptors like CO and O-atoms adsorb. For the first time, a quantitative relationship between the SH intensity and the coverage was established for the case of O-atom adsorption. The sensitivity of SH to adsorption at different sites was established for CO on top- and bridge-sites. In Ch. VI, section C, a study of alkali metal adsorption follows the continuous evolution of the electronic properties of the Rh surface towards that of an

alkali metal. The SH response of an alkali metal is larger than that of a transition metal like Rh presumably due to the more free-electron nature of the former. The surface specificity of SHG was tested directly by observing that the SH from alkali metals was determined by the top two atomic layers. A SHG study of CO and O_2 adsorption on alkali-metal-covered Rh in section D and of hydrocarbon adsorption and benzene dehydrogenation in section E are good examples of SH sensitivity to changes on the surface during chemical processes.

The thesis ends with a short conclusion in which some directions for future work are suggested.

References

1. See for example, G. A. Somorjai, Chemistry in Two Dimensions: Surfaces (Cornell Univ. Press, Ithaca, NY, 1981).

2. See for example, Y. J. Chabal and A. J. Sievers, Phys. Rev. Lett. 44, 944 (1980); D. L. Allara, D. Teicher, and J. F. Durana, Chem. Phys. Lett. 84, 20 (1981); R. B. Bailey, T. Iri, and P. L. Richards, Surf. Sci. 100, 626 (1980).

3. C. K. Chen, T. F. Heinz, D. Ricard, and Y. R. Shen, Phys. Rev. Lett. 46, 1010 (1981); J. M. Chen, J. R. Bower, C. W. Wang, and C. H. Lee, Optics Commun. 9, 132 (1973).

4. T. F. Heinz, C. K. Chen, D. Ricard, and Y. R. Shen, Phys. Rev. Lett. 48, 478 (1982).

5. T. F. Heinz, H. W. K. Tom, and Y. R. Shen, Phys. Rev. A 28, 1883 (1983).

6. H. W. K. Tom, T. F. Heinz, and Y. R. Shen, Phys. Rev. Lett. 51, 1983 (1983).

7. H. W. K. Tom, C. M. Mate, X. D. Zhu, J. E. Crowell, T. F. Heinz, G. A. Somorjai, and Y. R. Shen, Phys. Rev. Lett. 52, 348 (1984).

8. C. V. Shank, R. Yen, and C. Hirlimann, Phys. Rev. Lett. 51, 900 (1983).

II. SECOND-ORDER OPTICAL PROCESSES AT SURFACES

A. Radiation from the Surface of a Nonlinear Medium

The experiments discussed in this thesis concern the detection and analysis of radiation fields generated from surfaces between two centrosymmetric media due to the material system's second-order nonlinear response to the strong optical fields of a laser. The typical experimental geometry is shown in Fig. 1. Electric fields incident from linear medium 1 (only one field $\vec{E}_{inc}(\omega)$ is shown) induce a nonlinear source polarization at angular frequency ω_s in both the surface region and bulk region of nonlinear medium 2. This source polarization, in turn, generates an electric field at ω_s, $\vec{E}(\omega_s)$, back into medium 1 which is detected.

The surface is defined here to extend over that layer of material necessary so the linear response of bulk media 1 and 2 are completely characterized by the local dielectric constants ε_1 and ε_2 (for convenience taken to be isotropic). The surface region not only contains the one or two atomic layers (Thomas-Fermi screening length[1]) of homogeneous material over which the normal component of the incident electric fields are discontinuous but also the layers of material made different from the bulk by the presence of surface electronic states, defects, damage, compression, reconstruction, and of course, surface adsorbates. Because this layer of material is thin (say $\leq$ 5 nm) compared to an optical wavelength, the radiation from it may be thought as that from a single surface layer of nonlinear source polarization $\vec{P}_S^{NLS}$ of δ-function thickness where $\vec{P}_S^{NLS}$ is the integral of the nonlinear source polarization over the thickness of the real surface region. The choice of the local

dielectric constant ε' is arbitrary for the thin surface region and can be incorporated into $\vec{P}_S^{NLS}$. The nonlinear source polarization of the bulk is denoted $\vec{P}_B^{NLS}$. Since both bulk and surface polarizations are induced by the same incident fields and the tangential component of the wavevector is conserved across the interface, both $\vec{P}_B^{NLS}$ and $\vec{P}_S^{NLS}$ have the same wavevector $\vec{k}_s$ defined in medium 2, regardless of the choice of ε'.

The radiation fields generated by a general nonlinear source polarization $\vec{P}^{NLS}$ can be calculated from the wave equation[2]:

$$\vec{\nabla} \times \vec{\nabla} \times \vec{E} + (\varepsilon/c^2)(\partial^2/\partial t^2)\vec{E} = (-4\pi/c^2)(\partial^2/\partial t^2)\vec{P}^{NLS} \qquad (1)$$

subject to

$$\vec{\nabla} \cdot \varepsilon\vec{E} = -4\pi\, \vec{\nabla} \cdot \vec{P}^{NLS}$$

where the linear response of the medium is incorporated into the frequency-dependent dielectric constant ε. It can be shown that the radiation field $\vec{E}(\omega_s)$ calculated using surface and bulk nonlinear source polarizations of the form:

$$\vec{P}^{NLS} = \begin{cases} 0 & z < 0 \\ (\vec{P}_s^{NLS}\delta(z) + \vec{P}_b^{NLS})\exp(i\vec{k}_s \cdot \vec{r} - i\omega_s t) & z \geq 0 \end{cases} \qquad (2)$$

is the same as that using only an effective surface nonlinear source polarization,[3] $\vec{P}^{NLS} = \vec{P}_{eff}^{NLS}\,\delta(z)\exp(i\vec{k}_s \cdot \vec{r} - i\omega_s t)$ where

$$P^{NLS}_{eff,j} = P^{NLS}_{s,j} + i(k_{2,z} + k_{s,z})^{-1} P^{NLS}_{B,j} \quad \text{for } j = x,y$$

$$P^{NLS}_{eff,z} = P^{NLS}_{S,z} + i(\varepsilon'/\varepsilon_2)(k_{2,z} + k_{s,z})^{-1} P^{NLS}_{B,z} \qquad (3)$$

where $\vec{k}_1$ and $\vec{k}_2$ are the wavevectors of the freely propagating waves reflected into medium 1 and transmitted into medium 2, respectively, and $\vec{k}_s$ is taken to be in the x-z plane. The subscripts x, y, z denote x-, y-, and z-components. The x-component of all the wavevectors is constrained by the continuity of the electric field at z = 0 such that $k_{1,x} = k_{2,x} = k_{s,x} \equiv k_x$. This formulation of the problem with $\vec{P}^{NLS}_{eff}$ is convenient because contributions from the bulk and surface are easily compared without solving the full boundary problem. The form of Eq. (3) is reasonable since one should be able to construct the solution using the superposition of thin slabs of polarization $\vec{P}^{NLS}_B$. Each slab will radiate just like the top surface slab with polarization $\vec{P}^{NLS}_S$ except they will have slightly different phase factors. The factor $(k_{2,z} + k_{s,z})^{-1}$ is the effective thickness of the bulk media slab over which the radiation is phase-matched.

The radiation from a surface layer with source polarization $\vec{P}^S \times \exp(i\vec{k}_s \cdot \vec{r} - i\omega_s t)$ and with isotropic local dielectric ε' can be derived using the boundary conditions[4]:

$$\Delta B_x = -4\pi i \frac{\omega_s}{c} P^S_y \; ; \; \Delta B_y = +4\pi i \frac{\omega_s}{c} P^S_x$$

$$\Delta E_x = -\frac{4\pi}{\varepsilon'} \frac{\partial P^S_z}{\partial x} \; ; \; \Delta E_y = -\frac{4\pi}{\varepsilon'} \frac{\partial P^S_z}{\partial y}$$

$$\Delta B_z = 0$$

$$\Delta D_z = -4\pi\left(\frac{\partial P_x^S}{\partial x} + \frac{\partial P_y^S}{\partial y}\right). \tag{4}$$

Denoting the $\hat{p}$- and $\hat{s}$-polarized components of the electric field with subscripts, the electric field radiated back into medium 1 due to the surface polarization $\vec{P}^S$ is:[5]

$$E_p(\omega_S) = \frac{i4\pi k_1}{\varepsilon_2 k_{1,z} + \varepsilon_1 k_{2,z}}\left[k_{2,z}P_x^S + (\varepsilon_2/\varepsilon')k_x P_z^S\right]$$

$$E_s(\omega_S) = \frac{i4\pi k_1}{k_{1,z} + k_{2,z}}\left[(\varepsilon_1)^{-1}k_1 P_y^S\right] \tag{5}$$

where k_1 is the magnitude of $\vec{k}_1$ and the wavevector components are as defined above. Inserting $\vec{P}^{NLS}_{eff}$ defined in Eq. (3) for $\vec{P}^S$ in Eq. (5), one can calculate the nonlinear radiation reflected from an arbitrary nonlinear medium. We now consider the specific form of $\vec{P}^{NLS}_{eff}$ for centrosymmetric media.

B. Second-Order Nonlinear Source Polarization for Centrosymmetric Media

The usual way to describe the response to electromagnetic radiation is to expand the polarization $\vec{P}$ in a power series of the local electric field. The term second-order in the electric field is

$$\vec{P}(\omega_S) = \overleftrightarrow{\chi}^{(2)}(\omega_S = \omega_1 + \omega_2):\vec{E}(\omega_1)\vec{E}(\omega_2) \tag{6}$$

where $\overleftrightarrow{\chi}^{(2)}(\omega_S = \omega_1 + \omega_2)$ is the nonlinear susceptibility tensor and the summation over all frequencies $\omega_1 \geq \omega_2$ subject to $\omega_1 + \omega_2 = \omega_S$ is as-

sumed. For Difference-Frequency Generation $\omega_2 \rightarrow -\omega_2$ and $\vec{E}(\omega_2) \rightarrow \vec{E}^*(\omega_2)$ in Eq. (6).

The nonlinear source polarization in the bulk region of a centrosymmetric medium cannot have the form of Eq. (6). In centrosymmetric media the third rank tensor $\overleftrightarrow{\chi}^{(2)} = 0$ and since the local response of the medium vanishes, the normally negligible nonlocal response of the medium must also be considered. Because the distance an electron moves in an optical period is far less than an optical wavelength [e.g. $kV_{Fermi} << \omega$], one can expand the nonlocal contribution to the polarization in a quickly converging series of progressively higher-order spatial derivatives of the electric fields. The lowest-order term of the nonlocal contribution to the second-order polarization is

$$\vec{P}(\omega_s) = \overleftrightarrow{\chi}^{(2)}_{nonlocal}(\omega_s = \omega_1 + \omega_2):\vec{E}(\omega_1)\vec{\nabla}\vec{E}(\omega_2)$$

$$+ \overleftrightarrow{\chi}^{(2)}_{nonlocal}(\omega_s = \omega_2 + \omega_1):\vec{E}(\omega_2)\vec{\nabla}\vec{E}(\omega_1) \qquad (7)$$

where again the summation over all $\omega_1 \geq \omega_2$ where $\omega_1 + \omega_2 = \omega_s$ is understood. The fourth rank tensor $\overleftrightarrow{\chi}^{(2)}_{nonlocal}$ does not vanish in centrosymmetric media. Thus $\vec{P}^{NLS}_B$ in centrosymmetric media has the form of Eq. (7).

Since most of the nonlinear media of interest in this thesis are either isotropic (liquids, fused silica, evaporated films) or crystalline with cubic symmetry, it is useful to deduce the form of $\vec{P}^{NLS}_B$ in such cases. We also specialize to the case of second-harmonic generation in which $\omega_1 = \omega_2 \equiv \omega$. For cubic media, $\overleftrightarrow{\chi}^{(2)}_{nonlocal}(2\omega)$ has only 4 independent non-zero elements. Following the convention of Bloembergen

and coworkers,[6] the ith component of $\vec{P}_B^{NLS}$ in cubic media is

$$P_{B,i}^{NLS}(2\omega) = (\delta - \beta - 2\gamma)(\vec{E}(\omega) \cdot \vec{\nabla})E_i(\omega) + \beta E_i(\omega)(\vec{\nabla} \cdot \vec{E}(\omega))$$

$$+ \gamma\nabla_i(\vec{E}(\omega) \cdot \vec{E}(\omega)) + \zeta E_i(\omega)\nabla_i E_i(\omega) \qquad (8a)$$

where δ, β, γ, ζ are frequency dependent material parameters. For isotropic media Eq. (3) applies except $\zeta = 0$ because $E_i\nabla_i E_i$ does not transform as a vector. Recently, anisotropy in the SH radiation from cubic media has been observed.[7,8] The experiment reported in Chap. IV[3] enabled the assignment of part of the anisotropy to the ζ term in Eq. (8a).

Using Maxwell's Equations, Eq. (8a) may also be written in the form:

$$P_{B,i}^{NLS}(2\omega) = (\delta - \beta)(\vec{E}(\omega) \cdot \vec{\nabla})E_i(\omega) + \beta E_i(\omega)(\vec{\nabla} \cdot \vec{E}(\omega))$$

$$+ (2i\omega/c)\gamma(\vec{E}(\omega) \times \vec{B}(\omega))_i + \zeta E_i(\omega)\nabla_i E_i(\omega). \qquad (8b)$$

In the literature,[9] the first two terms of Eq. (8b) are often called the electric quadrupole term while the $\vec{E} \times \vec{B}$ term is called the magnetic dipole term. Strictly speaking this is incorrect. $\vec{P}_B^{NLS}(2\omega)$ can be derived quantum-mechanically using second-order perturbation theory from a multipole-expanded form of both the interaction Hamiltonian and the nonlinear current density $\vec{J}^{NLS}(2\omega) = -2i\omega\vec{P}^{NLS}(2\omega)$.[6] In isotropic media the magnetic-dipole terms lead to a polarization proportional to $\vec{E} \times \vec{B}$ while the electric-quadrupole terms lead to a polarization proportional to $\vec{E}(\vec{\nabla} \cdot \vec{E})$ and another proportional to $2(\vec{E} \cdot \vec{\nabla})\vec{E} + (i\omega/c)\vec{E} \times \vec{B}$. Thus

the coefficient γ comes from both magnetic-dipole and electric-quadrupole sources.

Using the electric-quadrupole term only, Bloembergen et al.[6] have derived an approximate expression for the bulk polarization in isotropic media due to bound electrons. In the low frequency limit for which the closure approximation is valid, they find

$$\beta = -2\gamma = 3(4n_{be})^{-1}|\chi^{(1)}(\omega)|^2, \quad \delta = 0 \tag{9}$$

with a total bound electron density n_b and a linear susceptibility $\chi^{(1)}(\omega)$ which is a scalar for cubic or isotropic media. For metals at frequencies below the interband transitions, the conduction electrons contribute the most to the nonlinear response of the medium. Treating the conduction electrons as a free electron gas with effective mass m^*, it is possible to derive $\vec{P}_B^{NLS}$. Classical[10] and quantum-mechanical[11] results yield

$$\beta = e/(8\pi m^* \omega^2)$$

$$\gamma = \beta\omega_p^2/4\omega^2 \quad \text{where } \omega_p^2 = 4\pi n_c e^2/m^*$$

$$\delta = \beta + 2\gamma \tag{10}$$

where n_c is the density of conduction electrons. Efforts to include the band structure of the material in similar calculations have been reported.[12] However, such evaluations are still approximate where the matrix elements are uncertain.

In homogeneous media $\vec{\nabla} \cdot \vec{E} = 0$ by Gauss's Law. Therefore β can never be measured directly. Furthermore, for excitation by only one plane wave $(\vec{E} \cdot \vec{\nabla})\vec{E}$ also vanishes. Thus for an isotropic nonlinear medium excited by a single plane wave, the bulk nonlinear polarizability is simply

$$\vec{P}_B^{NLS}(2\omega) = \gamma\vec{\nabla}\left(\vec{E}(\omega) \cdot \vec{E}(\omega)\right). \tag{11}$$

The polarization in Eq. (11) is longitudinal and can only radiate at the discontinuity of the surface. As a consequence, the radiation from this bulk polarization is indistinguishable from that from a surface polarization. For excitation by any number of plane waves, the $\vec{\nabla}$ in Eq. (11) may be replaced by ik_s, the wavevector of the source polarization. With the aid of Eq. (3), it is easy to show that the radiation from $\vec{P}_B^{NLS}$ in Eq. (11) is the same as that from a surface polarization:

$$P_{s,z}^{NLS}(2\omega) = -\gamma\left(\vec{E}(\omega) \cdot \vec{E}(\omega)\right) \tag{12}$$

where $\vec{E}(\omega)$ is defined in medium 2. As a result [see Eq. (13)], γ can never be distinguished from surface response parameters. Thus the nonlinear bulk parameters for isotropic media can not be measured in an experiment using a single plane wave.

In contrast to the bulk which has only nonlocal contributions to the second-order polarization, the surface has a local contribution to the source polarization with the form $\vec{P}_s^{NLS}(2\omega) = \overleftrightarrow{\chi}^{(2)}:\vec{E}(\omega)\vec{E}(\omega)$. This term is non-zero at the surface because inversion symmetry is broken at the interface between two media. Such terms can be derived from the

electric-dipole operator in a multipole expansion of the nonlinear polarizability.[6] The dielectric constant of the layer, ε', is chosen to be either ε_1 or ε_2 depending on whether $\overleftrightarrow{\chi}^{(2)}$ relates $\vec{P}_S^{NLS}$ to fields just inside or outside medium 2.

The large discontinuity of the normal component of the electric field $E_\perp$ over the surface can cause a substantial nonlocal response to the incident field. By integrating the nonlocal response over the surface thickness one removes the dependence of $\vec{P}_S^{NLS}$ on the rapidly changing fields normal to the surface and arrives at the purely local relationship between the polarization and the incident fields in Eq. (6). This integration has been performed[6] for the terms in Eqs. (8) to derive expressions for the nonlocal contribution to the elements of $\overleftrightarrow{\chi}^{(2)}$. However, the ability to solve even for the nonlocal contribution to $\overleftrightarrow{\chi}^{(2)}$ is questionable since the nonlocal response at the boundary may not be adequately described by Eq. (7) which would require $k_{surf}v_{Fermi} \ll \omega$. Since $k_{surface}$ is $\approx k_{Thomas\text{-}Fermi}$ for metals, the condition for using Eq. (7) is $\omega_p \ll \omega$ where ω_p is the plasma frequency of the metal. Rudnick and Stern[13] were able to account for all orders of the nonlocal response using a $\vec{k}$-dependent dielectric constant and Bower[9] extended this approach to include intra- and inter-band transitions. Both calculations point to the critical importance of surface electronic states and in so doing emphasize the limitation of performing such calculations. Neither calculation considers the electric-dipole contribution to $\overleftrightarrow{\chi}^{(2)}$ which would also necessarily depend strongly on surface structure and electronic states. In addition, there may be contributions to the surface polarization induced by large DC electric fields at the surface[14,15] [$\sim \overleftrightarrow{\chi}^{(3)}:\vec{E}_{DC}\vec{E}(\omega_1)\vec{E}(\omega_2)$]. Despite the detailed mechanism, all

contributions to the surface polarization may be written in the form of Eq. (6).

The symmetry of the surface dictates the form of $\overleftrightarrow{\chi}^{(2)}$. For 4m or higher symmetry $\overleftrightarrow{\chi}^{(2)}(2\omega = \omega + \omega)$ has only 3 independent elements: $\chi^{(2)}_{\perp\perp\perp}$, $\chi^{(2)}_{\perp\parallel\parallel}$, and $\chi^{(2)}_{\parallel\perp\parallel} = \chi^{(2)}_{\parallel\parallel\perp}$ where the subscripts $\perp$ and $\parallel$ indicate components perpendicular and parallel to the surface. Using Eq. (6) for the surface and Eqs. (11) and (12) for the bulk, the SH effective surface polarization for an isotropic nonlinear medium excited by a single plane wave at frequency ω has the form

$$P^{NLS}_{eff,\perp}(2\omega) = \left(\chi^{(2)}_{\perp\perp\perp} - (\varepsilon'(\omega)/\varepsilon_2(\omega))^2\gamma\right)E^2_\perp + \left(\chi^{(2)}_{\perp\parallel\parallel} - \gamma\right)E^2_\parallel$$

$$P^{NLS}_{eff,\parallel}(2\omega) = 2\chi^{(2)}_{\parallel\perp\parallel}(\varepsilon'(\omega)/\varepsilon_2(\omega))E_\perp E_\parallel \qquad (13)$$

where $E_\perp$ and $E_\parallel$ are the perpendicular and parallel components of the incident electric field in the surface layer with local dielectric constant ε'. We note here that for excitation at normal incidence to the surface, there is no SHG from isotropic or cubic media with 4m or higher surface symmetry since $P_{eff,\parallel} = 0$ because $E_\perp = 0$ and $P_{eff,\perp}$ cannot radiate in a direction perpendicular to the surface.

In using SHG as a surface probe, the sensitivity to the surface will be limited by the size of the bulk contribution with respect to that of the surface. The nonlocal terms of $\vec{P}^{NLS}_B$ are a factor of ka (where a is an atomic dimension) smaller than the local terms of the surface region. This factor of ka is cancelled by the factor of $(ka)^{-1}$ for the efficiency with which the bulk radiates in comparison to a surface region of finite thickness $\approx$ a. In Eq. (13), we see explicitly that the surface

susceptibility $\overleftrightarrow{\chi}^{(2)}$ and the bulk susceptibility Υ enter the radiation formulas with about the same weight. This suggests that there will be many cases in which SHG can be a useful surface probe because the SH response will not be dominated by Υ. In particular, by isolating the surface term $\chi^{(2)}_{\parallel\perp\parallel}$ in Eq. (13), one can eliminate the effect of the bulk entirely. This is accomplished experimentally by using an excitation beam with both $\hat{s}$- and $\hat{p}$-polarized components and observing the $\hat{s}$-polarized SH output.

While microscopic calculations of the surface nonlinear susceptibility $\overleftrightarrow{\chi}^{(2)}$ are at a primitive stage at this point, it is quite clear that adsorbate-induced changes in the surface electronic states and the intrinsic nonlinearity of adsorbates can also effect $\overleftrightarrow{\chi}^{(2)}$. It is in these changes that SHG finds its most useful application. We now consider the dependence of $\overleftrightarrow{\chi}^{(2)}$ on the presence of surface adsorbates.

C. $\overleftrightarrow{\chi}^{(2)}$ for Molecular Adsorbates on Surfaces

In the case of molecules adsorbed to noninteracting substrates, the nonlinearity of the adsorbate layer is simply the sum of the intrinsic nonlinearities of each molecule. For each adsorption site n, we can associate a molecular polarizability $\overleftrightarrow{\alpha}^{(2)}_n(\omega_s = \omega_1 + \omega_2)$. The surface nonlinear susceptibility due to the molecules is

$$\overleftrightarrow{\chi}^{(2)}_m(\omega_s = \omega_1 + \omega_2) = \sum_{\substack{\text{unit} \\ \text{area}}} \overleftrightarrow{\alpha}^{(2)}_n(\omega_s = \omega_1 + \omega_2) : \overleftrightarrow{L}_n(\omega_s)\overleftrightarrow{L}_n(\omega_1)\overleftrightarrow{L}_n(\omega_2) \tag{14}$$

where the tensor $\overleftrightarrow{L}_n(\omega)$ is the local-field factor that corrects for the effect of induced-dipoles at other sites and all induced-image dipoles on the field at frequency ω at site n. In three dimensions, such cor-

rections are called Lorentz corrections.[16] Bagchi et al.[17] have extended the calculation to the two dimensional case of molecular adsorbates on surfaces. These corrections can be ignored when the sites are far enough apart (ie., the linear polarizability $\alpha^{(1)}$ is $< d^3$ where d is the distance between dipoles) and the molecule-substrate distance large enough. In addition, harmonic components[18] and/or strong spatial gradients[19] in the induced-image-dipole field can affect the nonlinear polarizability at site n. Such corrections, here included in $\overleftrightarrow{\alpha}_n^{(2)}$ will also be negligible for large enough molecule-substrate distances.

If the coverage is low enough and there is only one kind of adsorbate,[20]

$$\overleftrightarrow{\chi}_m^{(2)}(\omega_s = \omega_1 + \omega_2) = N\langle\overleftrightarrow{\alpha}^{(2)}(\omega_s = \omega_1 + \omega_2)\rangle_{\text{mol orient}} \qquad (15)$$

where N is the surface density of the adsorbates and the brackets indicate the average over all molecular orientations. $\overleftrightarrow{\chi}_m^{(2)}$ in Eq. (15) may be zero either if the molecule is centrosymmetric ($\overleftrightarrow{\alpha}^{(2)} = 0$) or, if the molecules are ordered in a centrosymmetric way so that the average over molecular orientations is zero. Provided $\overleftrightarrow{\chi}_m^{(2)} \neq 0$, the coverage dependence of $\overleftrightarrow{\chi}_m^{(2)}$ allows one to use SHG or Sum-Frequency Generation (SFG) to obtain adsorption isotherms or other measurements of coverage. Including the contribution to the radiation from the weakly interacting substrate, the SH and SF intensities (I) will depend on coverage as:

$$I = |A + BN|^2 \qquad (16)$$

provided the average orientation is not coverage dependent. In this formula B/A may be complex.

From Eq. (15) it is easy to see that the frequency-dependence of the SH or SF response will be that of the molecular polarizability. The molecular polarizability may be derived using second-order time-dependent perturbation theory:[21]

$$\alpha^{(2)}_{ijk}(\omega_s = \omega_1 + \omega_2) = \frac{1}{\hbar^2}\left[\sum_{nn'} \frac{1}{\omega_1 + \omega_{ng} + i\Gamma_{ng}}\left\{\frac{p^i_{n'g}\, p^j_{gn}\, p^k_{nn'}}{\omega_s + \omega_{n'g} + i\Gamma_{n'g}} - \frac{p^i_{nn'}\, p^k_{n'g}\, p^j_{gn}}{\omega_s + \omega_{nn'} + i\Gamma_{nn'}}\right\} + \frac{p^j_{ng}}{\omega_1 - \omega_{ng} + i\Gamma_{ng}}\left\{\frac{p^i_{gn'}\, p^k_{n'n}}{\omega_s - \omega_{n'g} + i\Gamma_{n'g}} - \frac{p^i_{n'n}\, p^k_{gn'}}{\omega_s - \omega_{nn'} + i\Gamma_{nn'}}\right\}\right] + [\text{same with } j \leftrightarrow k \text{ and } \omega_1 \leftrightarrow \omega_2] \tag{17}$$

where the ground state $|g\rangle$ is assumed to be fully occupied and nondegenerate. The transitions between states $|n\rangle$ and $|n'\rangle$ have dipole matrix elements $p^i_{nn'}$ in the ith direction, energy $\hbar\omega_{nn'}$, and linewith $\Gamma_{nn'}$. The basis set of states can be the unperturbed free molecule states if the substrate is noninteracting or may be extended to include the states of the interacting substrate-molecule system. In the latter case the basis set and therefore $\overleftrightarrow{\alpha}^{(2)}(\omega_s)$ will be coverage dependent and Eq. (16) will probably not be valid.

For SHG, when 2ω is nearly resonant with ω_{ng} for a particular excited state $|n\rangle$, the resonant part of Eq. (17) may be separated out. The polarizability[20] becomes:

$$\alpha^{(2)}_{ijk}(2\omega - \omega_{ng}) = \left[\overleftrightarrow{\alpha}^{(2)}_{ijk}\right]_{NR} - \frac{1}{\hbar^2\pi}\tilde{\alpha}^{(1)}(2\omega)p^i_{gn} \cdot \left\{\sum_{n' \neq g} \frac{p^k_{nn'}\, p^j_{n'g} + p^j_{nn'}\, p^k_{n'g}}{\omega - \omega_{n'g} + i\Gamma_{n'g}}\right\} \tag{18}$$

where $[\alpha^{(2)}_{ijk}]_{NR}$ is the non-resonant part of the polarizability and where $\tilde{\alpha}^{(1)}(2\omega)$ is the linear polarizability normalized by $\int \mathrm{Im}(\tilde{\alpha}^{(1)}(2\omega)) \times d(2\omega) = 1$. Now, provided the non-resonant term has negligible dispersion and ω is not nearly resonant with other transitions, the nonlinear polarizability $\alpha^{(2)}_{ijk}(2\omega)$ has the same frequency-dependence as $\tilde{\alpha}^{(1)}(2\omega)$. It should be possible to obtain electronic spectra of an adsorbate layer by looking for resonant-enhancement in the SH intensity as the frequency 2ω is swept through resonance. The SHG lineshape should be $\approx |\tilde{\alpha}^{(1)}(2\omega)|^2$.

Note that the Eqs. (17) and (18) can be extended to include inhomogeneously-broadened degenerate states. Such states are automatically included in the linear polarizability $\tilde{\alpha}^{(1)}(2\omega)$. The lineshape obtained with SHG will be slightly more complicated than with a linear measurement since resonances of both the real and imaginary parts of $\tilde{\alpha}^{(1)}(2\omega)$ will appear in $|\tilde{\alpha}^{(1)}(2\omega)|^2$. In addition, the matrix elements in Eq. (18) may add some structure to $\overleftrightarrow{\alpha}^{(2)}(2\omega)$ that is not present in $\tilde{\alpha}^{(1)}(2\omega)$. However, since the optical transition of most molecules are broadened by a closely-spaced manifold of rotational and vibrational states, the spectra obtained with resonant SHG should be very similar in lineshape to $|\tilde{\alpha}^{(1)}(2\omega)|^2$.

A similar expression to Eq. (18) is obtained when ω is nearly resonant with frequency ω_{ng}. In principle, spectroscopy may also be obtained in this way. In practice, however, the restriction that 2ω remain non-resonant while ω is resonant with an electronic transition is a severe limitation. Perhaps more importantly, near a resonance of $\tilde{\alpha}^{(1)}(\omega)$, the molecule might adsorb enough power from the incident beam to either desorb or undergo laser-induced chemistry or fragmentation.

Before going on to the next section on experimental work, it is appropriate to summarize the three previous theoretical sections. Basically, a phenomenological model of the nonlinear response of a centrosymmetric media has been developed in which the surface region is treated quite differently from the bulk region. The form of the radiation may be predicted in terms of certain material parameters. Theoretical expressions for the parameters of the bulk response have been derived for the case of localized electrons and the free electron gas in isotropic media. Experiments to measure these isotropic bulk parameters are not possible. Theoretical expressions for the surface response parameters are lacking because of the absence of precise information about surface electronic states. This has not prevented, however, the successful use of SHG to detect changes on the surface due to adsorbates -- as we shall see in section D. For the case of molecular adsorbates on a noninteracting substrate, the susceptibility of the molecular layer can be analyzed quite readily.

D. Previous Experimental Work

SHG reflected from a silver sample was first observed by Brown et al.[22] in 1965. Between 1965 and 1973 researchers continued investigation on silver,[6,13,15,23,24] gold,[6] alkali metals,[25] semiconductors,[11] several kinds of insulating materials,[6,23,26] and even some liquids.[26] The qualitative aspects of this early work showed that the wavevector- and polarization-dependence of SH radiation from isotropic nonlinear media could be correctly described as being from a layer of surface polarization with the form of Eq. (6). Bloembergen et al.[6] and Wang and Duminski[23] performed experiments to measure some of the components of

$\overleftrightarrow{\chi}^{(2)}_{eff}$ in Eq. (13). In addition, the trend was established that the nonlinear response of metals exceeds that of semiconductors which in turn exceeds that of transparent materials, each by an order of magnitude.[23] This result is reasonable since at optical frequencies the linear response shows that free or delocalized electrons are generally more polarizable than tightly bound electrons in insulators.

Efforts were made to compare the experimental parameters with calculated values. In general, however, these early investigations [except Ref. 27] were done on materials held in air without careful control of surface preparation or cleanliness. As indicated in the previous section and as born out by the experimental work discussed below and in this thesis, the surface preparation and the presence of adsorbates greatly influence the SH intensity. Thus, quantitative aspects of this early work should be considered with some precaution.

The earliest work showed, in fact, that the SHG from silver films did not change as the silver aged in air on the time scale of hours.[6,22] The lack of sensitivity to surface adsorbates was thought to be consistent with adsorbate molecules having intrinsic nonlinearities that were small compared to those of metals. Brown and Matsuoka,[15] however, observed a 4-fold decrease in SHG from a silver film prepared at 10^{-7} torr when the film was exposed to air. Rudnick and Stern[13] saw an increase in SHG when their silver film prepared in UHV was exposed to air. In both cases, the nature of the adsorbates was unknown.

J. M. Chen et al.[27] was the first to see SHG on a sample manipulated solely in ultrahigh vacuum (10^{-10} torr). He observed a 10-fold increase in the SHG when he deposited a monolayer of sodium atoms on Ge(111) and Ge(100). This experiment established the surface specific nature of SHG

to adsorbates. While the potential for using SHG as a general surface probe was suggested by this work, the surface sensitivity could be attributed to the very large intrinsic nonlinearity of the metallic adsorbate with respect to the bulk and surface response of the Ge substrate. Experiments involving Cs films on semiconductors[25] and also alkali metals on the transition metals Cu and Ag[28] were also performed by J. M. Chen et al. but never published in complete form.

It remained for C. K. Chen et al.[29] to establish that even adsorbates without substantial intrinsic nonlinearities could significantly change the SHG from a surface. Observing SHG from a silver electrode in an electrochemical cell, they were able to see a 10 × increase in the SHG upon the formation of the first 5 layers of AgCl, relatively little change in the SHG during the continued formation of ~ 500 layers of AgCl, and the subsequent return to the original SHG signal level when the Cl was removed from the Ag electrode. Not only did this experiment show that it was the breaking of the symmetry at the Ag-AgCl interface that allowed a large nonlinear response to the incident field (as opposed to the nonlinearity of bulk AgCl which is centrosymmetric), but also that the interface giving rise to the SH radiation was on the order of 5 atomic layers thick.

The effect of molecular adsorbates on the SHG from silver electrodes was also investigated by C. K. Chen et al. Adsorption of a monolayer of pyridine[29] and cyanide[30] produced changes in the Ag interface SHG of 50× and 5×, respectively. That the SHG changed significantly for adsorbates but was insensitive to the number of molecules in the electrochemical solution once the adsorbate layer was saturated, indicated that the nonlinearity of the ordered adsorbate layer was much larger than the

nonlinearity of the centrosymmetrically-oriented molecules in solution. C. K. Chen et al.[31] also obtained an adsorption isotherm and followed the transient adsorption behavior of pyridine on a Ag electrode, assuming that the change in SHG was due entirely to the change in the number of adsorbed molecules. Such an assumption was recognized to be crude even at the time of writing since, by Eq. (15), the molecular contribution to the nonlinearity depends not only on the surface density N but also on the average orientation which could be coverage-dependent. In addition, the authors monitored the adsorption of pyridine on the Ag electrode with both surface-enhanced Raman and SHG[30] and found that the two signals did not depend on bias voltage in the same way. This showed that either orientational or other coverage-dependent changes to the average Raman cross-section and the second-order nonlinear polarizability could be occurring since both signals could not be strictly proportional to N.

That the molecular polarizability $\overleftrightarrow{\alpha}^{(2)}(2\omega)$ could be changed by the metal substrate was shown dramatically by T. F. Heinz et al.[32] He found that the SHG from a Ag electrode increased 10× on the adsorption of a monolayer of the centrosymmetric molecule pyrazine. The nonlinearity of the pyridine-Ag system is only about a factor of 2 larger than that of the pyrazine-Ag system even though $\overleftrightarrow{\alpha}^{(2)}(2\omega) = 0$ for free pyrazine. Thus, a substantial portion of the pyridine-Ag nonlinearity may come from sources other than the free-molecule nonlinearity. This is reasonable since the basis set in the quantum-mechanical calculation of the polarizability [Eq. (17)] should be that of the combined substrate-molecule system rather than that of the free molecule especially if the excitation or SH frequency is nearly resonant with metal-molecule charge

transfer states. This was indeed the case. For excitation at 1.06 μm, the fundamental was nearly resonant and SH resonant with the Ag-pyridine charge transfer state.[33] Calculations have also shown that appropriately large polarizabilities may be induced in a molecule close to a metal surface by interactions with the image-dipole field.[18,19] The work on pyrazine suggested that SHG may be a useful probe of metal-molecule interactions.

In contrast to the case of molecules adsorbed on metal substrates, SH from a monolayer of molecules on an insulating substrate is straightforward. In this case, interaction between the molecule and substrate is weak and $\overleftrightarrow{\alpha}^{(2)}(2\omega)$ may be taken to be that of the free molecule. The susceptibility of the adsorbate layer has the form of Eq. (14) or (15). T. F. Heinz et al.[20] exploited the dependences of $\overleftrightarrow{\chi}_m^{(2)}$ on both frequency and average orientation. Using the resonant-enhancement of $\overleftrightarrow{\alpha}^{(2)}(2\omega)$ near a molecular resonance as shown in Eq. (18), they were able to obtain a spectrum of the $S_o \rightarrow S_2$ transition of Rh 6G and Rh B110 dye monolayers on fused silica substrates. By assuming that for the resonant case there was only one large element of the $\overleftrightarrow{\alpha}^{(2)}(2\omega)$ tensor, the form of $\overleftrightarrow{\chi}_m^{(2)}$ in Eq. (15) could be greatly simplified. The authors measured a ratio of the elements of $\overleftrightarrow{\chi}_m^{(2)}$ and thereby measured a ratio of the moments of the molecular orientation angles. By noting that the SH intensity did not change when the substrate was rotated about its normal, they could conclude that the molecular distribution in the plane of the substrate was isotropic. As the two other molecular Euler angles were uncertain, the measured ratio of the orientation-angle moments was compared with that calculated for different models of the orientation. The ability to obtain surface optical spectroscopy and to measure the aver-

age orientation extended the capabilities of SHG beyond the ability to detect coverage.

Since the tensorial nature of $\overleftrightarrow{\chi}^{(2)}$ depends on the average directionality of the electron wavefunctions or bonds giving rise to the nonlinear response it is not surprising that SHG should be sensitive to the arrangement of molecular adsorbates and the crystalline structure of the substrate surface layer. It is surprising that only recently,[34] Guidotti et al.[7] observed anisotropy in the SH from crystalline Si and Ge as the samples were rotated about their surface normals. C. V. Shank et al.[8] used the anisotropy in the SH from Si(111) to measure the crystalline order of the sample surface. By measuring the SHG from a weak probe pulse delayed in time from an excitation pulse with energy above the threshold for forming an amorphous surface layer, they observed the surface order change from crystalline (rotationally-anisotropic SH) to disordered (rotationally-isotropic SH) within 3 picoseconds of the excitation pulse.

References

1. See for example, C. Kittel, Introduction to Solid State Physics, 5th edition (John Wiley, New York, 1976), p.296.
2. J. A. Armstrong, N. Bloembergen, J. Ducuing, and P. S. Pershan, Phys. Rev. 127, 1918 (1962).
3. H. W. K. Tom, T. F. Heinz, and Y. R. Shen, Phys. Rev. Lett. 51, 1983 (1983).
4. A thorough derivation of these boundary conditions can be found in Appendix I of T. F. Heinz, Ph.D. Thesis, Department of Physics, University of California, Berkeley, 1982.
5. This problem can also be solved by using a source polarization, $\vec{P}$, in a layer of finite thickness d and then allowing $d \to 0$ while keeping the product $\vec{P}d$ fixed. N. Bloembergen and P. S. Pershan, Phys. Rev. 128, 606 (1962).
6. N. Bloembergen, R. K. Chang, S. S. Jha, and C. H. Lee, Phys. Rev. 174, 813 (1968); 178, 1528(E) (1969).
7. D. Guidotti, T. A. Driscoll, and H. J. Gerritsen, Solid State Commun. 46, 337 (1983); T. A. Driscoll and D. Guidotti, Rapid Commun. of Phys. Rev. B 28, 1171 (1983). They attribute the anisotropy to a breaking of centrosymmetry at the surface induced by the electron-hole plasma generated by the fundamental pump beam. We disagree with their interpretation (see discussion section of Chap. IV).
8. C. V. Shank, R. Yen, and C. Hirlimann, Phys. Rev. Lett. 51, 900 (1983).
9. J. R. Bower, Phys. Rev. B 14, 2427 (1976).

10. S. S. Jha, Phys. Rev. 140, A2020 (1965).

11. S. S. Jha, Phys. Rev. 145, 500 (1966).

12. H. Cheng and P. B. Miller, Phys. Rev 134, A683 (1964): S.S. Jha and C. S. Warke, Phys. Rev. 153, 751 (1967).

13. J. Rudnick and E.A. Stern, Phys. Rev. B 4, 4274 (1971).

14. In bulk material this effect was first reported in R.W. Terhune, P.D. Maker, and C. M. Savage, Phys. Rev. Lett. 8, 404 (1962). The effect on surfaces using the double charge layer in an electrochemical cell was reported in C.H. Lee, R.K. Chang, and N. Bloembergen, Phys. Rev. Lett. 18, 167 (1967).

15. F. Brown and M. Matsuoka, Phys. Rev. 185, 985 (1969).

16. See for example, J. M. Ziman, Principles of the Theory of Solids, 2nd edition (Cambridge Univ. Press, Cambridge, 1979), p.266.

17. A. Bagchi. R. G. Barrera, and B. B. Dasgupta, Phys. Rev. Lett. 44, 1475 (1980); A. Bagchi. R. G. Barrera, and R. Fuchs, Phys. Rev. B 25, 7080 (1982).

18. P. R. Antoniewicz, Phys. Rev. B 26, 2285 (1982).

19. P. Ye and Y. R. Shen, Phys. Rev. B 28, 4288 (1983).

20. T. F. Heinz, C. K. Chen, D. Ricard, and Y. R. Shen, Phys. Rev. Lett. 48, 478 (1982).

21. N. Bloembergen and Y. R. Shen, Phys. Rev. 133, A37 (1964). Note that this definition of $\overleftrightarrow{\alpha}$ is consistent with the molecular polarization induced by two plane waves with frequencies ω_1 and ω_2 being written $\vec{p}(\omega_s) = \overleftrightarrow{\alpha}:\vec{E}(\omega_1)\vec{E}(\omega_2)$. With this definition the polarizability for second-harmonic generation $\vec{p}(2\omega) = \overleftrightarrow{\alpha}(2\omega):\vec{E}(\omega)\vec{E}(\omega)$ where $\overleftrightarrow{\alpha}(2\omega = \omega + \omega)$ is the same as $\lim_{\omega_1 \to \omega} \overleftrightarrow{\alpha}(2\omega = \omega_1 + \omega_2)$. This definition is consistent with the surface layer polarization being written

$\vec{P}_s(\omega_s) = \overleftrightarrow{\chi}(\omega_s = \omega_1+\omega_2):\vec{E}(\omega_1)\vec{E}(\omega_2)$ and $\vec{P}_s(2\omega) = \overleftrightarrow{\chi}(2\omega=\omega+\omega):\vec{E}(\omega)\vec{E}(\omega)$. This convention should not be confused with one where $\vec{P} = \overleftrightarrow{\chi}':\vec{E}\vec{E}$ because for two plane waves, i.e., $\vec{E} = \vec{E}(\omega_1)e^{-i\omega_1 t} + \vec{E}(\omega_2)e^{-i\omega 2t}$, $\vec{P} = \overleftrightarrow{\chi}'(\omega_s = \omega_1 + \omega_2):\vec{E}(\omega_1)\vec{E}(\omega_2) + \overleftrightarrow{\chi}'(\omega_s = \omega_2 + \omega_1)\vec{E}(\omega_2)\vec{E}(\omega_1)$ and $\overleftrightarrow{\chi}'(2\omega = \omega_1 + \omega_2)$ does not remain continuous as $\omega_1 \to \omega$.

22. F. Brown, R. E. Parks, and A. M. Sleeper, Phys. Rev. Lett. 14, 1029 (1965).

23. C. C. Wang and A. N. Duminski, Phys. Rev. Lett. 20, 668 (1968).

24. J. E. Sipe, V. C. Y. Su, M. Fukui, and G. I. Stegeman, Phys. Rev. B 21, 4389 (1980) and references therin.

25. C. S. Wang, J. M. Chen, and J. R. Bower, Optics Commun. 8, 275 (1973).

26. C. C. Wang, Phys. Rev. 178, 1457 (1969).

27. J. M. Chen, J. R. Bower, C. S. Wang, and C. H. Lee, Optics Commun. 9, 132 (1973).

28. J. M. Chen, J. R. Bower, and C. S. Wang, Jpn. J. Appl. Phys. Suppl. 2, Pt. 2, 711 (1974).

29. C. K. Chen, T. F. Heinz, D. Ricard, and Y. R. Shen, Phys. Rev. Lett. 46, 1010 (1981).

30. C. K. Chen, T. F. Heinz, D. Ricard, and Y. R. Shen, Phys. Rev. B 27, 1965 (1983).

31. C. K. Chen, T. F. Heinz, D. Ricard, and Y. R. Shen, Chem. Phys. Lett. 83, 455 (1981).

32. T. F. Heinz, C. K. Chen, D. Ricard, and Y. R. Shen, Chem. Phys. Lett. 83, 180 (1981).

33. Ph. Avouris and J. E. Demuth, J. Chem. Phys. 75, 4783 (1981).

34. In fact, the authors in Ref. 6 state that they could not find any

rotational anisotropy in the SH from surfaces of Si or Ge oriented along [111], [100], or [110] axes.

Figure Captions

Fig. 1 Typical geometry for observing second-order nonlinear optical response of nonlinear medium 2. Incident field $\vec{E}_{inc}(\omega)$ induces polarizations in the surface and bulk which in turn radiate field $\vec{E}(\omega_s)$ back into medium 1.

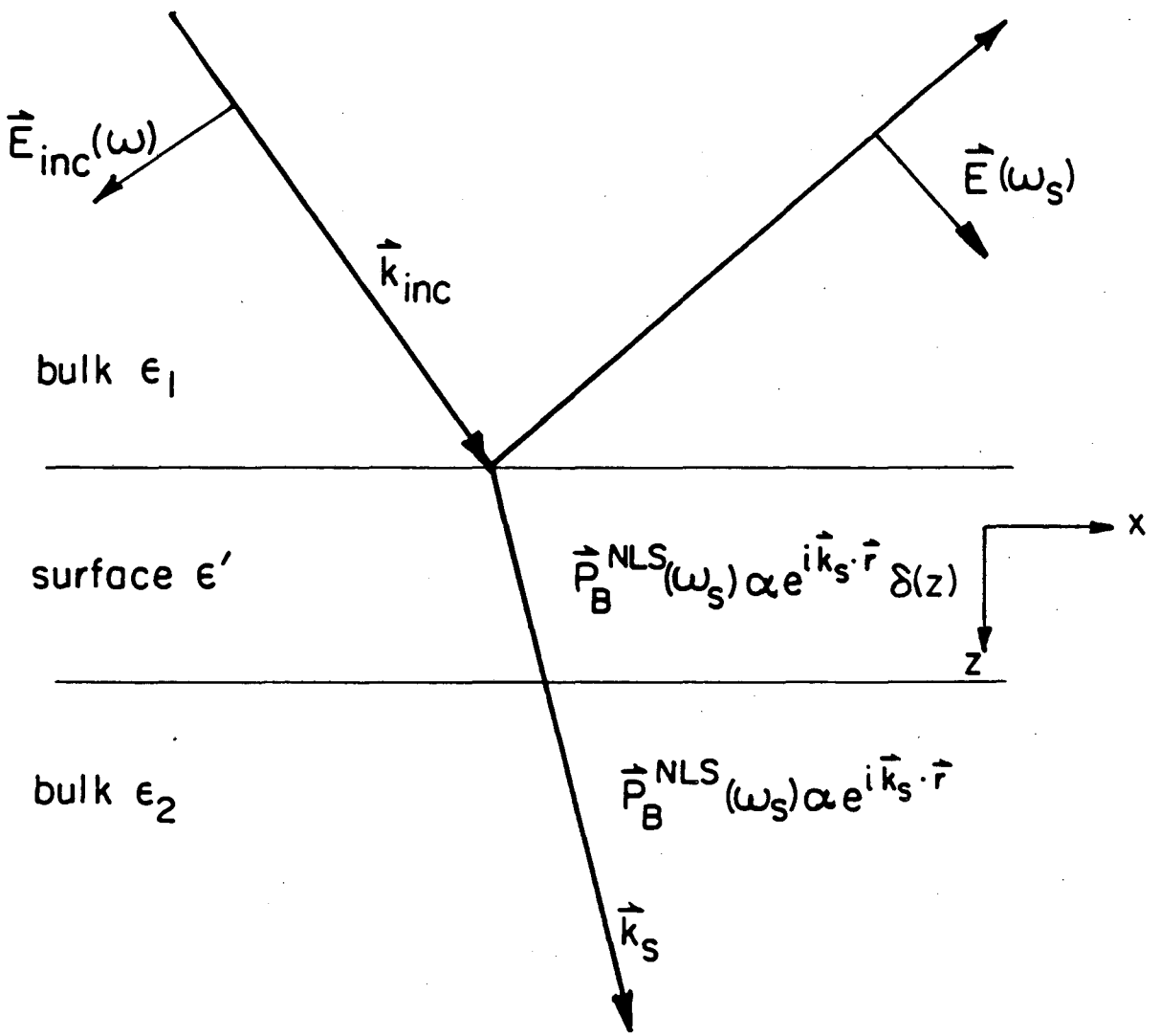

XBL 844-6832

Fig. 1

III. EXPERIMENTAL SETUP FOR DETECTION AND ANALYSIS OF SHG FROM CENTROSYMMETRIC MEDIA

Since the experiments in this thesis deal with the detection and analysis of SHG and SFG from centrosymmetric media, it is appropriate here to describe the experimental setup in some detail. While the basic experimental setup is the same as that used in the very earliest experiments (see Ch. II, sect. D for references), the setup and detection scheme as well as typical numbers used in more recent experiments may prove interesting and useful to potential users of SHG as a surface tool. In addition the experiments reported in this thesis use an interference technique for measuring the phase of the second-harmonic electric field. Knowing both the amplitude and phase of the SH field is required for much of the analysis of the SH signal.

A. Basic Experimental Setup

The experimental setup for detecting SHG reflected from a surface is shown in Fig. 1. Optional elements are surrounded by dashed lines and are discussed in section B. The first element in the setup is, of course, the laser which must generate pulses of typically 100 ns or less duration to achieve the intensities required to observe surface SHG. In these experiments, excitation pulses were derived from a Nd:YAG laser (Quanta Ray DCR IA) with 7-10 ns time duration and 10 Hz repetition rate. Laser pulses at 1.06 μm can be doubled in phase-matched KDP to provide excitation pulses at 532 nm. The latter may be used to pump dyes or a stimulated Raman cell to obtain other excitation wavelengths. The laser pulses are incident on the sample at an angle usually $\geq 45°$

after passing through appropriate lenses (L1, L2) to telescope the beam to the desired size, a polarizer (P1), and a color filter (F1). The color filter blocks the undesired SHG from the KDP crystal of the laser harmonic generator,[1], the polarizer,[2], and surfaces of the beam steering elements. The filter also blocks luminescence from the flashlamps of the laser. The filter is placed at normal incidence because, as shown in Ch. 2, SHG from the surface and bulk of isotropic media excited at normal incidence is forbidden.

SH signal levels can be quite substantial even for fairly low excitation laser intensities. The energy in the SH pulse is proportional to $I^2(\omega)A\tau$ where $I(\omega)$ is the field intensity at the fundamental frequency ω, A is the area of the excitation beam and τ is the time duration of the pulse. When laser power is not a limitation, $I(\omega)$ may be fixed at some level below the sample damage threshold and the SH signal increased simply by expanding the excitation beam area. Such is the case for metals and semiconductors which have fairly large optical nonlinear responses. For example, using $\hat{p}$-polarized input at 532 nm and observing the $\hat{p}$-polarized SH output, only 6 mJ focussed to a 1 mm^2 cross-sectional area incident at 67.5° on the clean Rh(111) surface in UHV or 35 mJ focussed to a 30 mm^2 cross-sectional area incident at 45° on the Si(111) surface were required to generate ≈ 1000 SH photons per pulse. $I(\omega)$ was chosen to be lower than the surface damage threshold by a factor of 10 for Rh and 2 for Si. By using a detection system sensitive enough to work with 2 SH photons/pulse generated at the surface as we did in our experiments, one could use as little as 0.1 mJ/pulse at the fundamental frequency. SHG experiments like those reported here and even measurements of optical spectra of surfaces via SHG[3] may be easily implemented

using one of several commercially available pulsed lasers priced around ~ $30,000 with outputs ≈ 20 mJ/10ns [4] and commercial tunable dye lasers which can generate $\geq$ 1 mJ/10 ns pulse. On the other hand, SHG from materials with small nonlinearities requires the full output of high power lasers. For glass, $|\chi^S| \approx 10^{-18}$ esu and 170 mJ/pulse focussed to 20 mm^2 were required to generate ≈ 10 SH photons/pulse.

From a smooth optically flat surface, the SH is generated in a coherent well-collimated beam in roughly the same direction as the specular reflection of the incident beam.[5] Using color filters (F2) to pass the SH and reject the fundamental frequency, the desired SH output polarization is selected by polarizer (P2) and then focussed into the slits of a monochromator (M). As $I(2\omega)$ can be on the order of 10^{-17} of $I(\omega)$ and a monochromator typically rejects ≈ 10^5, filters (F2) must reject on the order of 10^{-12} of the incident light. Care should be taken to eliminate nonlinear fluorescence from the sample at the SH frequency by spatial filtering. The intensity on both Stokes and anti-Stokes sides of the SH frequency should be no larger than the noise level.

The SHG is then detected by a photomultiplier tube (PMT) and processed either by a gated pulse counter or by a gated integrator. In our experiments we used a Hamamatsu 919 photomultiplier which had a quantum efficiency around 8% at 532 nm and 20% at 265 nm. Because of the difference in color filters and monochromator efficiency, the quantum efficiency for the whole detection path for excitation at both 1.06 μm and 532 nm was ~ 5%. Photomultiplier tubes with higher quantum efficiency at 532 nm are available. The noise level was limited by the dark counts in the PMT and using a gate of 1 μs for the 10 Hz signal (ie., 10^{-5} duty cycle) the noise level was < 10^{-3} counts/pulse. For a signal-to-noise

ratio of 100 we only needed 2 SH photons/pulse to be generated at the sample. Unfortunately such low count rates are limited by photon counting statistics and 400 counts are required to get a 5% measurement. For signal levels below 0.3 counts/pulse we simply counted the fraction of pulses, Λ, during which 1 or more photoelectrons were emitted by the photocathode and corrected this rate for the probability of multiple-photon events. Assuming the latter obeys Poisson statistics the corrected rate, λ,[6] is given by $\lambda = -\ln(1 - \Lambda) = \Lambda + \Lambda^2/2 + \ldots$. Note that the correction can be quite substantial: for $\Lambda = 0.3$ counts/pulse the correction is 15%. For signals above 0.3 counts/pulse, the PMT output was integrated with a 1 μs gate. For the experiments on Rh (Ch. VI), SHG could be measured during rapid adsorption and desorption processes with a signal averaging time of 1 sec and accuracy of 5%. For the experiments on silicon (see Figs. 4 and 5 of Ch. IV) a 2% measurement was obtained with a 10s averaging time. Data for the work on p-nitrobenzoic acid on fused silica (Ch. V) typically required averages over several minutes to an hour to obtain 5% accuracy.

B. Optional Measurements: Laser Reference Channel, Calibration, SH Phase Measurement

While the output of the Quanta Ray laser was fairly stable provided the cooling water stayed within 10°C of its temperature with the lamps off, fluctuations in the laser intensity could be normalized out by measuring the ratio of the SHG from the sample and that from another source of SHG such as a quartz plate (Q1) generating SH in transmission in a reference channel (see Fig. 1). Note that the square of a linear measurement of the laser output would not give as accurate a reference sig-

nal as a SH measurement since the two have different dependences on the laser beam's temporal and spatial profile. By placing the quartz plate at the same distance from the beam splitter as the sample, the reference signal will accurately account for propagation effects in the spatial mode profile. This method was used to normalize the measurements of SH from silicon (see Figs. 2-5, Ch. IV) which took 1 hour per 360° rotation scan.

For calibration, the sample SHG signal is compared to the SHG from a quartz plate (Q2) placed in the sample beam path. Since both reference and sample are measured with the same detection system, detection efficiency is normalized out. To compensate for beam propagation effects, (Q2) is placed as close to the sample as possible. For a quartz plate cut with the optic axis ($\hat{e}_3$) and the 2-fold axis ($\hat{e}_1$) in the plane and aligned to a Maker fringe[7] near normal incidence, the SH field generated in transmission may be calculated by the equation:

$$\vec{E}_Q(2\omega)' = \hat{e}_1 \frac{4\pi 2 d_{111}^{(2)} (\hat{e}_1 \cdot \vec{E}_Q(\omega))^2}{n_o(2\omega)(n_o(\omega) - n_o(2\omega))} \qquad (1)$$

where $\vec{E}_Q$ is the field amplitude inside the quartz plate, $n_o(\omega)$ is the frequency dependent ordinary index of refraction and $d_{111}^{(2)}$ is the $\hat{1}\hat{1}\hat{1}$ component of the second order susceptibility $\overleftrightarrow{d}^{(2)}$. Here we use the convention of Bloembergen et al.[8] that $\vec{E}(t) = \vec{E}(\omega)e^{-i\omega t} + c.c.$ and therefore the susceptibility $\overleftrightarrow{\chi}^{(2)} = 2\overleftrightarrow{d}^{(2)}$. For quartz $d_{111}^{(2)} = 1.1 \times 10^{-9}$ esu.[9] Note that the quartz and sample SHG will be coherent since they are induced by the same incident field; thus, care must be taken to block SH from the sample by placing appropriate filters and to detect only SHG from the quartz during calibration measurements.

In contrast to the case above, the coherence of the quartz and sample SHG is exploited to measure the relative phase of the SH field from the sample surface $\vec{E}_S(2\omega)$. The phase is determined by interfering $\vec{E}_S(2\omega)$ with the SH field of the quartz plate and adjusting the quartz SH field amplitude $\vec{E}_Q(2\omega)$ and phase ϕ_Q to values $\vec{E}_{Q,null}(2\omega)$ and $\phi_{Q,null}$ to obtain a null in the interference fringes. At the null of the fringe, $I(2\omega) = |\vec{E}_S(2\omega) + \vec{E}_{Q,null}(2\omega)\exp(i\phi_{Q,null})|^2 = 0$ and one finds: $\vec{E}_S(2\omega) = -\vec{E}_{Q,null}(2\omega)\exp(i\phi_{Q,null})$. The phase can be determined when $|\vec{E}_Q| \neq |\vec{E}_S|$ by finding the minimum in $I(2\omega)$, however, it is experimentally more accurate to determine the minimum close to a null where the contrast ratio is high. Because the quartz amplitude $\vec{E}_Q(2\omega)$ has an unknown phase,[10] we can only measure relative phases between two different SH fields from the sample surface. For example, in the experiments on p-nitrobenzoic acid on fused silica (Ch. V, sec. A) we measured the change in $\phi_{Q,null}$ for the SH fields from the substrate alone, $\vec{E}_{sub}$, and from the substrate covered with molecules, $\vec{E}_{sub} + \vec{E}_{mol}$. With the relative phase and amplitude of these two fields we were then able to deduce the field from the molecules alone, $\vec{E}_{mol}$. We found that for 532 nm excitation, $\vec{E}_{mol}$ was shifted in phase by $\exp(-i90°) = -i$ from $\vec{E}_{sub}$. In cases where $|\vec{E}_{mol}|$ is comparable to $|\vec{E}_{sub}|$ this phase measurement is essential to allowing accurate subtraction of the substrate signal. In cases where both substrate and the molecular layer may be considered off resonant, one can assume the nonlinear susceptibilities are real.

Experimentally, one detects a projection of $\vec{E}_S(2\omega) + \vec{E}_Q(2\omega)\exp(i\phi_Q)$ along a polarization direction set by the output polarizer (P2). The SH field $\vec{E}_Q(2\omega)$ generated in a quartz plate cut perpendicular to the $\hat{e}_2$-axis and excited at normal incidence is linearly polarized along the

$\hat{e}_1$-axis and proportional to $(\vec{E}_Q(\omega) \cdot \hat{e}_1)^2$ (only the susceptibility tensor component $d^{(2)}_{111}$ contributes in this geometry). Using such a configuration (see Fig. 2), the amplitude of the component of $\vec{E}_Q(2\omega)$ along the output polarizer direction is adjusted by simply rotating the quartz plate about its normal until the projections of the quartz $\hat{e}_1$-axis on the incident and output polarizer directions are appropriate.[11]

The phase is adjusted by varying the distance through which the SH and the fundamental beams are dispersed by propagation in the air between the sample surface and the quartz. For a quartz plate placed a distance L after the sample, the SH field $\vec{E}_S(2\omega)$ evolves a phase $(2\omega/c)n(2\omega)L$ in propagating to the quartz plate while the square of the incident fundamental-frequency field which generates the quartz SHG has acquired a phase factor $(2\omega/c)n(\omega)L$ in that same distance. A displacement of ΔL changes the phase factor between the sample and quartz SH fields by $\Delta\phi = (2\omega/c)\big(n(2\omega) - n(\omega)\big)\Delta L$. Here $n(\omega)$ is the frequency dependent index of refraction of air. For an excitation wavelength λ_{exc} = 532 nm, the dispersion $n(2\omega) - n(\omega) = 1.99 \times 10^{-5}$ and ΔL = 1.33 cm for a phase shift of 2π. For λ_{exc} = 1.06 μm the dispersion is much smaller and ΔL = 14.5 cm for a phase shift of 2π.

In practice, the phase measurement has several technical difficulties. First, the quartz plate is birefringent ($\hat{e}_3$ is the extraordinary ray) so the SH field from the sample and quartz can acquire an additional phase factor that depends on the rotation angle of the plate. By using a quartz plate which is also a $\lambda/2$ retardation plate at the fundamental or SH frequency, the incident or sample SH polarizations will be rotated but will have the same phase when the quartz plate is rotated. The new polarization directions may be accounted for analy-

tically. For our experiments using excitation at λ_{exc} = 532 nm, it was convenient to use a multiple-order quartz $\lambda/2$ plate prepared for 532 nm which coincidentally was a $2n\pi$-retardation plate (ie., no birefringence) for the SH wavelength at λ = 266 nm. This quartz plate could be placed after the sample without changing the polarization or phase of the SH field that passed through it.

A second difficulty arises due to the imperfect spatial overlap of the quartz and sample SH fields. This results in an imperfect cancellation between $\vec{E}_S$ and $\vec{E}_Q \exp(i\psi_Q)$. In Fig. 3, data from a fairly good null measurement are shown; the intensity $I(2\omega)$ of the quartz and two sample SH fields are plotted against phase angle ψ_Q in degrees near interference minima. Instead of the perfect cancellation case of $I(2\omega) \propto |\exp(i\psi_Q) + 1|^2$, the curves in Fig. 3 are fit by $I(2\omega) \propto b^2 + |\exp(i\psi_Q) + 1|^2$ where b is the fraction of the SH fields that cannot be nulled. For these cases b is ≈ 0.6 and curve fitting allows ψ^Q_{null} to be measured to $\pm 3°$.

Imperfect spatial overlap is caused by several effects. The spatial profile of the incident beam can change in the distance L between the sample and the quartz. For an excitation beam with the donut mode of the Nd:YAG laser with an unstable resonator configuration, propagation effects made b on the order of 2 for L = 10 cm in air. This situation can be improved by using a laser with better mode quality. Even without mode propagation effects, however, dispersion in the air makes the SH from the sample slightly non-collinear[5] with the incident field and therefore with the SH field from the quartz plate. Even for propagation in air, this effect is not negligible. After a distance ≈ 0.5 meters in air from a sample at 45° to the incident beam, the sample and

quartz SH field at 266 nm are separated by ≈ 5 μm which was enough to make b ≈ 0.5 using a 5 mm diameter beam with a donut-mode pattern. The effect was much more pronounced in the case of our p-nitrobenzoic acid experiments on glass at the liquid-solid interface. There the SH had to propagate from the interface back through the substrate (see Ch. V, Fig. 2). Even after passing through a thin substrate (1/8" thick) at 45° incidence the separation between interface and quartz SH at 266 nm was 45 μm and the corresponding value of b rose to 2. This effect could be greatly reduced, however, by using an excitation beam with better mode quality: using the filled-in mode pattern of the beam after propagating the donut-mode to the far-field zone,[12] we made the interference null measurements with b ≈ 0.6 shown in Fig. 3. In this figure, the curve B is the SH interference between the quartz plate and the substrate-ethanol interface, the curve A is the SH interference for the same quartz plate but with the substrate-PNBA solution interface, and one deduces a phase shift of 49.7° between the SH fields from the two interfaces.

In closing this chapter, we note that any nonlinear medium can be used to generate the SH to reference, calibrate and interfere with the SHG from the sample surface. Quartz was chosen here because the amplitude could be easily varied by rotating the sample about its normal.

References

1. The 532 nm excitation pulses which are generated in phase-matched KDP, can also generate SH pulses at 266 nm that, despite the lack of phase-matching at 266 nm, are more intense than the SH generated at the sample surface.
2. Sizeable SH can be generated from the bulk of prism polarizers which are necessarily made of non-centrosymmetric materials.
3. T. F. Heinz, C. K. Chen, D. Ricard, and Y. R. Shen, Phys. Rev. Lett. 48, 478 (1982).
4. See, for example, Laser Focus Buyer's Guide, Jan. 1983.
5. For a fundamental frequency beam incident at an angle $\theta(\omega)$ from a medium with an isotropic dielectric constant $\varepsilon(\omega)$, the SH is reflected at the angle $\theta(2\omega)$ where $\theta(2\omega) = \arctan[\sin\theta(\omega)/\sqrt{\varepsilon(2\omega)/\varepsilon(\omega) - \sin^2\theta(\omega)}]$.
6. T. F. Heinz, Ph.D. thesis, Department of Physics, U.C. Berkeley, 1982, Appendix III.
7. P. D. Maker, R. W. Terhune, M. Nisenhoff, and C. M. Savage, Phys. Rev. Lett. 8, 21 (1962).
8. See, for example, N. Bloembergen, Nonlinear Optics, (W. A. Benjamin, Inc., Reading, MA, 1977), 3rd printing, p.135.
9. CRC Handbook of Lasers with Selected Data on Optical Technology, Robert J. Pressley, ed. (Chemical Rubber Co., Cleveland, OH, 1971), p.497.
10. The phase depends on the phase of $d_{\{11\}}^{(2)}$ and the thickness of the plate.
11. Although the phase of $\vec{E}_Q$ is unknown it does not change when $|\vec{E}_Q|$ is

varied by rotating the quartz plate about its normal as long as the plate is cut perpendicular to the $\hat{e}_2$-axis and is excited at normal incidence.

12. A. E. Siegman, Appl. Optics 13, 353 (1974).

Figure Captions

Fig. 1 Experimental setup for SHG from surface. Components described in text. Dashed boxes enclose: 1) Optional reference channel for measuring SH from quartz plate (Q1) against which sample SH may be normalized for laser fluctuations, and 2) Optional quartz plate (Q2) for generating SH in beam path against which sample SH intensity may be compared in absolute calibration measurement and against which sample SH field may be interfered in phase measurement.

Fig. 2 Geometry for SHG from quartz plate for calibration measurement. The quartz plate is cut perpendicular to the $\hat{e}_2$-axis so only nonlinear tensor element $d_{11}^{(2)}$ contributes to SHG. The SH field, $\vec{E}_Q(2\omega)$, is parallel to $\hat{e}_1$ and proportional to the square of the projection of incident field $\vec{E}(\omega)$ along $\hat{e}_1$.

Fig. 3 SH intensity generated from the sample and collinear quartz plate as a function of the ϕ_Q, the adjustable phase between the quartz plate and the sample. Curve A and B are for the ethanol/silica interface with and without adsorbed PNBA, respectively.

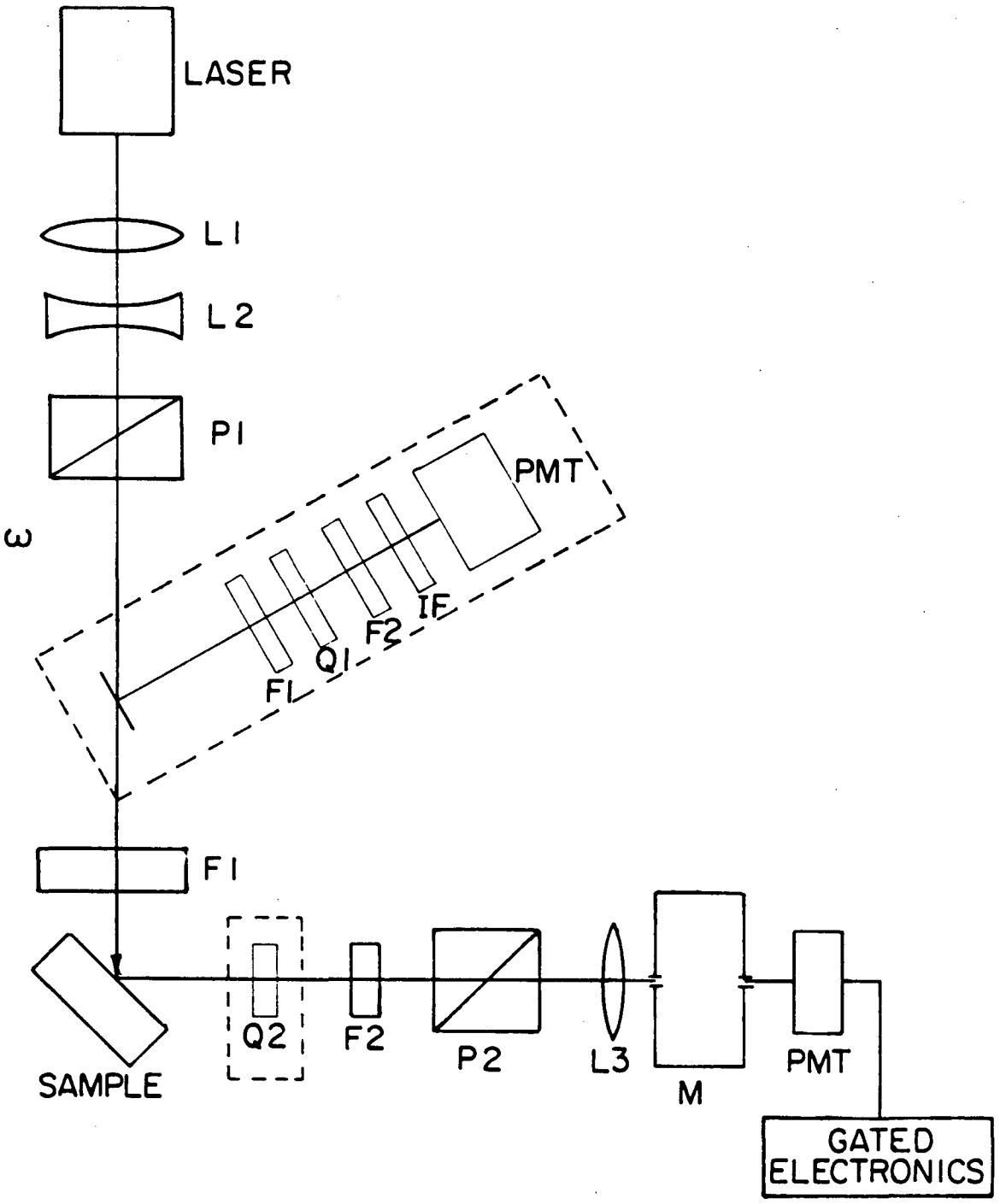

XBL 844-6831

Fig. 1

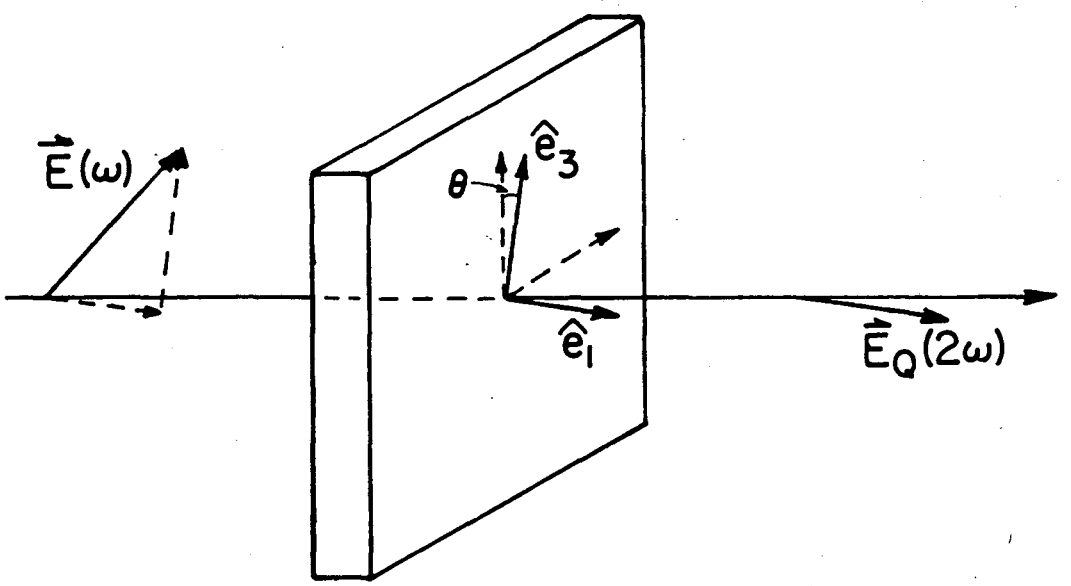

XBL 844-6834

Fig. 2

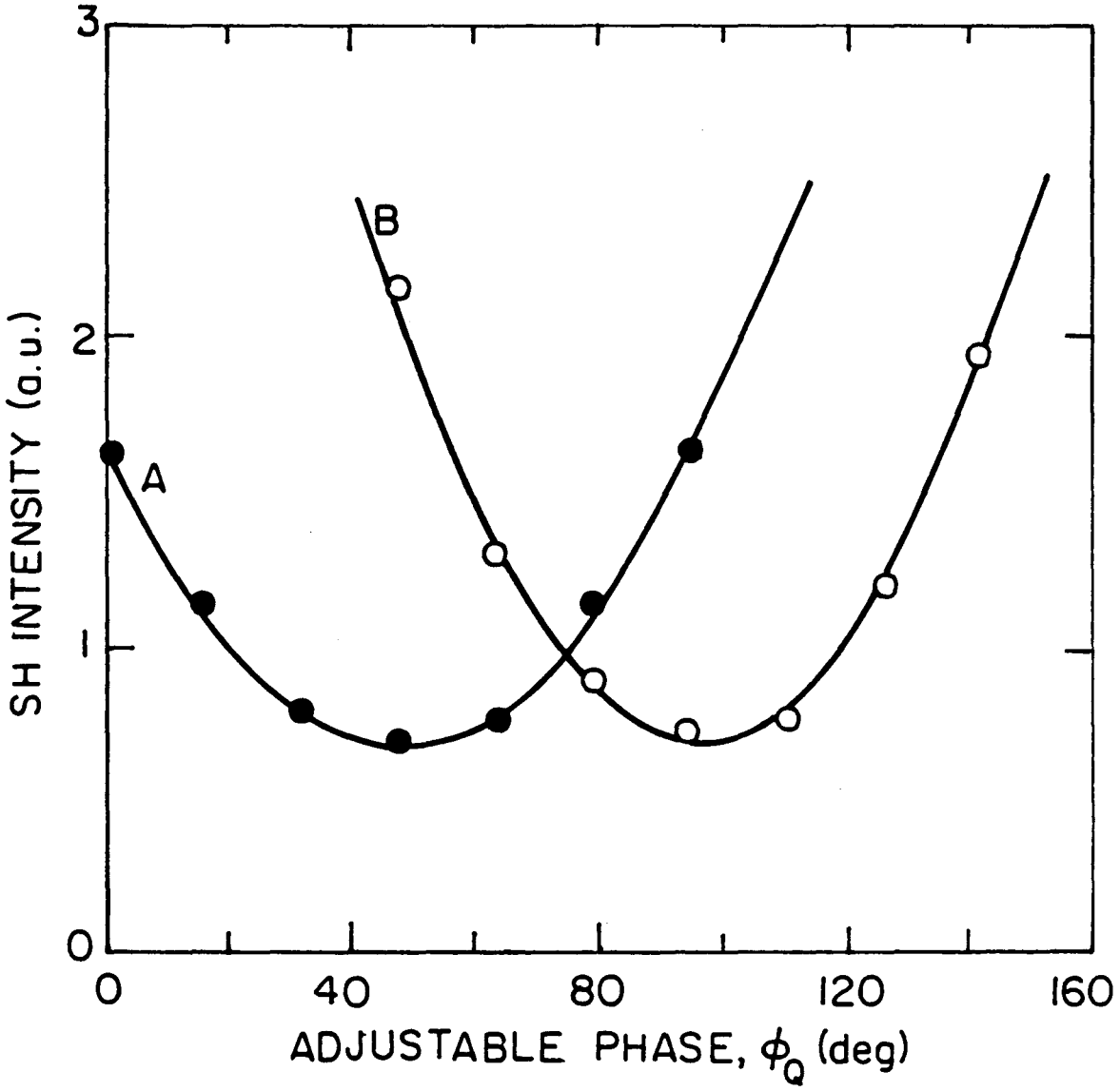

XBL 844-6833

Fig. 3

IV. USE OF SECOND-HARMONIC GENERATION TO PROBE STRUCTURAL SYMMETRY OF SURFACES OF CUBIC MEDIA: INVESTIGATION OF SILICON (100) AND (111)

In Ch. II, we presented the theory for SH radiation reflected from a nonlinear medium characterized by an arbitrary polarization and wrote down the nonlinear polarizations for the surface and bulk regions of an isotropic centrosymmetric media. While the early work of Bloembergen et al.[1] indicated that the SH from crystalline Si and Ge was independent of the cut and orientation of the face, more recent investigations[2,3] show just the opposite. In this chapter, we consider the SH from surfaces of cubic media. After appropriate theoretical considerations, experimental results for SH from Si (100) and (111) surfaces are presented which verify the forms of the nonlinear polarizations and enabled a determination of the elements of the surface and bulk nonlinear susceptibilities. The latter allowed us to determine the relative contribution of the surface and bulk to the total SH under all excitation geometries. In Section C we comment on other experimental work on SH from crystalline Si in light of our experiment. Conclusions are presented in Section D.

A. Theoretical Considerations[4]

We consider here the SH reflected from a nonlinear cubic media (characterized by linear dielectric constant ε_2) induced by a field $\vec{E}(\omega)$ with incident wavevector $\vec{k}(\omega)$ inside medium 2. From Ch. II we know that the $\hat{p}$- and $\hat{s}$-polarized reflected fields in medium 1 (with dielectric constant ε_1) are:

$$E_p = \alpha(k_x P_{eff,z} + k_{2z} P_{eff,z})$$

$$E_s = \beta(k_o P_{eff,y}) \tag{1}$$

where $\vec{k}(\omega) = (k_x(\omega), 0, k_z(\omega))$, the nonlinear source wavevector is $\vec{k}_s \equiv 2\vec{k}(\omega) \equiv (k_x, 0, k_{sz})$, $k_o = 2\omega/c$, $\vec{k}_2 = (k_x, 0, \sqrt{\varepsilon_2 k_o^2 - k_x^2})$ and the SH propagates along $\vec{k}_1 = (k_x, 0, -\sqrt{\varepsilon_1 k_o^2 - k_x^2})$. In the above, $\alpha = 4\pi i k_1(\varepsilon_2 k_{1z} + \varepsilon_1 k_{2z})$ and $\beta = 4\pi i k_o/(k_{1z} + k_{2z})$. The effective nonlinear polarization is

$$\vec{P}_{eff} = \vec{P}_S^{NLS} + i/(k_{sz} + k_{2z})\vec{P}_B^{NLS} \tag{2}$$

where $\vec{P}_S^{NLS}$ and $\vec{P}_B^{NLS}$ are the nonlinear polarizations of the surface and of the bulk and Eq. (2) applies when $\vec{P}_S^{NLS}$ is embedded in the surface of medium 2. In Ch. II, we considered the SH from isotropic media. Here, we lower symmetry by going from isotropy to cubic symmetry and increase the number of non-zero elements of the surface and bulk nonlinear susceptibilities. The additional susceptibilities lead to the rotational anisotropy observed experimentally.

In the bulk region of cubic media, the second-order nonlinear polarization takes on the non-local form given in Eq. (8a) of Ch. II. For excitation by a single plane wave the ith component of the polarization of the bulk reduces to

$$P_{B,i}^{NLS}(2\omega) = \gamma\nabla_i(\vec{E}(\omega) \cdot \vec{E}(\omega)) + \zeta E_i(\omega)\nabla_i E_i(\omega) \tag{3}$$

where the frequency-dependence on 2ω of the material parameters γ and ζ are understood and the i-directions are along principal axes of the cubic crystal. The γ term transforms as a vector and does not depend on

the orientation of the principal axes. The ζ term, on the other hand, leads to rotational anisotropy as it depends on the orientation of the principal axes. The form of the ζ term (designated $\vec{P}_B^{\zeta}$) for the (100) and (111) surfaces is given in Appendix I.

In the surface region, the nonlinear polarization is characterized by a sheet of polarization $\vec{P}_S^{NLS}(2\omega)$, with a local relationship to the electric field at the fundamental frequency given by $\vec{P}_S^{NLS} = \overleftrightarrow{\chi}^{(2)}(2\omega = \omega + \omega):\vec{E}(\omega)\vec{E}(\omega)$. The symmetry of $\overleftrightarrow{\chi}^{(2)}$ will be dictated by the symmetry of the surface. A perfectly truncated (100) crystalline surface has 4m symmetry. For 4m or higher symmetries $\overleftrightarrow{\chi}^{(2)}(2\omega)$ is the same as for isotropic media. As shown in Ch. II, we can include the contribution to SHG from the isotropic (Υ) bulk term to write the isotropic part of the effective surface nonlinear polarization as

$$P^{iso}_{eff,\perp} = (\chi^{(2)}_{\perp\parallel\parallel} - \Upsilon)E_\perp^2 + (\chi^{(2)}_{\perp\parallel\perp} - \Upsilon)E_\parallel^2$$

$$P^{iso}_{eff,\parallel} = 2\chi^{(2)}E_\parallel E_\perp \qquad (4)$$

where $E_\perp$ and $E_\parallel$ are the perpendicular and parallel components of the incident fields in medium 2.

The surface region of the (111) surface has 3m symmetry. Although the top layer of atoms of a perfectly truncated (111) would have 6m symmetry, the electronic properties of the surface (as distinct from those properties of the bulk region) are determined by the top 2 or more layers. In addition, atomic steps and the resulting domains of (111) planes will cause even the top-most Si atomic layer to have 3m symmetry on the scale of the laser beam diameter. For 3m symmetry, $\overleftrightarrow{\chi}^{(2)}(2\omega)$ has

the 3 independent elements associated with isotropy above plus another independent element that leads to rotational anisotropy. The additional surface element is $\chi^{(2)}_{\xi\xi\xi} = -\chi^{(2)}_{\xi\eta\eta} = -\chi^{(2)}_{\eta\xi\eta}$ where the $\hat{\xi}$-axis is defined by the projection of the [100] crystal axis on the surface, and the $\hat{\eta}$-axis is 90° from the $\hat{\xi}$ in the surface plane (see Fig. 1a). The anisotropic surface polarization due to the element $\chi^{(2)}_{\xi\xi\xi}$ is:

$$P^{anis}_{s,x} = \chi^{(2)}_{\xi\xi\xi}\{-(E_x^2 - E_y^2)(3\sin^2\psi\cos\psi - \cos^3\psi)$$

$$+ 2E_xE_y(3\cos^2\psi\sin\psi - \sin^3\psi)\}$$

$$P^{anis}_{s,y} = \chi^{(2)}_{\xi\xi\xi}\{(E_x^2 - E_y^2)(3\cos^2\psi\sin\psi - \sin^3\psi)$$

$$+ 2E_xE_y(3\sin^2\psi\cos\psi - \cos^3\psi\} \qquad (5)$$

where the x-z plane is the plane of incidence and the angle ψ for the (111) face is defined as the angle between the $\hat{\xi}$- and $\hat{x}$-axes (see Fig. 1a). The fields are again defined in medium 2. Inspection of Eqs. (4) and (5) and Appendix I reveals that the polarizations take on simpler forms if one uses excitation polarizations that make $E_{\parallel} = 0$, $E_{\perp} = 0$ or $E_x^2 - E_y^2 = 0$.

Using the formulas for the SH radiation from surface and bulk polarizations given in Eqs. (1)-(5), it is easy to show that the rotational dependence of the SH radiation intensity will be of the form $|\vec{E}(2\omega)|^2 = |A + B\,f(\psi)|^2$ where:

1) A is a linear combination of the isotropic terms in $\vec{P}^{iso}_{eff}$ [Eq. (2)] and $\vec{P}^{\zeta}_{B}$ (Appendix I) with susceptibilities

$$\chi^{(2)}_{\perp\perp\perp} - \gamma,\ \chi^{(2)}_{\perp\parallel\parallel} - \gamma,\ \chi^{(2)}_{\parallel\perp\parallel}, \text{ and } \zeta.$$

2) B is a linear combination of the ψ-dependent terms in $\vec{P}_s^{anis}$ [Eq. (3)] and $\vec{P}_B^{\zeta}$ (Appendix I) with susceptibilities

   ζ for the (100) face, and

   $\chi^{(2)}_{\xi\xi\xi}$ and ζ for the (111) face.

3) $f(\psi)$ is 4-fold symmetric for the (100) face and 3-fold symmetric for the (111) face.

ψ is defined for the (100) face as the angle between the in-surface-plane [100]-axis and the lab frame $\hat{x}$-axis (see Fig. 1b). The linear combination of susceptibilities in A and B are fully specified by the geometry of excitation and detection.

By choosing the appropriate input and output polarization combinations one can vary A/B or $f(\psi)$ and observe different dependences of the SHG on the rotational angle ψ. From Eq. (4), one sees that for purely $\hat{p}$- or $\hat{s}$-polarized input the isotropic contribution to the $\hat{s}$-polarized SH field proportional to $P^{iso}_{eff,y} = 2\chi^{(2)}_{\parallel\perp\parallel}E_\perp E_s = 0$ and thus A is always zero and the SH output is proportional only to the anisotropic susceptibilities through B. By actually measuring A/B for different linear combinations of the surface and bulk nonlinear susceptibilities one can measure the susceptibilities and thus the relative importance of each one to the total SHG reflected from the medium. The detailed form of the SH fields in four particular geometries: $E_{p,p}$, $E_{p,s}$, $E_{s,x}$, $E_{s,p}$ are given in Table I for (100) and (111) faces where $E_{m,n}$ is the $\hat{m}$-polarized SH field for $\hat{n}$-polarized input. The subscripts are p and s for $\hat{p}$- and $\hat{s}$-polarized and x for mixed polarization with $E_x^2 - E_y^2 = 0$ in medium 2. To summarize the results of Table I, the susceptibilities that appear in $\vec{E}(2\omega)$ in these four polarization combinations are

indicated in Table II.

B. Experimental Results and Discussion

The experimental setup for observing SHG from the sample surface was described in Ch. III. The Si samples were 0.008" thick Syton-etched optically flat wafers with only a native oxide layer. Crystalline order and orientation were verified with x-ray diffraction. The samples were mounted on a rotation stage at an angle of 45° to the incident beam of excitation pulses of wavelength 532 nm provided from the frequency-doubled output of a Q-switched Nd:YAG laser. The fluence of the 10 ns pulses was limited to 5 mJ/cm^2, well below the damage threshold. The intensity of SHG from Si surfaces was recorded as the samples were rotated about their normals. In Figs. 2-5 we show the SHG intensity as a function of the rotation angle, ψ, from the Si (111) and (100) faces for $\hat{p}$-polarized input fields and $\hat{s}$- and $\hat{p}$-polarized SH output fields (ie. $E_{s,p}$ and $E_{p,p}$). The sample SHG was normalized against SHG in a reference channel to eliminate the effect of laser fluctuations during the hour required to complete a 360° rotation scan. A 10s time constant on the integrater enabled a 1° angular resolution.

In Figs. 2-5 the experimental data are indicated in solid lines. The data are fit (dashed lines in figures) with the forms derived in section A and listed in Table I. The fits are extremely good and verify that the form of the nonlinear polarizations for the bulk and surface are correct. The data are consistent with the choice of symmetries being no higher than 3m and 4m for the (111) and (100) surfaces, respectively.

As indicated in Table II, only the susceptibilities giving rise to

rotational anisotropy contribute to the SH field for $E_{s,p}$. Thus $E_{s,p}$ for the Si(111) is proportional to the 3-fold function $3\cos^2\psi \sin\psi - \sin 3\psi$, and the SH intensity $(|E_{s,p}|^2)$ which is shown in Fig. 2 has 6 equally spaced maxima and minima. Similarly in Fig. 3, $E_{s,p}$ from the Si (100) depends on the 4-fold angular function $\sin 4\psi$ which gives an SH intensity with 8 equally spaced maxima and minima. The sign change in $E_{s,p}$ from lobe to lobe was verified by interfering the silicon SH field with that from a quartz plate.

Both isotropic and anisotropic susceptibilities contribute to the SH field $E_{p,p}$. The SH fields have the form $A + B f(\psi)$. For the Si (111) surface, $f(\psi) = 3\sin^2\psi \cos\psi - \cos^3\psi$ and as shown in Fig. 4, $|E_{p,p}|^2$ is well fit $B/A = 1.0$. Note that equal contributions from isotropic and anisotropic susceptibilities enable the contributions to completely cancel when $f(\psi) = -1$. For the Si (100) face (see Fig. 5) $f(\psi) = \sin^4\psi + \cos^4\psi$ and the data is fit with $B/A = -0.23$. In this case, the anisotropic amplitude is smaller than the isotropic amplitude and the minima never reach zero as they do for the Si (111) face.

The larger size of the anisotropic amplitude B with respect to the isotropic amplitude A for the (111) face comes from two effects. First, the (111) face has an additional contribution from an anisotropic surface susceptibility $\chi^{(2)}_{\xi\xi\xi}$ while the (100) face does not. Secondly and perhaps most importantly, geometrical factors (see $E_{p,p}$ in Table I) make the ratio of B for the (100) and (111) faces $\zeta\delta$ to 2.83 $(\chi^{(2)}_{\xi\xi\xi} - \zeta\delta(0.454e^{-i1.5^\circ}))$ assuming a 45° angle of incidence.

Exploiting the absence of the surface anisotropic term $\chi^{(2)}_{\xi\xi\xi}$ for the Si (100) face, we used the amplitude of the SH field $E_{s,p}$ shown in Figs. 2 and 3 to measure the anisotropic susceptibilities $|\chi^{(2)}_{\xi\xi\xi} - a\zeta|$ and $|\zeta|$

from the (111) and (100) faces, respectively. The expression for constant a may be found in Table I and a value 0.062 exp(- i36°) is derived using the dielectric constants for Si: $\varepsilon(\omega) = 17.0 + i0.4$ and $\varepsilon(2\omega) = -13.9 + i15.4$ [ref. 5]. Using the phase measurement described in Ch. III, we determined the relative phase of $\chi^{(2)}_{\xi\xi\xi} - a\zeta$ and ζ and thus determined that $\chi^{(2)}_{\xi\xi\xi} = 3.6e^{i22°}a\zeta$. Note that this means the anisotropy in the SH from the Si (111) face is due mostly to the surface. The non-zero value of $\chi^{(2)}_{\xi\xi\xi}$ proves that the surface layer must have 3m symmetry.

Table II shows that for the special polarization geometries when one observes $E_{p,s}$ and $E_{s,x}$, only one isotropic surface susceptibility ($\chi^{(2)} - \gamma$) and $\chi^{(2)}_{\parallel\perp\parallel}$, respectively, contributes to the isotropic part of the SHG through coefficient A. By measuring A/B in these 2 polarization geometries we find $(\chi^{(2)}_{\perp\parallel\parallel} - \gamma)/\zeta$ and $\chi^{(2)}_{\parallel\perp\parallel}/\zeta$. Using these values of the susceptibilities and the measured value of A/B for $E_{p,p}$, one can then solve for the remaining susceptibility $\chi^{(2)}_{\perp\perp\perp} - \gamma$. The observed values of the susceptibilities for the Si (111) sample were:

$$\chi^{(2)}_{\xi\xi\xi} = 1.6 \exp(i22°)\zeta'$$

$$\chi^{(2)}_{\parallel\perp\parallel} = 5.1 \exp(-i148°)\zeta'$$

$$\chi^{(2)}_{\perp\parallel\parallel} - \gamma = 3.1 \exp(-i50°)\zeta'$$

$$\chi^{(2)}_{\perp\perp\perp} - \gamma = 55 \pm 5 \exp(-i120° \pm 7°)\zeta'$$

where $\zeta' = \zeta\, k_o/(k_{2z} + k_{sz}) = 0.138 \exp(-i35.6°)\zeta$. These values of the

susceptibilities fully specify the SHG from the Si (111) surface for all excitation geometries.

The value of $\chi^{(2)}_{\xi\xi\xi}$ appears to be smaller than that of the isotropic part of $\overleftrightarrow{\chi}^{(2)}$. This is understandable since $\chi^{(2)}_{\xi\xi\xi}$ is derived from the lack of inversion symmetry in the surface plane, while the other elements of $\overleftrightarrow{\chi}^{(2)}$ are related to the lack of inversion symmetry perpendicular to the surface. Despite the relatively small value of the anisotropic tensor element, this term still makes an appreciable contribution to the SH signal due to its higher radiation efficiency compared with the isotropic term. This higher efficiency stems from the larger Fresnel factors for electric fields in the medium lying parallel rather than perpendicular to the surface. While the value of the isotropic bulk susceptibility γ cannot be separated from that of $\chi^{(2)}_{\perp\parallel\parallel}$ and $\chi^{(2)}_{\perp\perp\perp}$, the similarity between $\chi^{(2)}_{\perp\parallel\parallel} - \gamma$ and $\chi^{(2)}_{\parallel\perp\parallel}$ suggest that γ does not dominate the isotropic elements of $\overleftrightarrow{\chi}^{(2)}$ and may be comparable to the relatively small value of bulk parameter ζ.

The values of the surface susceptibilities may be strongly sample dependent due to the somewhat complex structure of the sample surface. The surface region giving rise to the surface susceptibilities extends from the air to the crystalline Si bulk and includes the air-silica interface, SiO_2 overlayer, the SiO_2-Si interface, any amorphous Si left disordered by the sample polishing process that is not consumed in the oxidation process, and the interface between disordered Si and ordered bulk Si. The contribution to the SHG from the air-silica interface and bulk silica layers is negligible as our work on silica substrates held in air indicates it should be at least two orders of magnitude smaller than the SHG observed from the Si surface. For Syton-etched samples,

the amount of disordered Si left after the natural oxidation process is probably also negligible because the natural oxide layer is ~ 20 Å thick and should completely consume the amorphous Si layer which should be ~ 3 Å before oxidation. The absence of a thick amorphous layer is certainly consistent with the susceptibility $\chi^{(2)}_{\xi\xi\xi}$, which can only arise from the interface with ordered Si, being comparable to the isotropic susceptibilities $\chi^{(2)}_{\|\perp\|}$ and $\chi^{(2)}_{\perp\|\|} - \gamma$. Since the penetration depth at 2ω is ~ 100 Å, a thick layer of amorphous Si would significantly reduce $\chi^{(2)}_{\xi\xi\xi}$.

C. Comments on Previous SHG Investigations of Crystalline Si

The earliest work on SHG from crystalline Si by Bloembergen et al.[1] reported that they did not see anisotropy in the SH from their Si (111), (100) and (110) surfaces. Their sample penetration may have left a thick amorphous Si layer above the ordered bulk. If their amorphous layer was ~ 200 Å thicker than the one on our Syton-etched samples, the observed values of the anisotropic susceptibilities $\chi^{(S)}_{\xi\xi\xi}$ and ζ would be 5 times smaller and more difficult to observe. The same result would apply if the laser fluence used in their experiments had been high enough to destroy the order of the surface.

It is interesting to note that the Syton-etched Si wafers used in standard micro-electronics fabrication have remarkably similar SH responses. The data for $\hat{p}$-polarized SH for $\hat{p}$-polarized input excitation at 45° incidence shown in Fig. 5 is the same as that observed by Guidotti et al.,[2] and by Shank et al.,[3] despite the different sources for the Si samples in each case. This again suggests that the Syton-etch process leaves a disordered Si layer that is narrow enough to be adequately consumed in the natural oxidation process so the final

SiO_2-Si interface has the bulk symmetry.

Guidotti et al.[2] attribute the anisotropy in the SH to symmetry breaking in the surface due to the creation of a high density electron-hole plasma. Their explanation cannot be correct as they find a strictly quadratic dependence of SH on the fundamental input beam intensity when a higher-order dependence is expected for any effect that depends on the density of the electron-hole plasma and secondly, their data[7] is similar to our data which was obtained with laser fluences well below those needed to obtain high densities of electrons and holes.

Detection of atomic-scale surface order via an optical technique such as SHG can be a unique tool especially in time-resolved experiments on order-disorder phase transitions. Time-resolved low energy electron diffraction (LEED)[8] and x-ray diffraction[9] have been reported. But LEED is useful only for the first 2 nm of dense media due to the short penetration depth of the electrons, while x-ray diffraction is not surface specific due to the long penetration depth of x-rays. SHG can probe interfaces between dense media and can therefore be used as in the case of our Si sample to probe the SiO_2-Si interface beneath layers of SiO_2. In addition, SHG can be used at an interface as thin as 1 or 2 nm.

Recently Shank et al.[3] used SHG to monitor the subpicosecond time-scale evolution of the surface order of a Si (111) wafer after it had been excited with a laser pulse near or exceeding the damage threshold intensity. At various delay times after the high intensity pump laser pulse, they observed the $\hat{p}$-polarized SH intensity generated by a weaker $\hat{p}$-polarized input probe pulse at 45° incidence. For pump pulse intensities below the damage threshold they saw the same dependence of the SH intensity on rotation angle as shown in our Fig. 4. For pump pulses

above the damage threshold they observed the anisotropic part of the SH intensity vanish, ie., $I(2\omega) = |A + B\, f(\psi)|^2 \rightarrow |A|^2$, after 3 picoseconds. The latter showed that surface order was destroyed in 3 picoseconds. Had Shank et al. used the $\hat{s}$-polarized SH intensity instead of the $\hat{p}$-polarized SH intensity they would have had a background free probe of the surface order since SH in that polarization geometry comes only from the anisotropic terms of the nonlinear susceptibility. Upon loss of surface order the SH intensity $I(2\omega) = |B\, f(\psi)|^2$ as in our Fig. 3 would vanish at all values of ψ as B decreased to zero.

D. Conclusions

Rotational anisotropy in the SHG from surfaces may be used to monitor order on atomic scales at interfaces. We have fully characterized the SH response of the Si (111) and Si (100) surfaces by deriving the forms of the surface and bulk nonlinear polarizations and by measuring all the nonlinear susceptibilities. Our results are fully consistent with the (111) surface having 3m symmetry and the (100) surface having 4m symmetry. From our analysis, we find that the surface and bulk can make comparable contributions to the SH generated in reflection from Si samples. Similar measurements may be extended to determine or monitor changes in the symmetry of ordered adsorbed or epitaxially-grown layers.

The measurement of anisotropic bulk parameter ζ deserves some attention. As indicated in Ch. II, the isotropic bulk parameter γ cannot be separated from $\chi^{(2)}_{\perp\perp\perp}$ and $\chi^{(2)}_{\perp\parallel\parallel}$ experimentally. Thus, calculated expressions for γ and ideas about the relative bulk and surface contributions to SHG have not been checked. The parameter ζ has not been discussed in

previous theoretical works but should be calculable since bulk electronic properties are relatively well known. If calculations of ζ prove adequate then one can begin to trust calculations of Υ and become more confident in assigning the bulk and surface isotropic contributions to SHG.

References

1. N. Bloembergen, R. K. Chang, S. S. Jha, and C. H. Lee, Phys. Rev. 174, 813 (1968).
2. D. Guidotti, T. A. Driscoll, and H. J. Gerritsen, Solid State Commun. 46, 337 (1983); T. A. Driscoll and D. Guidotti, Phys. Rev. B (Rapid Commun.) 28, 1171 (1983).
3. C. V. Shank. R. Yen, and C. Hirlimann, Phys. Rev. Lett. 51, 900 (1983).
4. H. W. K. Tom, T. F. Heinz, and Y. R. Shen, Phys. Rev. Lett. 51, 1983 (1983).
5. R. Hulthén, Physica Scripta 12, 342 (1975); H. R. Phillipp and E. A. Taft, Phys. Rev. 120, 37 (1960).
6. Syton-etched samples have been polished to optical flatness in a Syton slurry and then cleaned in a chemical that preferentially etches amorphous Si leaving at most one or two layers of disordered material before oxication (employee at Wacker Chemical, Portland, OR, private commun.). Ellipsometric techniques have been used to determine that the disordered layer may be as thin as the optical equivalent of 1 Å using the right etchants (D. E. Aspness and A. A. Studna, Appl. Phys. Lett. 39, 316 (1981)).
7. The data reported in Ref. 2 were obtained with picosecond excitation pulses and with error bars large enough that our theoretical curves may be drawn through their experimental points.
8. G. Mourou and S. Williamson, Appl. Phys. Lett. 41, 44 (1982); R. S. Becker. G. S. Higashi, and J. A. Golovchenko, Phys. Rev. Lett. 52, 307 (1984).

9. B. C. Larson, C. W. White, T. S. Noggle, and D. Mills, Phys. Rev. Lett. 48, 337 (1982); B. C. Larson, C. W. White, T. S. Noggle, J. F. Barhorst, and D. M. Mills, Appl. Phys. Lett. 42, 282 (1983).

TABLE I SH fields for four specific polarization geometries

(100) face

$$E_{p,p} = \alpha E_p^2 k_x (k_x(\omega)/k(\omega))^2 \{[(\chi^{(2)}_{\perp\perp\perp} - \gamma) + (\chi^{(2)}_{\perp\parallel\parallel} - \gamma)(k_z(\omega)/k_x(\omega))^2$$

$$- 2\chi^{(2)}_{\parallel\perp\parallel}(k_z(\omega)/k_x(\omega))(k_{2z}/k_x)] - \zeta\delta(k_z(\omega)/k_o(\omega))/2$$

$$- \zeta\delta(k_z(\omega)/k_x(\omega))^2(k_{2z}/k_o)(\cos^4\psi + \sin^4\psi)/2\}$$

$$E_{p,s} = \alpha E_s^2 k_x[(\chi^{(2)}_{\perp\parallel\parallel} - \gamma) - \zeta\delta(k_{2z}/k_o)(\sin^2 2\psi)/4]$$

$$E_{s,x} = 2\beta E_p E_s k_o(k_x(\omega)/k(\omega))[\chi^{(2)}_{\parallel\perp\parallel} + \zeta\delta(k_z(\omega)/k_o(\omega))(\sin^2 2\psi)/4]$$

$$E_{s,p} = - \beta E_p^2 k_o(k_z(\omega)/k(\omega))^2(k_x(\omega)/k_o(\omega))\zeta\delta(\sin 4\psi)/8$$

(111) face

$$E_{p,p} = \alpha E_p^2 k_x (k_x(\omega)/k(\omega))^2 \{[(\chi^{(2)}_{\perp\perp\perp} - \gamma) + (\chi^{(2)}_{\perp\parallel\parallel} - \gamma)(k_z(\omega)/k_x(\omega))^2$$

$$- 2\chi^{(2)}_{\parallel\perp\parallel}(k_z(\omega)/k_x(\omega))(k_{2z}/k_x)] - \zeta\delta[(k_z(\omega)/k_o(\omega))/6 \cdot (k_z^2(\omega)$$

$$- k_x^2(\omega))/k_x^2(\omega) - (k_{2z}/k_o)/12 \cdot (k_z^2(\omega) - 2k_x^2(\omega))/k_x^2(\omega)]$$

$$+ [(k_{2z}/k_x)(k_z(\omega)/k_x(\omega))^2(\chi^{(2)}_{\xi\xi\xi} - \zeta\delta(72)^{-1/2}((k_x/k_{2z})(k_x(\omega)/k_o(\omega))$$

$$+ (k_z(\omega)/k_o(\omega))(k_z^2(\omega) - 2k_x^2(\omega))/k_z^2(\omega)))](\cos^3\psi - 3\sin^2\psi\cos\psi)\}$$

TABLE I (Continued)

$$E_{p,s} = \alpha E_s^2 k_x\{(\chi^{(2)}_{\perp\parallel\parallel} - \gamma) - \zeta\delta((k_z(\omega)/k_o(\omega))/6 + (k_{2z}/k_o)/12)$$

$$+ (k_{2z}/k_x)[\chi^{(2)}_{\xi\xi\xi} - \zeta\delta(72)^{-1/2}((k_x(\omega)/k_o(\omega))(k_x/k_{2z})$$

$$+ (k_z(\omega)/k_o(\omega)))](3\sin^2\psi\cos\psi - \cos^3\psi)\}$$

$$E_{s,x} = 2\beta E_p E_s k_o(k_x(\omega)/k(\omega))\{[\chi^{(2)}_{\parallel\perp\parallel} - \zeta\delta(k_z(\omega)/k_o(\omega))/12]$$

$$+ \zeta\delta(72)^{-1/2}(k_z(\omega)/k_o(\omega))(k_x(\omega)/k(\omega))(E_p/E_s)(3\cos^2\psi\sin\psi - \sin^3\psi)$$

$$+ (k_{2z}/k_x)[\chi^{(2)}_{\xi\xi\xi} - \zeta\delta(72)^{-1/2}(k_z^2(\omega) - k_x^2(\omega))/(k_o(\omega)k_z(\omega))](\cos^3\psi$$

$$- 3\sin^2\psi\cos\psi)\}$$

$$E_{s,p} = \beta E_p^2 k_o(k_z(\omega)/k(\omega))^2[\chi^{(2)}_{\xi\xi\xi} - \zeta\delta(72)^{-1/2}(k_z(\omega)/k_o(\omega))(k_z^2(\omega)$$

$$- 2k_x^2(\omega))/k_z^2(\omega)](3\cos^2\psi\sin\psi - \sin^3\psi)$$

$E_{m,n}$ is the $\hat{m}$-polarized part of SH field $\vec{E}(2\omega)$ with $\hat{n}$-polarized excitation.

p = $\hat{p}$-polarized; s = $\hat{s}$-polarized; x = mixed-polarized with $E_x^2 - E_y^2 = 0$ in medium 2.

$\alpha = 4\pi i k_1/(\varepsilon_1 k_{1z} + \varepsilon_1 k_{2z})$; $\beta = 4\pi i k_o/(k_{1z} + k_{2z})$; $\delta = k_o/(k_{sz} + k_{2z})$ where the k's are defined as:

$\vec{k}(\omega)$ is incident wavevector in medium 2 = $(k_x(\omega), 0, k_z(\omega))$; $k_o(\omega) = \omega/c$; $k_o = 2\omega/c$; $\vec{k}_s \equiv 2\vec{k}(\omega) \equiv (k_x, 0, k_{sz})$; $\vec{k}_1 = (k_x, 0, -k_{1z}) = (k_x, 0, -\sqrt{\varepsilon_1 k_o^2 - k_x^2})$; $\vec{k}_2 = (k_x, 0, k_{2z}) = (k_x, 0, \sqrt{\varepsilon_2 k_o^2 - k_x^2})$.

TABLE II Nonlinear susceptibilities appearing in $E(2\omega)$ for four specific polarization geometries.

(100) face-4m surface symmetry

Susceptibility	Polarization Geometry			
	$E_{s,p}$	$E_{s,x}$	$E_{p,s}$	$E_{p,p}$
ζ	x	x	x	x
$\chi^{(2)}_{\parallel\perp\parallel}$		x		x
$\chi^{(2)}_{\perp\parallel\parallel} - \gamma$			x	x
$\chi^{(2)}_{\perp\perp\perp} - \gamma$				x

(111) face-3m surface symmetry

Susceptibility	Polarization Geometry			
	$E_{s,p}$	$E_{s,x}$	$E_{p,x}$	$E_{p,p}$
ζ	x	x	x	x
$\chi^{(2)}_{\xi\xi\xi}$	x	x	x	x
$\chi^{(2)}_{\parallel\perp\parallel}$		x		x
$\chi^{(2)}_{\perp\parallel\parallel} - \gamma$			x	x
$\chi^{(2)}_{\perp\perp\perp} - \gamma$				x

Figure Captions

Fig. 1 Coordinate geometry for (111) and (100) faces. a) For the (111) face, the projection of the [100] axis on the surface defines $\hat{\xi}$ while $\hat{\eta}$ is in the surface plane perpendicular to $\hat{\xi}$. Rotation about the surface normal is defined by ψ, the angle between $\hat{x}$ and $\hat{\xi}$. b) For the (100) face, angle ψ lies between the $\hat{x}$ and the in-surface-plane [100]-axis.

Fig. 2 SH intensity vs. rotation angle ψ for the Si(111) surface for $\hat{p}$-polarized excitation and $\hat{s}$-polarized SH field (eg., $|E_{s,p}|^2$). —— expt., --- theor. fit to $|B(3\cos^2\psi \sin\psi - \sin^3\psi)|^2$.

Fig. 3 Same as Fig. 2, except for the Si(100) face the --- theoretical fit is to $|B\sin 4\psi|^2$.

Fig. 4 SH intensity vs. rotation angle ψ for the Si(111) surface for $\hat{p}$-polarized excitation and SH field (eg., $|E_{p,p}|^2$). —— expt., --- theoretical fit to $|A + B(3\sin^2\psi \cos\psi - \cos^3\psi)|^2$ with B/A = 1.0.

Fig. 5 Same as Fig. 4, except for the Si(100) face and the --- theoretical fit is to $|A + B(\cos^4\psi + \sin^4\psi)|^2$ with B/A = - 0.23.

a) (111) face, $\hat{z}$ along [111]

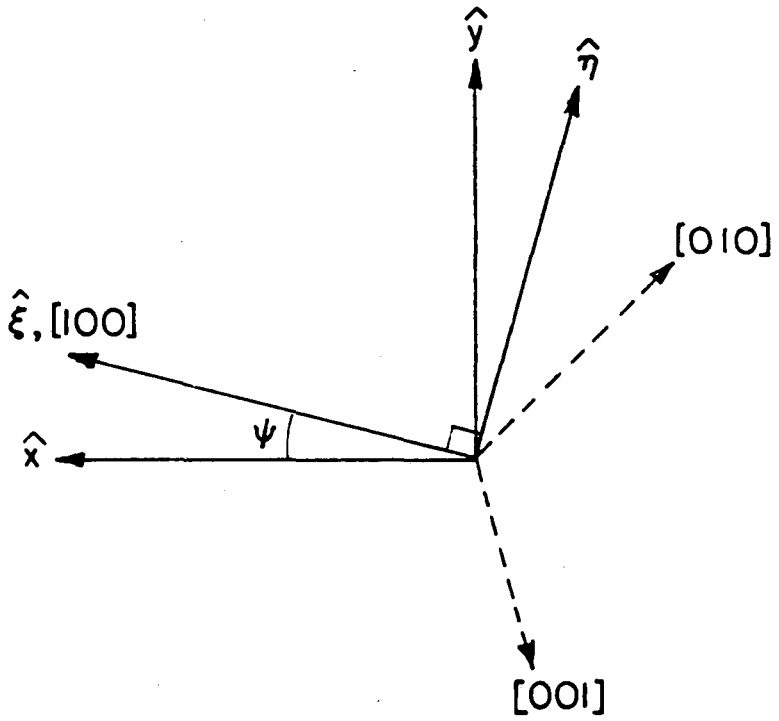

b) (100) face, $\hat{z}$ along [001]

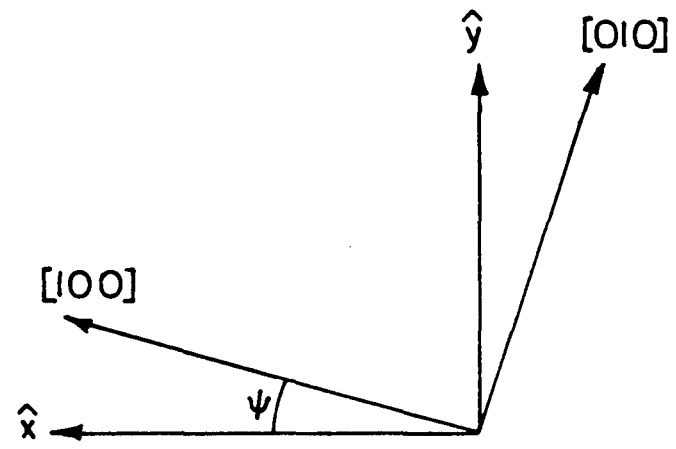

XBL 844-6855

Fig. 1

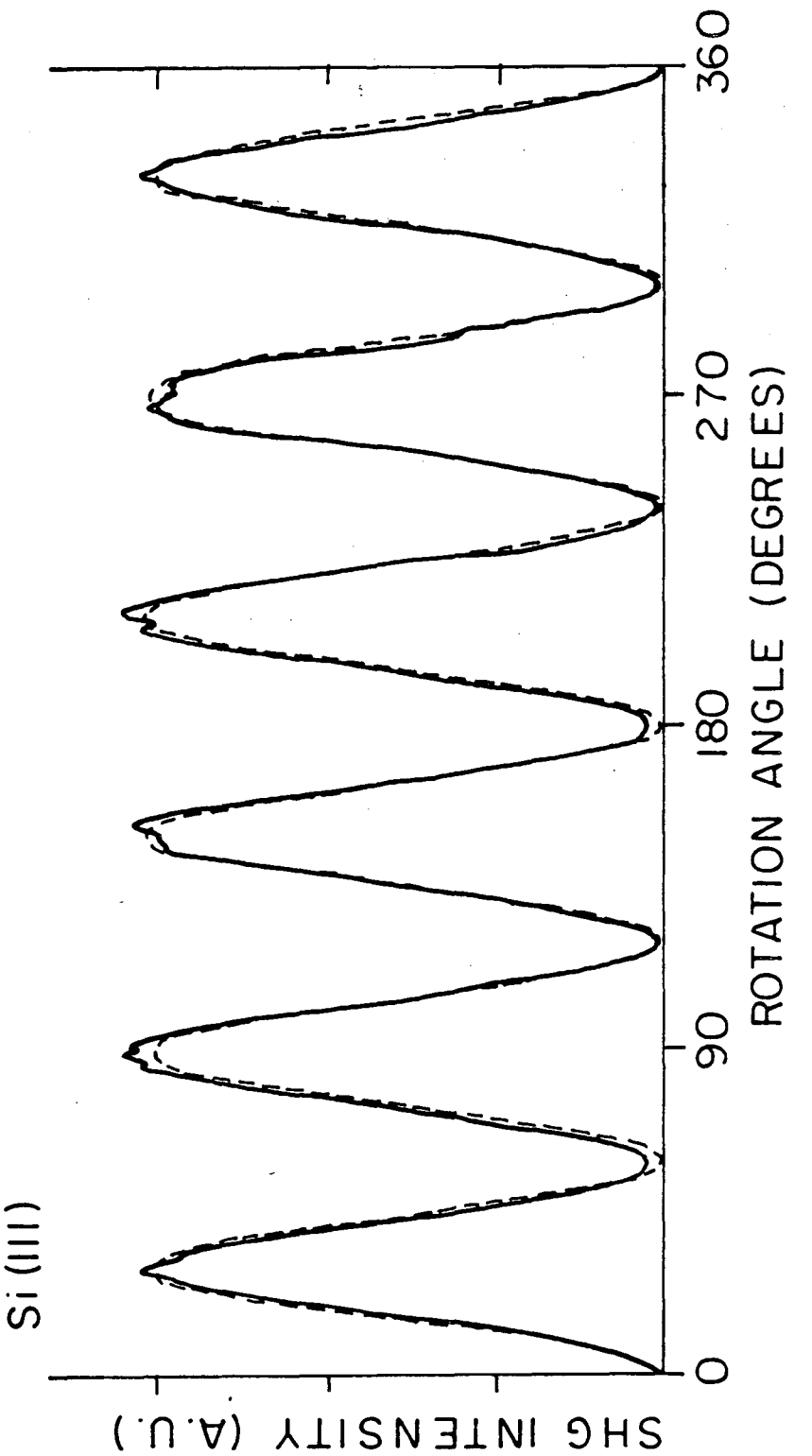

XBL836-5869A

Fig. 2

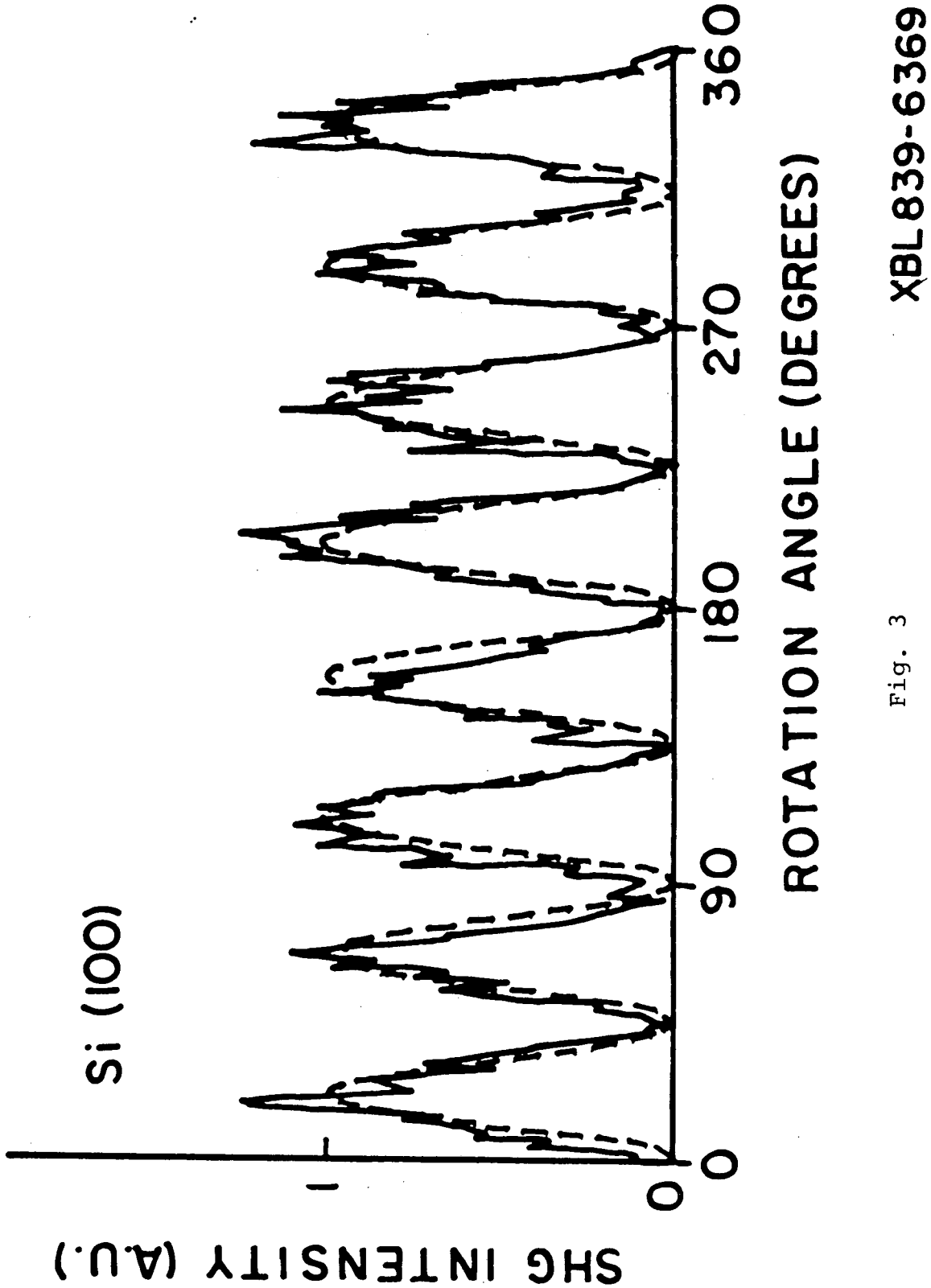
SHG INTENSITY (A.U.)
Si (100)
0
1
0
90
180
270
360
ROTATION ANGLE (DEGREES)
XBL839-6369

Fig. 3

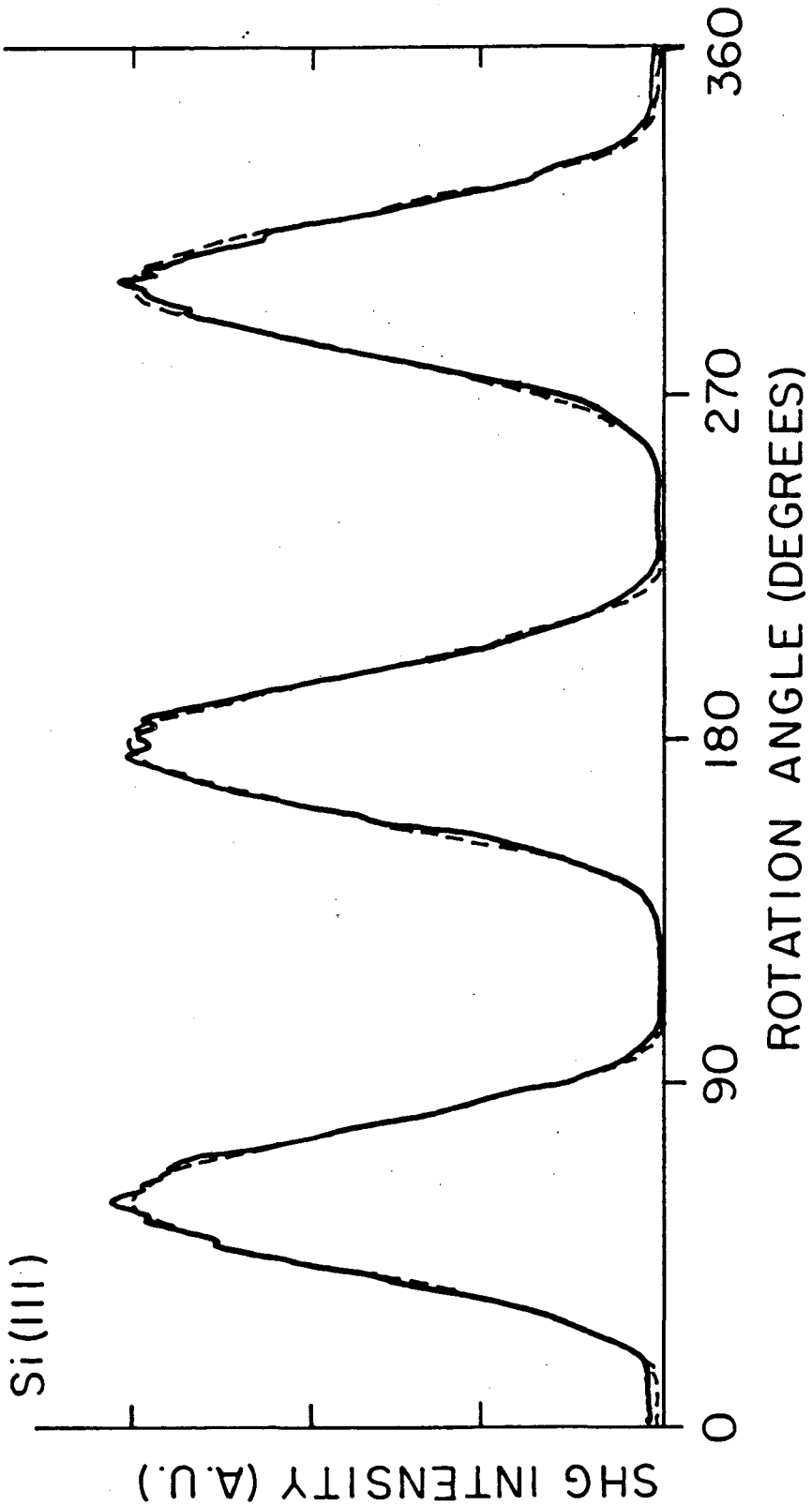

XBL836-5868A

Fig. 4

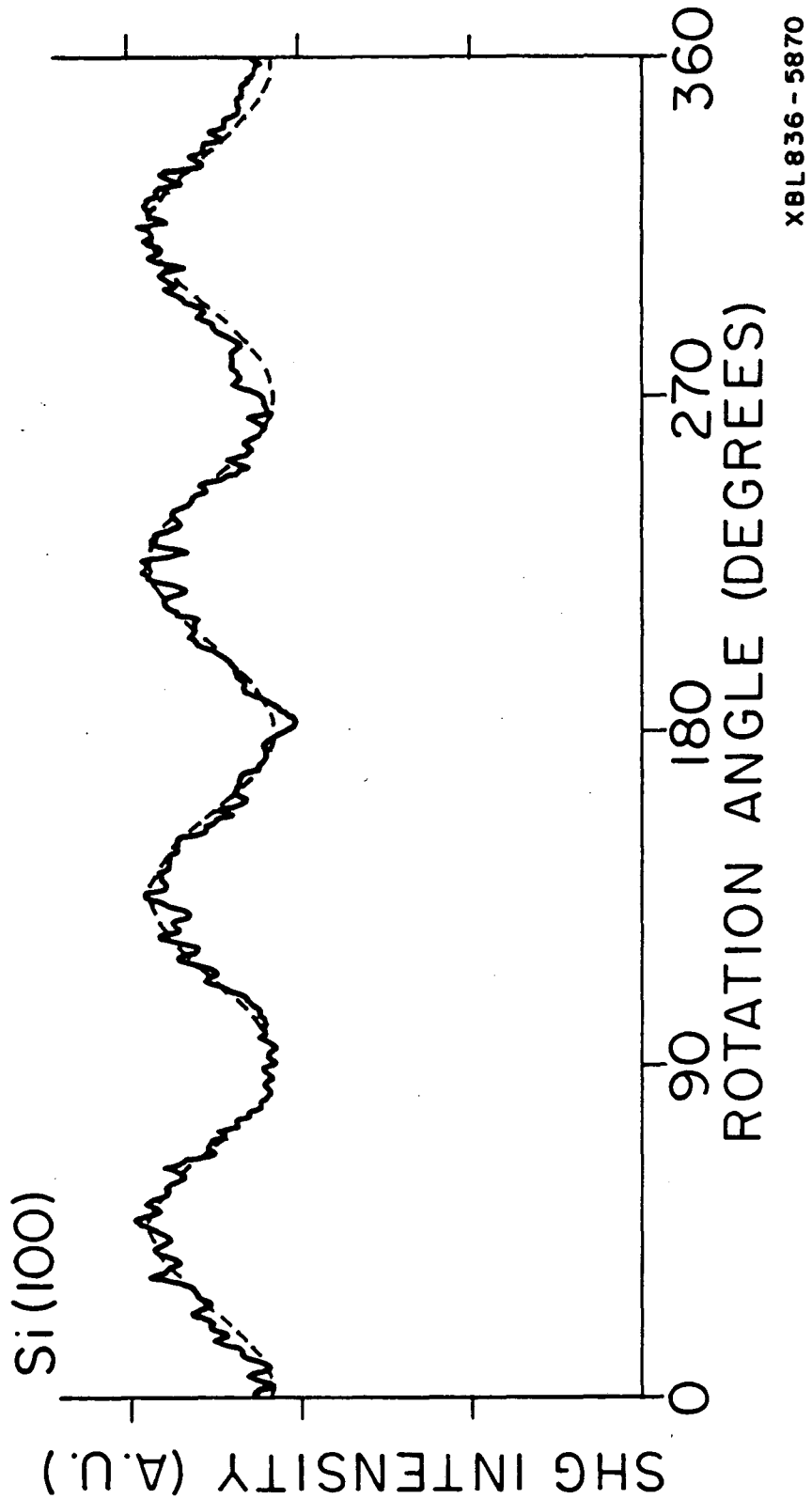
SHG INTENSITY (A.U.)
Si (100)
0
90
180
270
360
ROTATION ANGLE (DEGREES)
XBL836-5870

Fig. 5

V. USE OF SECOND-ORDER PROCESSES TO PROBE MOLECULES ADSORBED TO NONINTERACTING SUBSTRATES

To demonstrate the basic features of the second-order optical surface probes, it is convenient to work on systems of molecules adsorbed to noninteracting substrates. By noninteracting, we mean that the molecule-substrate interaction perturbs the electronic and vibrational properties of the free molecule and clean substrate very weakly. In such systems, the second-harmonic (SH) or sum-frequency (SF) field due to the substrate is the same with or without adsorbed molecules. The field due to the molecular layer, $\vec{E}_{mol}$, can be obtained by subtracting the field due to the clean substrate, $\vec{E}_{sub}$, from the field due to the molecule-covered substrate, $\vec{E}_{sub} + \vec{E}_{mol}$, by the techniques discussed in Ch. III, section B. Moreover, the field $\vec{E}_{mol}$ can be simply related to the nonlinear polarizability of the free molecule, $\overleftrightarrow{\alpha}^{(2)}$, for which symmetry and spectroscopic information may be available. The relationship between $\vec{E}_{mol}$ and the nonlinear susceptibility of the molecular layer

$$\overleftrightarrow{\chi}^{(2)}_{mol} = N_s \langle \overleftrightarrow{\alpha}^{(2)} \rangle_{orient} \qquad (1)$$

was discussed in Ch. II. Here, N_s is the surface density, the brackets indicate the average over orientations in the layer and local-field corrections are neglected assuming the layer to be sufficiently dilute and the substrate (typically an insulator) to have a weak image-dipole. In this chapter, three experiments are presented in which the orientation of adsorbed molecules is obtained through the tensorial properties of $\overleftrightarrow{\chi}^{(2)}_{mol}$, the isotherm of adsorption of molecules from solution is

obtained through N_s and the vibrational spectrum is obtained through the resonant enhancement of $\overleftrightarrow{\alpha}^{(2)}(\omega_s = \omega_1 + \omega_2)$ when ω_1 is tuned through a vibrational transition and ω_2 is fixed. The first two experiments were performed on p-nitrobenzoic acid (PNBA) adsorbed to fused silica. The PNBA orientation measurement is a significant refinement over an earlier measurement of the orientation of Rh 6G on fused silica[1] as the ratio of moments of orientation angles is determined by a single highly accurate polarization measurement. Moreover, the PNBA data is less ambiguous because PNBA's orientation is specified by one angle while Rh 6G's orientation is specified by two angles with unknown correlations. The isotherm of PNBA adsorption to silica determined by SHG is more reliable than the isotherm of pyridine adsorption on Ag published earlier[2] because the coverage-dependence of $\vec{E}_{mol}$ for the PNBA layer is specified by Eq. (1) while the coverage-dependence of the nonlinear response of the strongly-interacting pyridine-Ag system is uncertain. The third experiment in this chapter (section C) performed on unknown hydrocarbons on a fused silica substrate is the first experiment to use SFG to obtain surface vibrational spectroscopy. In section D, the chapter ends with a discussion of what one might expect if one extended these three measurements to strongly-interacting systems (i.e., molecules on metals).

A. Average Orientation of PNBA on Air/Silica and Ethanol/Silica Interfaces[3]

It is clear from Eq. (1) that a determination of $\overleftrightarrow{\chi}^{(2)}_{mol}$ and an <u>apriori</u> knowledge of $\overleftrightarrow{\alpha}^{(2)}$ should allow one to infer information about the average orientation of the molecules adsorbed at a surface. More

specifically, Eq. (1) may be written:

$$\chi^{(2)}_{mol,ijk} = N_s \langle G^{ijk}_{\lambda\mu\nu} \rangle_{orient} \alpha^{(2)}_{\lambda\mu\nu} \qquad (2)$$

where the orientational average is taken over the tensor $\overleftrightarrow{G}$ whose elements are the product of the 3 projections of λ on i, μ on j, and ν on k where λ, μ, and ν are any of the molecular coordinates (ξ, η, ζ) and i, j and k are any of the substrate coordinates (x, y, z). It is useful to specify the orientation of the molecules by their Euler angles (ϕ, θ, ψ) where, by the usual definition, the orientation is obtained by first setting the molecular (ξ, η, ζ) in registry with (x, y, z), and then rotating ϕ about $\hat{z}$, θ about $\hat{\xi}$, and ψ about $\hat{\zeta}$.

Limitations of the SH technique to deducing average orientation are two-fold. First, as with all average measurements, the elements of G are averaged over the distribution function $f(\phi, \theta, \psi)$ and unknown correlations between angles may complicate the interpretation. Secondly, symmetry determines the number of independent non-zero elements in $\overleftrightarrow{\chi}_{mol}$ and $\overleftrightarrow{G}$ in Eq. (2) and may limit the number of non-negligible elements of $\overleftrightarrow{\alpha}^{(2)}$ that can be considered without making it impossible to determine $\langle \overleftrightarrow{G} \rangle$.

We now specialize to the most favorable case for deducing molecular orientation -- the case of uniaxial molecules characterized by a single dominant polarizability element $\alpha^{(2)}_{\zeta\zeta\zeta}$ and oriented with no preferred direction in the plane (ie., $\langle \sin^2\phi \rangle = 1/2$). In this case the orientation is fully specified by the tilt angle θ between $\hat{\zeta}$ and $\hat{z}$ and the non-zero elements of $\overleftrightarrow{\chi}^{(2)}_{mol}$ are:

$$\chi^{(2)}_{mol,\perp\perp\parallel} = N_s \alpha^{(2)}_{\zeta\zeta\zeta} \langle \cos^3\theta \rangle$$

$$\chi^{(2)}_{mol,\perp\parallel\parallel} = N_s \alpha^{(2)}_{\zeta\zeta\zeta} \frac{1}{2}\langle \cos\theta \sin^2\theta \rangle = \chi^{(2)}_{mol,\parallel\perp\parallel} . \qquad (3)$$

Any ratio of the elements of $\overleftrightarrow{\chi}^{(2)}_{mol}$ will give a value for moments of angle θ which will be independent of the coverage N_s and the absolute magnitude of $\alpha^{(2)}_{\zeta\zeta\zeta}$. Experimentally such a ratio is most easily obtained by taking the ratio of the $\hat{p}$- and $\hat{s}$-polarized parts (ie., cotangent of the polarization angle β) of $\vec{E}_{mol}$. Using Eqs. (5) and (6) of Ch. II and Eq. (3) for $\overleftrightarrow{\chi}^{(2)}_{mol}$, this ratio becomes

$$\cot\beta = \frac{E_p}{E_s} = A\{\chi^{(2)}_{mol,\perp\perp\perp} + B\chi^{(2)}_{mol,\perp\parallel\parallel} + C\chi^{(2)}_{mol,\parallel\perp\parallel}\}/\chi^{(2)}_{mol,\parallel\perp\parallel} \qquad (4)$$

where

$$A = \frac{1}{\varepsilon'} \frac{(k_{1z} + k_{2z})/k_o}{(k_1 k_{2z}/k_2^2 + k_{1z}/k_1)} \frac{k_x}{k_o} \frac{E_z}{2E_y}$$

$$B = (E_x^2 + E_y^2)/E_z^2$$

$$C = 2(k_{2z}/k_o)(\varepsilon'/\varepsilon_2)(E_x/E_z)$$

ε_1, ε', and ε_2 are the dielectric constants at 2ω above the layer, in the layer and in the substrate; $k_o^2 = 4\omega^2/c^2$, $k_1^2 = \varepsilon_1 k_o^2$, $k_2^2 = \varepsilon_2 k_o^2$; $k_{1z} = \sqrt{k_1^2 - k_x^2}$, $k_{2z} = \sqrt{k_2^2 - k_x^2}$; $k_x = 2k_x(\omega)$ where incident wavevector $\vec{k}(\omega) = (k_x(\omega), 0, k_z(\omega))$; and $\vec{E} = (E_x, E_y, E_z)$ is the incident field at frequency ω defined in the layer with dielectric constant ε'.

Rearranging Eq. (4), the ratio R of elements of $\overleftrightarrow{\chi}^{(2)}$ becomes

$$R = \frac{\chi^{(2)}_{mol,\perp\perp\perp} + B\,\chi^{(2)}_{mol,\perp\parallel\parallel}}{\chi^{(2)}_{mol,\parallel\perp\parallel}} = \frac{\cot\beta}{A} - C \qquad (5)$$

where β is the measured polarization angle of $\vec{E}_{mol}$ at 2ω while A, B,

and C are set by the excitation geometry. By Eq. (3), if B is set to 2 then $R = 2/\langle \sin^2\theta \rangle$.

We now consider the measurement of the orientation of p-nitrobenzoic acid (PNBA) on both the PNBA-ethanol solution/silica and air/silica interfaces. The former was prepared by placing PNBA-ethanol solution in a liquid cell with the optically flat silica (Suprasil) substrate as one wall. The latter was prepared by placing a ~ 1 mm thick layer of dilute PNBA-ethanol solution on a carefully cleaned Suprasil substrate and letting the layer evaporate over a 3 to 5 hour period. Studies of a number of carboxylic acids adsorbed to metal oxides using inelastic electron tunneling spectroscopy indicate that the species adsorbed out of solution is the symmetrically positioned bidentate carboxylate ion (RCO_2^-).[4,5] The free PNBA molecule and adsorbed ion are shown in Fig. 1.

For using the scheme above to determine orientation, the molecules must have no preferred orientation in the surface plane and the electronic response of the molecule must be uniaxial. The first condition was verified by observing that the SH intensity did not depend on the sample's angle of rotation about its normal. This is reasonable since the silica substrate surface should be isotropic in the surface plane. The second condition is met because the delocalized π-electrons in the benzene ring, which dominate the nonlinear response, are polarized by the NO_2- and CO_2- groups (both acceptors) along the molecular $\hat{\zeta}$-axis. The adsorbed PNBA molecule has C_{2v} symmetry which for SHG limits the independent non-zero polarizability elements to: $\alpha^{(2)}_{\zeta\zeta\zeta}$, $\alpha^{(2)}_{\zeta\xi\xi}$, $\alpha^{(2)}_{\xi\zeta\xi}$ = $\alpha^{(2)}_{\xi\xi\zeta}$, $\alpha^{(2)}_{\zeta\eta\eta}$, and $\alpha^{(2)}_{\eta\zeta\eta} = \alpha^{(2)}_{\eta\eta\zeta}$, where $\hat{\xi}$ is in the plane of the benzene ring. Because of the large static dipole moments of some of the excited states along $\hat{\zeta}$, the element $\alpha^{(2)}_{\zeta\zeta\zeta}$ should dominate $\overleftrightarrow{\alpha}^{(2)}$. This contention

is borne out by detailed calculations of $\overleftrightarrow{\alpha}^{(2)}$ for aniline, nitrobenzene, and p-nitroaniline[6] in which $\alpha^{(2)}_{\zeta\zeta\zeta}$ is about an order of magnitude greater than $\alpha^{(2)}_{\zeta\xi\xi}$ and $\alpha^{(2)}_{\xi\zeta\xi}$ and two orders of magnitude greater than $\alpha^{(2)}_{\zeta\eta\eta}$ and $\alpha^{(2)}_{\eta\zeta\eta}$ for excitations in the near-infrared and visible. For λ_{exc} = 532 nm, the SH wavelength 266 nm is in resonance with the low-lying $A_1 \rightarrow A_1$ transition (centered at 260 nm with 50 nm FWHM for PNBA in ethanol) polarized along $\hat{\zeta}$. On the SH resonance, $\alpha^{(2)}_{\zeta\zeta\zeta}$ and $\alpha^{(2)}_{\zeta\xi\xi}$ will be further enhanced with respect to the other elements of $\overleftrightarrow{\alpha}^{(2)}$.

For measurements on the solution/silica interface (see Fig. 2), the incident field was passed through the silica substrate to excite the molecules on the substrate's back face to which a liquid cell had been pressure mounted. The SH field passed out through the silica substrate and along the detection path and was spatially separated from the SH field reflected from the front face. The criterion B = 2 in Eq. (3) was met by using an incidence angle of 65° and a polarization angle of 32.7° measured from the horizontal for the incident field before entering the silica substrate. For the air/solid interface, the molecules were excited on the front face of the substrate and B was set to 2 by using an incidence angle of 50° and a polarization angle of 54.6°. The value of the dielectric constant for the molecular layer ε' was taken to be that of the ambient, either of ethanol or of air. We used refractive indices of 1.46 and 1.36 for fused silica and ethanol respectively.

Using λ_{exc} = 532 nm, we measured the magnitude and phase of the SH field of the substrate with and without molecules and inferred a phase difference between $\vec{E}_{mol}$ and $\vec{E}_{sub}$ of 75° ± 5° and 90° ± 5° for the solution/silica and air/silica interfaces, respectively. These phase shifts are reasonable since the substrate nonlinearity should be off-

resonant and real while the molecule nonlinearity should be almost purely imaginary as 2ω is very close to the resonance at 260 nm discussed above. The difference in the phase shifts at the two interfaces may be due to solvent effects which can shift the resonance peak center. Both phase shifts are positive and are consistent with the resonance peak center being at higher frequencies than 2ω.

From the polarization angle of $\vec{E}_{mol}$ measured with λ_{exc} = 532 nm, we deduced $\langle \sin^2\theta \rangle = 0.36$ for ~ 1/2 monolayer of PNBA at the solution/silica interface and $\langle \sin^2\theta \rangle = 0.88$ for 1/4 monolayer (N_s = 1.5 X $10^{14}/cm^2$) at the air/silica interface. Assuming a δ-function distribution of θ at θ_o, θ_o = 37° and 70° for the two interfaces, respectively. For comparison, if the distributions were Lorentzians with 10° FWHM, the center of the distribution would lie at 34° and 76°, respectively. It is clear from these values that the molecules at the solution/silica interface are tilted into the solvent and the molecules at the air/silica interface lie relatively flat. The difference in orientation may be due to the static dipole-dipole interaction between molecules that would favor a flat orientation more strongly in air where ε_{dc} = 1 than in ethanol with ε_{dc} = 24. In addition, chemical interactions between the NO_2- group and the silica[7] and which would pull the NO_2- group toward the substrate would be weaker at the ethanol/silica interface because nitrobenzene interacts strongly with ethanol. Nitrobenzene is completely miscible in ethanol.

The resonance in $\overleftrightarrow{\alpha}^{(2)}$ for λ_{exc} = 532 nm made it more certain $\alpha^{(2)}_{\zeta\zeta\zeta}$ dominated $\overleftrightarrow{\alpha}^{(2)}$ but increased the likelihood that local-field corrections that had been neglected in Eq. (1) could affect the orientation measurement. To check the importance of these effects we measured the orienta-

tion using λ_{exc} = 1.06 μm (2ω off-resonant) and 683 nm (2ω near-resonant with the extinction coefficient ~ 1.5% that at resonance). For the same 1/2 monolayer sample of PNBA at the solution/silica interface we found the values of R, $\langle\sin^2\theta\rangle$ and θ_o below:

λ_{exc}	R	$\langle\sin^2\theta\rangle$, θ_o		
		(i)	(ii)	(iii)
1.06 μm	5.3 ± .3	0.38, 38° ± 2°	0.43, 41°	0.31, 34°
683 nm	4.3 ± .3	0.47, 43° ± 2°	0.48, 44°	0.36, 37°
532 nm	5.5 ± .2	0.36, 37° ± 1°	0.40, 39°	0.29, 33°

where in column (i) $\alpha^{(2)}_{\zeta\xi\xi} = \alpha^{(2)}_{\xi\zeta\xi} = 0$ is assumed and the error bars in θ_o come from the slight (~ 5%) ellipticity in the SH polarization due to weak birefringence in the fused silica substrate. Note the values of θ_o all fall near 40° indicating that local field effects (expected to be weakest for λ_{exc} = 1.06μm) are not important.

If we consider the contribution of elements $\alpha^{(2)}_{\zeta\xi\xi}$ and $\alpha^{(2)}_{\xi\zeta\xi}$ we find that for an excitation geometry where B = 2, Eq. (5) becomes:

$$R = \frac{2}{\langle\sin^2\theta\rangle} \quad \frac{\left(1 - (\gamma + 2\delta)\,\langle\sin^2\psi\rangle\right)}{\left(1 + \gamma - \delta/\langle\sin^2\theta\rangle\right)} \tag{6}$$

where $\gamma = \alpha^{(2)}_{\zeta\xi\xi}/\alpha^{(2)}_{\zeta\zeta\zeta}$ and $\delta = \alpha^{(2)}_{\xi\zeta\xi}/\alpha^{(2)}_{\zeta\zeta\zeta}$ and ψ is the Euler angle describing the rotation of the molecule about its $\hat{\zeta}$-axis. In columns (ii) and (iii) we calculate $\langle\sin^2\theta\rangle$ and θ_o taking the cases of $\langle\sin^2\psi\rangle$ = 0 and 1, respectively where γ = -0.15 and δ = -.10. These values of γ and δ are the worst case values for PNBA as they were derived by Lalama and Garito[6] for p-nitroaniline with λ_{exc} = 1.06 μm). Again note that all

values of θ_o lie within 38° ± 5° indicating that the orientation measurements do not suffer by neglecting γ and δ.

The local-field effects for PNBA in ethanol solution were expected to be weak due to the optical dielectric constant of ethanol being 1.36. Even for the 1/4 monolayer (N_s = 1.5 X 10^{14}/cm^2) sample of PNBA on the air/silica interface, local field effects should be small. The local-field factors for a layer of rod-like molecules with tilt angle θ, linear polarizability of 10Å^3 and a surface density N_s = 2 X 10^{14}/cm^2 derived with the approach of Bagchi et al.[8] gives $L_{\parallel} \sim 1$ and $L_{\perp} \sim (1 + 1/4 \cos^2\theta)^{-1}$ where $\parallel$ and $\perp$ subscripts indicate the corrections to the fields parallel and perpendicular to the substrate surface.[9]

On resonance (λ_{exc} = 532 nm), we found that the molecular layer gave rise to a substantial nonlinearity. Approximately 100 $\hat{s}$-polarized SH photons were generated from the N_s = 1.5 X 10^{14}/cm^2 layer of PNBA on the air/silica interface using a 7 ns pulse of ~ 100 mJ incident energy focussed on 0.25 cm^2 incident at 50° with a polarization angle of 54.6°. By comparing the value of E_{mol} so generated against the SH field from a quartz reference plate (see Ch. III, section B for calibration technique), we determined $\chi^{(2)}_{mol,\ \parallel\perp\parallel}$ = 9.0 X 10^{-17} esu. This allowed us to infer via Eq. (3) a value for $\alpha^{(2)}_{\zeta\zeta\zeta}$ (λ_{exc} = 532 nm) = 4.0 X 10^{-30} esu assuming the molecules were all tilted at θ_o = 70° from the surface normal. Repeating the measurement on the same sample for λ_{exc} = 1.06 μm, we found that the magnitude of $\alpha^{(2)}_{\zeta\zeta\zeta}$ for 1.06 μm was 5.5 times smaller than for λ_{exc} = 532 nm.[10]

Before ending this section, it is appropriate to mention other techniques for deducing molecular orientation. Orientation may also be measured by linear light scattering through the tensor properties of the

linear susceptibility of the molecular layer $\overleftrightarrow{\chi}^{(1)}_{mol}$. In analogy to the analysis of $\overleftrightarrow{\chi}^{(2)}_{mol}$ which gives third-order moments of the Euler angles, ratios of the elements of $\overleftrightarrow{\chi}^{(1)}_{mol}$ give second-order moments of the Euler angles. Because linear scattering has no intrinsic surface specificity, discriminating the molecule contribution from the substrate contribution is much more difficult in the linear measurement than in the SHG measurement. Ellipsometric techniques to cancel the substrate contribution or special geometries such as waveguides[11] to increase the interaction length are usually necessary. Another more widely used technique for measuring orientation of molecules on metal substrates is to analyze the ratio of the intensities of vibrational spectral lines. Because electric fields at infrared frequencies are perpendicular to the surface, vibrational modes are suppressed the more tilted they are from the surface normal.[12] This technique is superior to linear and nonlinear (SH) techniques that probe the orientation of electronic transitions as adsorption to metals is less likely to perturb the direction of the vibrational modes than the direction of electronic transitions. Vibrational spectra of molecular adsorbates are routinely measured with electron energy loss spectroscopy,[13] but their measurement in gaseous or liquid ambients by purely optical (IR or Raman) techniques requires sophisticated detection schemes.[14-17] There are also techniques exploiting the angular-dependence of the emission of photoelectrons[18] and ions desorbed in electron- or photon-stimulated processes.[19] Recently, the polarization dependence of the near-edge x-ray-absorption fine-structure spectra (NEXAFS) has also been used to deduce the orientation of molecules on surfaces.[20] Their use is also limited to UHV environments. Thus, SHG emerges as a more versatile orientational probe than linear optical

scattering in the visible and often times as a more practical alternative to vibrational spectroscopies for probing interfaces between two dense media.

B. Isotherm of p-Nitrobenzoic Acid (PNBA) Adsorption from Ethanolic Solution to Fused Silica[3]

The adsorption isotherm, that is the coverage of adsorbates as a function of solution concentration, ρ, is one of the most important pieces of information obtainable about molecular adsorption. From it, one can deduce the number of adsorption species and information about the adsorption kinetics. In the simplest case of Langmuir kinetics[21] in which molecules adsorb to all unoccupied sites with equal probability and interactions between adsorbate molecules are negligible, the steady state adsorbate coverage is given by:

$$N_S/N_O = \rho/(\kappa + \rho), \qquad (7)$$

where N_S is the adsorbate surface density, N_O is the saturation density and κ is a constant at fixed temperature. For aqueous solutions, $\kappa = 55 \exp(-\Delta G/RT)$ where ΔG is the free energy of adsorption from aqueous solution, R is the gas constant 1.99 cal/mole/K, and the constant 55 normalizes for adsorption from aqueous solution.

In general, there are few techniques for measuring N_S at the liquid/solid interface. The use of dispersed media substrates with large surface to volume ratios makes it possible to study molecular adsorption and surface reaction products by chemical titration techniques[21] or

infrared spectroscopy.[22] For many applications, such as electrochemistry, it is necessary to have a flat substrate with a relatively small area and adsorbate coverage must be inferred by the magnitude of adsorbate-induced changes in the electrostatic (in electrochemical cells) or optical properties of the substrate. In the latter case, special detection schemes[14-17] or a surface sensitive technique must be used to suppress the signal from the molecules in solution with respect to the relatively few molecules adsorbed to the surface. Recently, enhancements in the surface local fields at roughened metal surfaces have been exploited to obtain Raman spectra of molecular adsorbates.[23] Such spectra can be enhanced over those expected from the same number of free molecules by a factor of 10^5 for roughened Ag surfaces. Enhancement factors for other roughened materials have been measured.[24] Optical fields can also be enhanced by using geometries in which surface waves are launched on the surface of the metal substrate.[25] Here we exploit the intrinsic surface specificity of SHG to measure the surface coverage of p-nitrobenzoic acid molecules on a small (laser beam probes only 1/4 cm^2) ethanol/silica interface for which enhancements in the optical fields are negligible.

PNBA molecules were adsorbed from ethanolic solution onto an optically flat Suprasil substrate which was pressure mounted as a wall of a liquid cell, (see Fig.2). SHG from the liquid/silica interface was detected as a function of the PNBA-ethanol solution concentration, ρ, as ρ was progressively increased by adding small doses of concentrated PNBA-ethanol solution to the liquid cell. We waited 1 hour between data points to allow for equilibration. The SH field from the molecules, $\vec{E}_{mol}$, as a function of ρ was deduced from the measured SH intensities

from the molecule-covered substrate by assuming the phase factor between $\vec{E}_{mol}$ and the substrate SH field, E_{sub}, was 75° ± 5° and independent of ρ. This phase factor was determined by measuring the amplitudes and phases of $\vec{E}_{sub}$ for the pure ethanol/silica interface and ($\vec{E}_{mol}$ + $\vec{E}_{sub}$) for the ρ = 0.5 mM PNBA-ethanol solution/interface and then subtracting analytically. The assumption that the phase factor did not depend on ρ or orientation was reasonable since the phase is determined by the phase of $\overleftrightarrow{\chi}^{(2)}_{mol}$ which, as discussed in section A, has the same phase as the dominant element of the molecular polarizability $\alpha^{(2)}_{\zeta\zeta\zeta}$ for PNBA.

In Fig. 3, we show the adsorption isotherm of PNBA from ethanolic solution to fused silica where we have made the approximation that N_s is proportional to $|\vec{E}_{mol}|$ at each value of ρ. As shown in the introduction to this chapter, $\vec{E}_{mol}$ is related to elements of $\overleftrightarrow{\chi}^{(2)}$ which depend both on N_s and on the average orientation of the molecules. In this experiment we measured the $\hat{p}$-polarized component of $\vec{E}_{mol}$ excited with a $\hat{s}$-polarized incident field at 532 nm. $|\vec{E}_{mol}|$ was then proportional to $\chi^{(2)}_{mol,\,\|\perp\|}$. The orientational dependence of E_{mol} was then given by that in Eq. (3), namely, that of $\chi^{(2)}_{mol,\|\perp\|} = N_s\alpha^{(2)}_{\zeta\zeta\zeta}\langle\cos\theta\sin^2\theta\rangle/2$, (neglecting local-field corrections), where the orientation of PNBA is fully specified by tilt angle θ between the molecular $\hat{\zeta}$-axis and the normal to the substrate surface. By measuring the orientation by the technique described in section A we found that $\langle\sin^2\theta\rangle$ = 0.36 and 0.28 for the molecules adsorbed when ρ = 0.5 mM and 0.05 mM. The corresponding values of $\langle\cos\theta\sin^2\theta\rangle$ assuming θ is distributed narrowly about θ_o are 0.29 and 0.24 for the two coverages respectively. As these values are the same to within our experimental accuracy, the approximation that

N_S is proportional to $|\vec{E}_{mol}|$ was reasonable.

The isotherm has the shape generally associated with Langmuir kinetics.[21] It increases monotonically to a saturation level without kinks which would have indicated the coverage-dependent onset of adsorption at a second site. Fitting the first three points to Eq. (7) we deduce a value of 8 kcal/mol for the free energy of adsorption from solution, ΔG, referenced to aqueous solution. This relatively low value is reasonable considering ΔG is the difference between the adsorption free energies for both chemisorption of PNBA to glass and solvation of PNBA in ethanol.

For high values of ρ, $|\vec{E}_{mol}|$ reaches a saturation value that does not change when ρ is increased from 2 to 10 mM (10 mM data point not shown). This indicates that, as expected by symmetry, the SH from the isotropically-oriented PNBA molecules in solution is suppressed with respect to that of the adsorbed molecules on the surface. If one considers that at 10 mM there are 6×10^{17} PNBA molecules in a 1 mm thick layer of solution in front of the interface while there are only at most 10^{15} molecules/cm^2 adsorbed on the surface, the suppression of SH from the solution is extremely efficient.

In summary, we have obtained an isotherm of adsorption at a liquid/solid interface without the benefit of special geometries or surface-enhanced local-field effects. By verifying experimentally that the molecular orientation does not change appreciable as a function of coverage, we could determine the surface coverage simply by measuring the magnitude of the SH field due to the molecules. The latter could be isolated from the SH from the substrate by measuring the relative phase between the molecule and substrate SH fields and subtracting.

C. Vibrational Spectra of Hydrocarbons on Fused Silica: Preliminary Results[26]

So far in this Chapter, we have considered the use of SHG to measure coverage and the orientation of molecules adsorbed to surfaces. In many cases, one would like to identify the species adsorbed to the surface or determine the coverage or orientation of only one of several species on the surface. To obtain this species specificity one may use the frequency-dependence of the second-order nonlinear response of the molecular adsorbate layer. The use of SHG to obtain electronic spectra of adsorbates by observing the enhancement of the SH intensity as 2ω is tuned through an electronic resonance[1] was discussed in Ch. II, section C. In this section, we discuss the use of sum-frequency generation (SFG) to obtain vibrational spectra of adsorbates by observing the enhancement of the SF intensity as one of the excitation frequencies is tuned through a vibrational resonance.

The frequency dependence of the SF intensity from a molecular layer is given by the square of the molecular polarizability $\overleftrightarrow{\alpha}^{(2)}(\omega_S = \omega_1 + \omega_2)$ which is written explicitly in Eq. (17) of Ch. II. Here ω_S is the sum frequency and ω_1 and ω_2 are the excitation frequencies. When ω_1 is close to a vibrational resonance with frequency ω_{vg} between the ground state $|g\rangle$ and the vibrational state $|v\rangle$, the expression for $\overleftrightarrow{\alpha}^{(2)}(\omega_S)$ reduces to:

$$\alpha^{(2)}_{ijk}(\omega_S = \omega_1 + \omega_2) = [\alpha^{(2)}_{ijk}]_{NR} + (\pi\hbar^2)^{-1}\tilde{\alpha}^{(1)}(\omega_1 - \omega_{vg})p^i_{vg} \times \sum_n \left\{ \frac{p^i_{gn}\, p^k_{nv}}{\omega_S - \omega_{ng} + i\Gamma_{ng}} - \frac{p^i_{nv}\, p^k_{gn}}{\omega_S + \omega_{nv} + i\Gamma_{nv}} \right\}, \qquad (8)$$

where the ground state is assumed to be fully occupied and nondegenerate. The transitions between state $|n\rangle$ and $|n'\rangle$ have dipole matrix elements $p^i_{nn'}$ in the i^{th} direction, energy $\hbar\omega_{nn'}$, and linewidth $\Gamma_{nn'}$. $[\alpha^{(2)}_{ijk}]_{NR}$ is the non-resonant contribution. The linear polarization $\tilde{\alpha}^{(1)}(\omega_1)$ has been normalized to $\int \mathrm{Im}(\tilde{\alpha}^{(1)}(\omega_1))d\omega_1 = 1$. We see from Eq. (8) that the frequency-dependence of $\overleftrightarrow{\alpha}^{(2)}(\omega_s = \omega_1 + \omega_2)$ is dominated by the vibrational resonance behavior of $\tilde{\alpha}^{(1)}(\omega_1)$.

In practical applications, one chooses ω_2 to be an easily generated fixed visible frequency and takes advantage of the fact that a visible signal at ω_s can be easily detected with sensitive photomultiplier tubes. The first term in braces in Eq. (8) indicates that by an appropriate choice of ω_2, an enhancement of the SF signal is obtained when ω_s is near an electronic resonance. Such an enhancement makes the signal easier to detect and suppresses $[\alpha^{(2)}_{ijk}]_{NR}$. In addition, because a visible frequency and the linewidth of an electronic resonance is so much larger than the range over which ω_1 is tuned around a vibrational resonance (50 cm^{-1}) or even over a complete vibrational spectrum (1000 to 3000 cm^{-1}), the energy denominators in braces are essentially independent of ω_1. If $[\alpha^{(2)}_{ijk}]_{NR}$ is negligible, $\overleftrightarrow{\alpha}^{(2)}(\omega_s = \omega_1 + \omega_2)$ is proportional to the linear polarizability at ω_1 and the vibrational lineshapes measured by SFG will be the same as those measured by linear IR spectroscopy. If necessary the phase and amplitude of the SF field can be measured and the effects of a large $[\alpha^{(2)}_{ijk}]_{NR}$ subtracted out analytically to get an easily interpretable SFG lineshape. We note that the ratios of the vibrational line intensities in a complete spectrum measured by SFG will not generally be the same as those measured by IR or Raman spectroscopy because of the different selection rules: for

both p_{vg} and the products $p_{gn}p_{nv}$ to be non-zero, the transition must be both IR- and Raman-active.

Surface vibrational spectra are currently obtained by electron energy loss spectroscopy[12] in ultrahigh vacuum environments, inelastic electron tunneling spectroscopy[4,5] in tunneling junctions, or a number of optical techniques (IR[14-16] and Raman[17,23]). In the latter case, the relatively small optical scattering cross-section of a monolayer of adsorbates, compared to the signals from the adsorbate molecules in the ambient and from the substrate, often necessitate the use of: 1) special geometries to increase the interaction areas such as dispersed media substrates[22] and waveguides,[11] or 2) special detection schemes such as ellipsometry,[14,27] wavelength modulation,[15] bolometers,[28] photoacoustic spectroscopy,[29] Raman gain spectroscopy,[17] and multi-channel detection,[30] or 3) local-field enhancements at roughened surfaces.[22] The advantage of SFG over other optical techniques is that special geometries or detectors are not required. SFG is intrinsically interface specific provided the surrounding media (i. e., substrate and ambient liquid or gas) are centrosymmetric. On the other hand, the vibrational frequency range accessible by SFG is limited by current laser technology to the region (850-1050 cm^{-1}) with the CO_2 laser and > 2800 cm^{-1} with F-center lasers, difference-frequency generation in dyes or a $LiNbO_3$ optical parametric oscillator.[31] Tunable IR can also be generated by Stimulated Raman Scattering but intensities are generally too low to be useful. Development of the free electron laser will overcome this limitation.

To demonstrate the feasibility of obtaining surface vibrational spectra using SFG we chose to probe the C-H stretch (n 3000 cm^{-1}) of

molecules on a fused silica (Optosil) substrate. The laser setup and typical energies of pulses used are shown in Fig. 4. Infrared radiation tunable around 3000 cm^{-1} was generated by a $LiNbO_3$ optical parametric oscillator (OPO) and amplifier (OPA) pumped with 15 ns pulses of 1.06 μm radiation from a cavity-extended Quanta Ray Nd^{3+}:YAG laser which had been propagated to the far-field to get good mode quality. The OPO was operated with ~ 5 cm^{-1} resolution to maximize the output power. The insertion of an intracavity etalon could have increased the resolution to 0.5 cm^{-1}. We mixed the IR with visible radiation at 532 nm generated by frequency-doubling in a KDP crystal the 1.06 μm radiation remaining after the OPA stage. As with SH, the IR and visible incident beams were incident on the sample (see Fig. 5) so the reflected SF radiation could be spatially separated from the reflected incident beams. The SF radiation was passed through appropriate filters, a monochromator and then detected by a photomultiplier tube. Sample SF intensities were normalized for the laser intensities against the SF generated from the surface of a quartz plate.

In Fig. 6, we show the normalized SF spectrum from an Optosil substrate that had been carefully cleaned with a series of organic solvents ending with vapor-deposited methanol. The data was obtained using ~ 6 mJ of IR and 60 mJ of 532 nm radiation focussed to ~ 3 mm^2. Signals were large enough to be detected without further enhancement by making ω_s closer to the UV. On the resonance at 2950 cm^{-1} there were ~ 100 SF photons/pulse. The resonance is most certainly due to adsorbates rather than an intrinsic feature of the substrate as the quartz (also SiO_2) reference signal was strictly proportional to the product of the incident energies and showed no dispersion. The resonance is probably due

to the C-H stretch modes of alkoxides which are known to adsorb to silica quite readily.[32] Alkane C-H stretches run from 2800 to 3000 cm^{-1}.

In our initial efforts we were unable to see significant differences between the spectra from a nominally clean sample and one with 6×10^{14}/cm^2 PNBA molecules adsorbed by evaporation from ethanolic solution. This may have been due to there being many more alkoxide radicals on the surface than PNBA molecules. Unfortunately, time did not allow us to try using 266nm (the 4th harmonic of the Nd^{3+}:YAG laser output) as the visible wavelength to exploit the electronic resonance of the PNBA molecules and thereby enhance the SF signal from the PNBA molecules.

Despite our lack of well-characterized spectra, these results definitely show that SFG is sensitive enough to detect vibrational spectra of molecules on surfaces (we observed a resonant enhancement of 10). Because of its intrinsic surface specificity and the ability to use it without special geometries or detection systems, SFG promises to be an extremely useful technique for obtaining vibrational spectra.

D. Extension to Molecules on Metal Substrates

The orientation, coverage, and vibrational spectrum were particularly easy to obtain in the cases above because the nonlinearity of the adsorbed molecule was not perturbed by the substrate and thus maintained its free-molecule electronic dipole moments, did not depend on relative coverage and had the same vibrational spectrum as the free molecule. The electronic properties of molecules adsorbed to metal substrates are quite complex. The molecular levels mix with the metallic surface bands and can accept from or donate to the metal conduction band, can perturb metal interband transitions, and can create new metal-molecule transi-

tions. Obviously, the nonlinear optical response will reflect the rich electronic properties of the metal-molecule system. One expects SHG to be extremely sensitive to chemisorbed molecules on surfaces.

On the other hand, interpreting the SH signal to deduce specific properties of the surface adsorbates is not straight-forward. For example, since the direction of the electronic transitions involving shared electrons between the metal and molecule will most likely be perpendicular to the surface and independent of the molecular orientation, SHG will not be a good tool for measuring molecular orientation. Similarly, because each molecule will interact with a substrate that has already been modified by the presence of adsorbed moelcules, the change in SH response due to an additional adsorbate will depend on the relative coverage. Thus SHG would not be a good way of measuring coverage unless the SH response had been independently calibrated to coverage.

Despite these difficulties, however, SHG can be a useful probe of the changes in electronic structure due to adsorbates. By using the resonant enhancement of SH when either ω or 2ω are resonant with an interband transition, one can follow the evolution of the surface electronic spectra during chemical processes.

Because vibrational modes maintain there integrity upon adsorption, vibrational spectra obtained with SFG can be used to measure coverage and with some analysis also the adsorbate orientation. The low-lying electronic resonance in the metal-molecule system can resonantly enhance SFG at the sum frequency. One would then expect to gain sensitivity due to these electronic resonance and to be able to perform measurements with a less powerful tunable IR source than was used in the experiment reported here on molecules adsorbed to an insulating substrate.

References

1. T. F. Heinz, C. K. Chen, D. Ricard, and Y. R. Shen, Phys. Rev. Lett. 48, 478 (1982).
2. C. K. Chen, T. F. Heinz, D. Ricard, and Y. R. Shen, Chem. Phys. Lett. 83, 455 (1981).
3. T. F. Heinz, H. W. K. Tom, and Y. R. Shen, Phys. Rev. A 28, 1883 (1983).
4. J. T. Hall and P. K. Hansma, Surf. Sci. 76, 61 (1978).
5. C. S. Korman and R. V. Coleman, Phys. Rev. B 15, 1877 (1977).
6. S. J. Lalama and A. F. Garito, Phys. Rev. A 20, 1179 (1979); K. D. Singer and A. F. Garito, J. Chem. Phys. 75, 3572 (1981).
7. Tunneling spectroscopy indicates that for o-nitrobenzoic acid both the NO_2^- and COO^- -groups are bound to the surface. See Korman and Coleman, ref. 5.
8. A. Bagchi, R. G. Barrera, and B. B. Das Gupta, Phys. Rev. Lett. 44, 1475 (1980); A. Bagchi, R. G. Barrera, and R. Fuchs, Phys. Rev. B 25, 7080 (1982).
9. P. Ye (private communication).
10. These values of $\alpha^{(2)}_{\zeta\zeta\zeta}$ are comparable to those calculated for other ρ-distributed benzene derivatives in ref. 6.
11. J. F. Raboit, R. Santo, N. E. Schlotter, and J. D. Swalen IBM,J. Res. Develop. 26, 209 (1982).
12. Ph. Avouris and J. E. Demuth, J. Chem. Phys. 75, 4783 (1981).
13. H. Ibach, H. Hopster and B. Sexton, Appl. of Surf. Sci. 1, 1 (1977).
14. P. R. Mahaffy and M. J. Digman, Surf. Sci. 97, 377 (1980).

15. P. Hollins and J. Pritchard, Surf. Sci. 89, 486 (1979).

16. Y. J. Chabal and A. J. Sievers, Phys. Rev. Lett. 44, 944 (1980).

17. J. P. Heritage and D. L. Allara, Chem. Phys. Lett. 74, 507 (1980); G. L. Eesley, IEEE J. of Quant. Electron, 17, 1285 (1981).

18. R. Brooks, N. V. Richardson and D. A. King, Surf. Sci. 117, 434 (1982); C. L. Allyn, T. Gustafsson, and E. W. Plummer. Chem. Phys. Lett. 47, 127 (1977).

19. F. P. Netzer and T. E. Madey, Phys. Rev. Lett. 47, 928 (1981).

20. J. Stöhr and R. Jaeger, Phys. Rev. B 26, 4111 (1982).

21. See for example, M. J. Rosen, Surfactants and Interfacial Phenomena (Wiley, New York, 1978).

22. L. H. Little, Infrared Spectra of Adsorbed Molecules, (Academic Press, New York, 1966).

23. Surface Enhanced Raman Scattering, eds. R. K. Chang and T. E. Burstein (Plenum, New York, 1982).

24. G. T. Boyd, Th. Rasing, J. R. R. Leite, and Y. R. Shen, "Study of Local-Field Enhancement on Rough Surfaces of Metals, Semi-Metals and Semiconductors Using Optical Second-Harmonic Generation", submitted to Phys. Rev. B.

25. Y. J. Chen and E. Burstein, Phys. Rev. Lett. 36, 1207 (1976); E. Kretschmann, Z. Phys. 241, 313 (1971).

26. The author acknowledges Ralph H. Page for his assistance in this work and for providing and operating the tunable IR and visible frequency laser sources necessary for its completion.

27. R. M. A. Azzam and N. M. Bashara, Ellipsometry and Polarized Light (North Holland, Amsterdam, 1972); D. E. Aspnes and A. A. Studna, Appl. Optics 14, 220 (1975).

28. R. B. Bailey, T. Iri, and P. L. Richards, Surf. Sci. 100, 626 (1980).

29. F. Trager, H. Confal and T. J. Chuang, Phys. Rev. Lett. 49, 1720 (1982).

30. A. Campion and D. R. Mullins, Chem. Phys. Lett. 94, 576 (1983).

31. For oscillator: S. J. Brosnan and R. L. Byer, IEEE J. of Quant. Electron. QE-15, 415 (1979). For amplifier: R. A. Baumgartner and R. L. Byer, IEEE J. of Quant. Electron. QE-15, 432 (1979).

32. S. Kitahiro, Bull. Chem. Soc. Jpn. 49, 3389 (1976).

Figure Captions

Fig. 1 Schematic picture of p-nitrobenzoic acid as a free molecule and adsorbed to fused silica.

Fig. 2 Experimental setup for observing second-harmonic generation from the p-nitrobenzoic acid-ethanol solution/silica interface.

Fig. 3 Isotherm of p-nitrobenzoic acid adsorption from ethanolic solution to fused silica.

Fig. 4 Laser setup for sum-frequency generation experiment producing ~ 6.5 mj and 60 mj per 10 ns pulse of tunable IR - 3μm and visible at 532 nm, respectively.

Fig. 5 Excitation geometry for sum-frequency generation experiment. SFG propagates away from reflected excitation beams.

Fig. 6 Sum-Frequency Intensity vs. IR frequency (in wave numbers) from the surface of a nominally clear Optosil substrate.

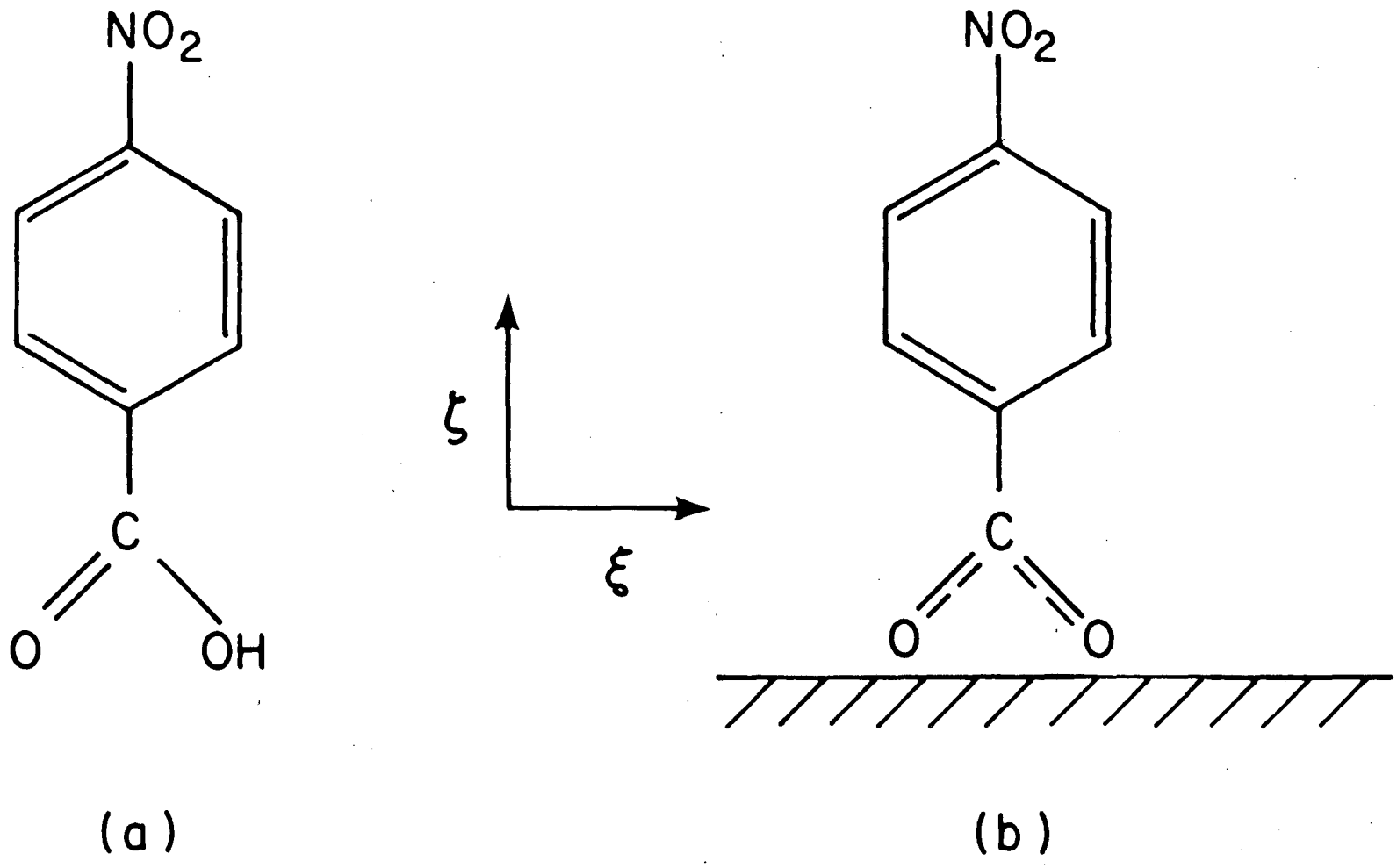

Fig. 1

XBL 8212-7390

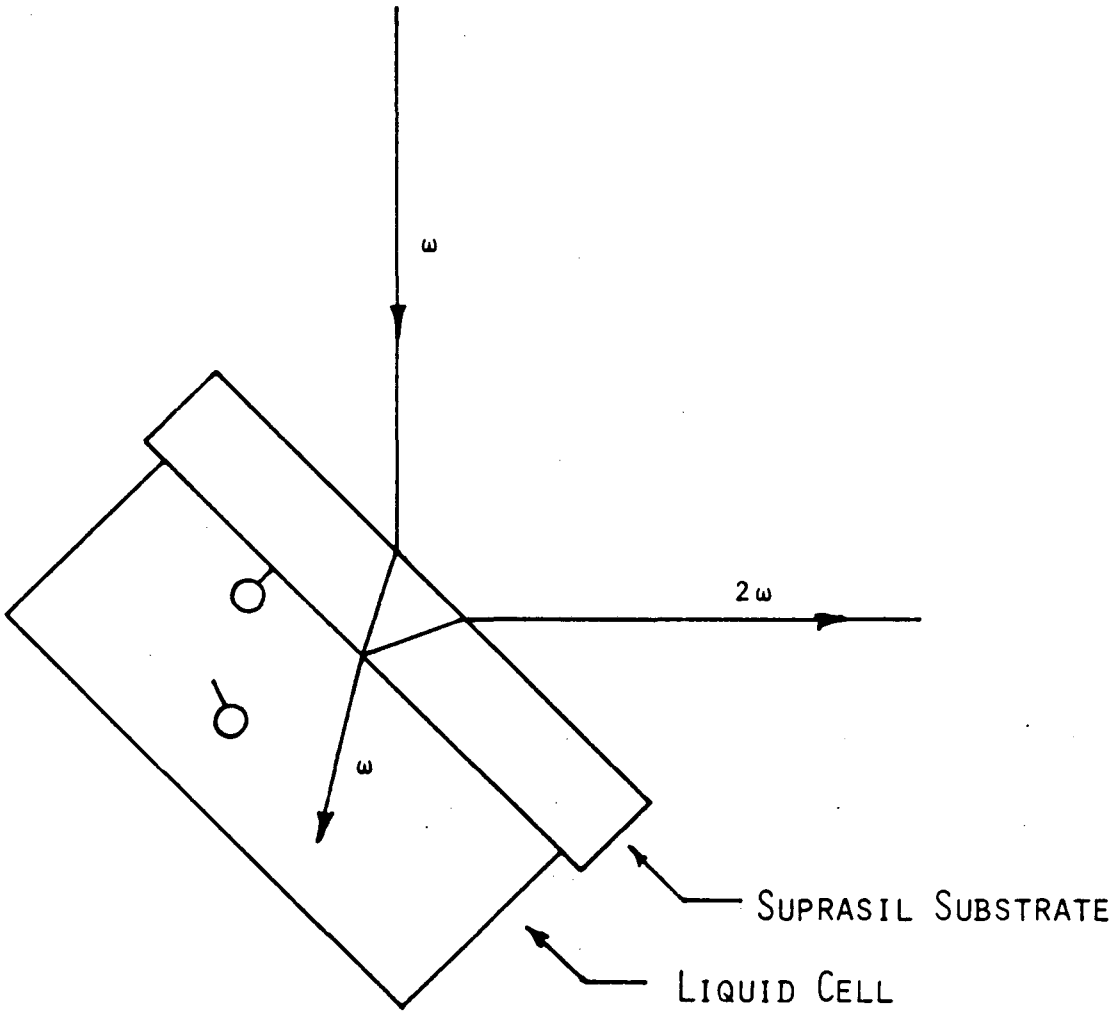

FIG. 2

XBL 844-1521

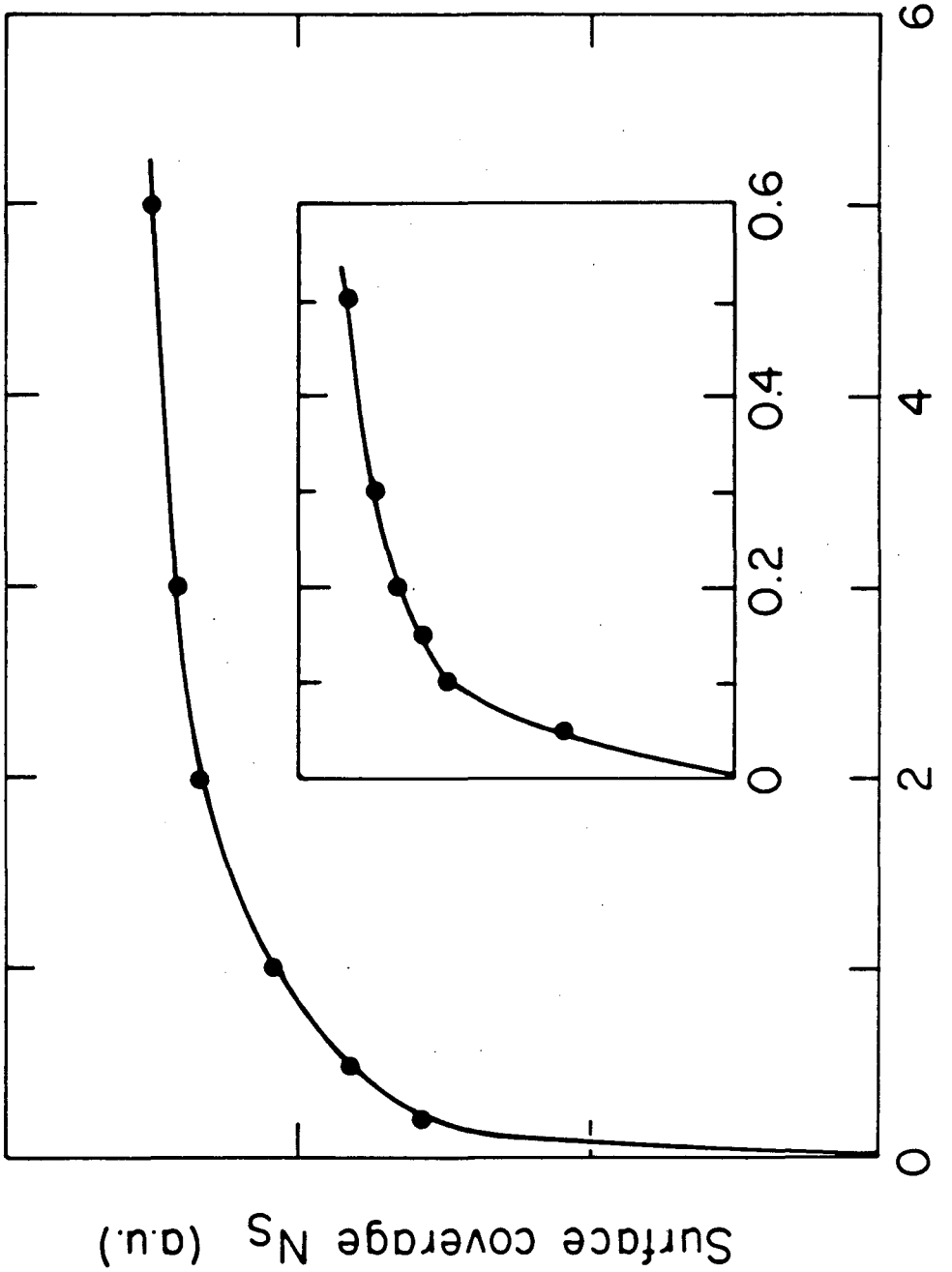

XBL8212-7391

Fig. 3

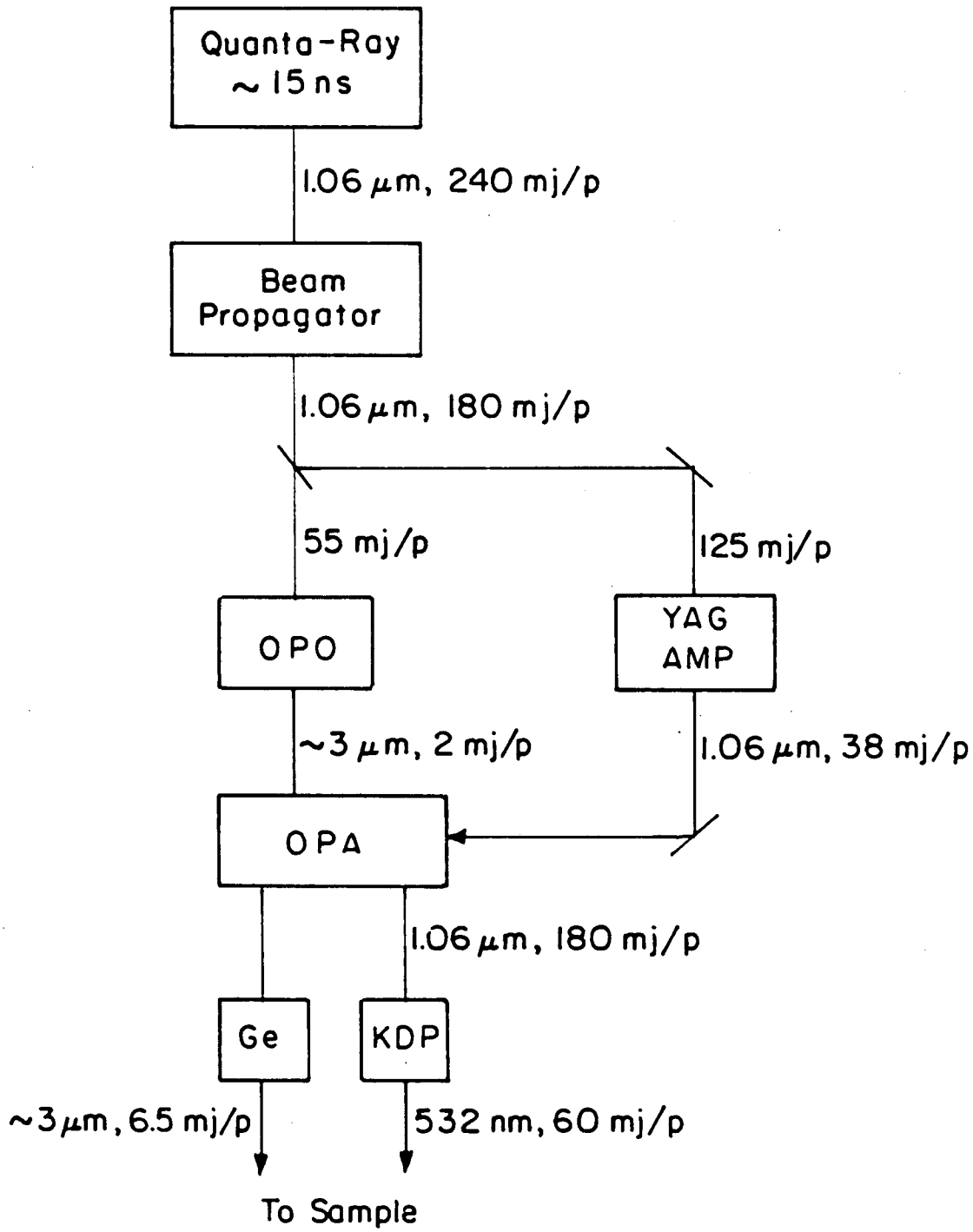
Quanta-Ray
~ 15 ns
1.06 μm, 240 mj/p
Beam
Propagator
1.06 μm, 180 mj/p
55 mj/p
125 mj/p
OPO
YAG
AMP
~3 μm, 2 mj/p
1.06 μm, 38 mj/p
OPA
1.06 μm, 180 mj/p
Ge
KDP
~3 μm, 6.5 mj/p
532 nm, 60 mj/p
To Sample
XBL 844-6856

Fig. 4

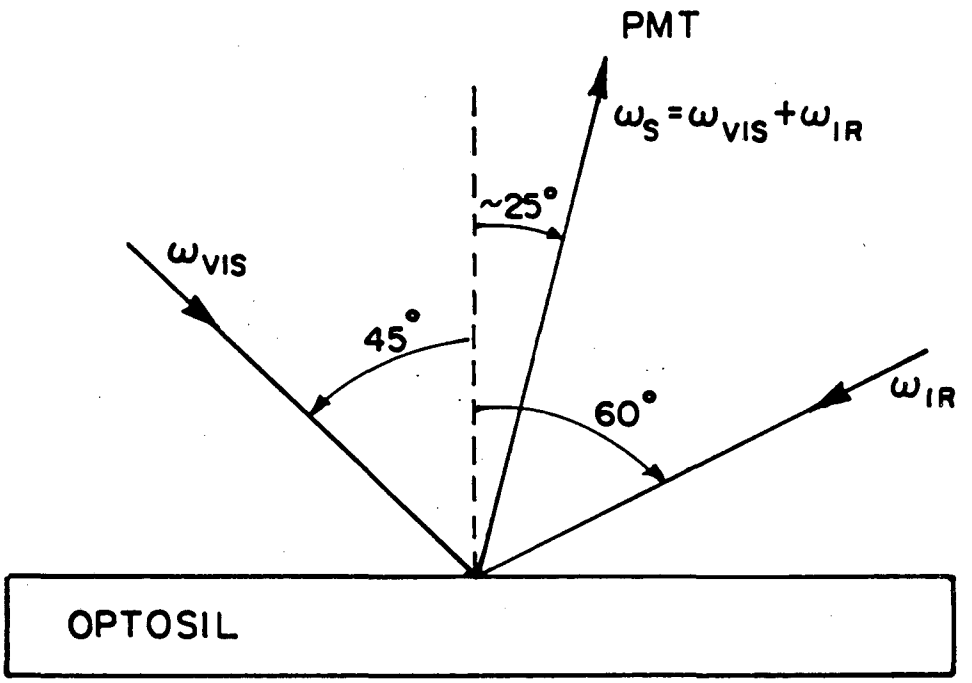

XBL 844-6857

Fig. 5

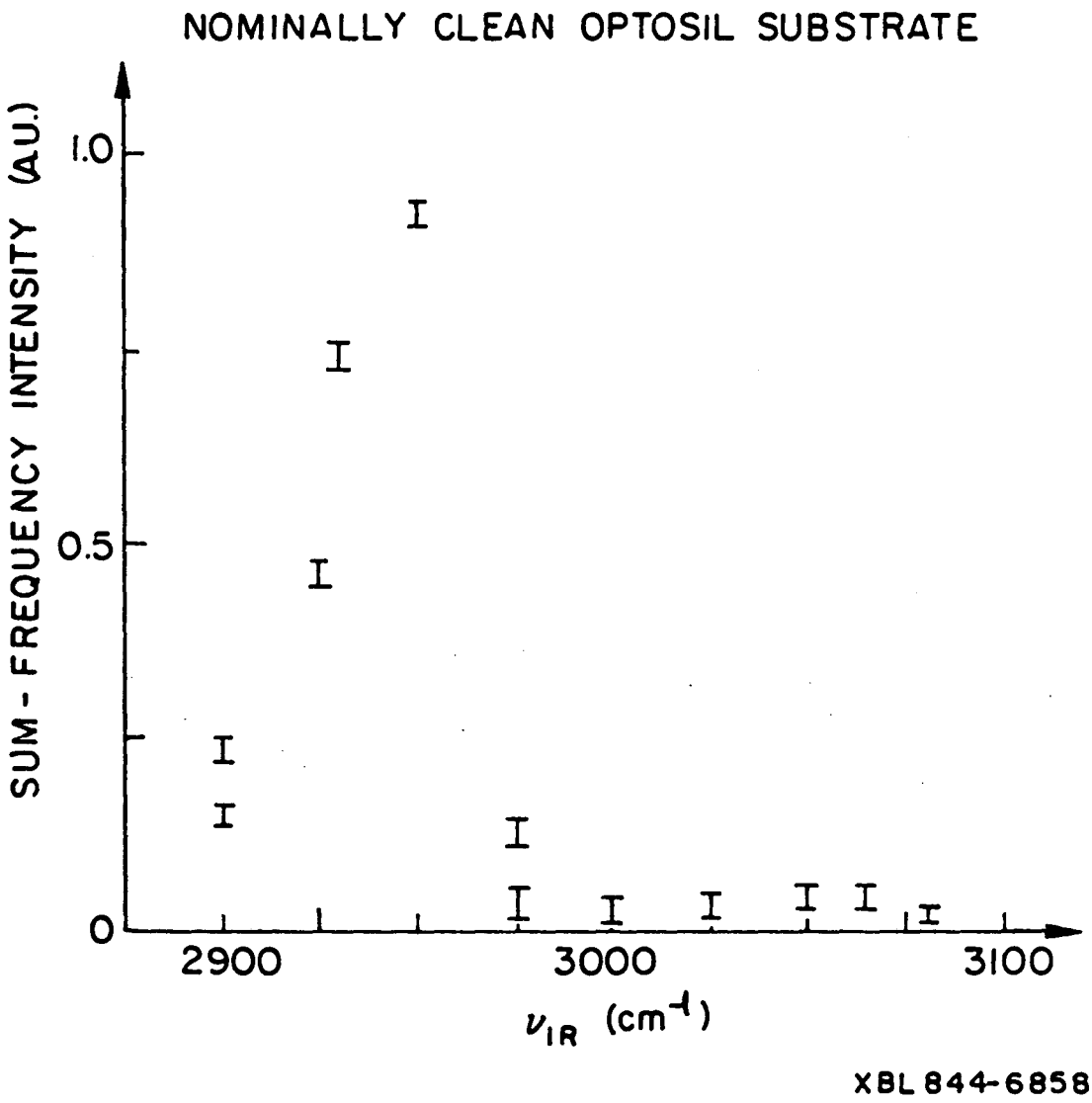
NOMINALLY CLEAN OPTOSIL SUBSTRATE
SUM-FREQUENCY INTENSITY (A.U.)
1.0
0.5
0
2900
3000
3100
ν_{IR} (cm^{-1})
XBL 844-6858

Fig. 6

VI. SECOND-HARMONIC GENERATION STUDIES OF SURFACES PREPARED IN ULTRAHIGH VACUUM: ADSORBATES ON Rh(111)

In previous chapters, we have discussed how SHG can be sensitive to surface structural symmetry, adsorbate coverage, and adsorbate orientation. In addition, SHG has been used to obtain electronic spectra of adsorbates[1] and preliminary results presented in Section C of Chapter V indicate that SFG can be used to obtain vibrational spectra. However, to establish SHG and SFG as viable new surface probes one must show that results obtained with SHG correlate with and supplement those obtained by more established surface science tools.

In this chapter we discuss the first application of SHG to probe well-characterized surface systems prepared in ultrahigh vacuum (UHV). We have used SHG to study the adsorption of O_2, CO, alkali metals, and aromatic hydrocarbons to atomically clean Rh(111). These are systems which have been actively investigated for their importance in catalysis involving hydrocarbon and oxidation reactions.[2] In all cases SHG had excellent sensitivity to the adsorbates and for the case of CO on Rh, SH was even sensitive to adsorption at different sites. SH results correlated well with other surface probes. In addition, because SHG is nondestructive and intrinsically fast (limited by the repetition rate of the excitation laser), we were able to monitor the surface continuously during adsorption and thermal processes which are often too fast for standard UHV surface probes.

The sample preparation and the apparatus will be described in Section A. Experimental results for the adsorption and coadsorption of O_2, CO, and alkali metals on Rh are presented in Sections B, C, and D.

Studies of the adsorption of benzene and pyridine and the dehydrogenation of benzene on Rh are presented in Section E. Results are briefly summarized in Section F.

A. Experimental

These experiments were conducted on a UHV chamber with a base pressure of ~ 2×10^{-10} torr. For optical access to the sample, two chamber ports were outfitted with special flanges to hold optically flat windows. The flanges had a square cut groove for a Viton O-ring against which the window sealed and a second wide groove to hold a larger-diameter concentrically-placed square-cross-section Teflon ring which served as a spacer to prevent the optical flat from compressing the Viton O-ring unevenly.

For the SHG measurements, Nd^{3+}:YAG laser pulses at 532 nm or 1.06 μm with ~ 7 ns pulse width and ~ 6 mJ pulse energy were $\hat{p}$-polarized and incident on the Rh sample at an angle of 67.5° with a beam diameter of 1 mm. At this intensity, no laser-induced desorption or surface damage could be detected. The SH radiation from the surface was mostly $\hat{p}$-polarized and was detected by the same system described in Ch. III. The SH intensity generated from the clean Rh surface was extremely large (about 1000 SH photons/pulse). With our 5%-efficient detection system and 10 Hz laser repetition rate, the measurements reported here are accurate to 5% with 1 sec time resolution. This fast time response is fairly unique among the traditional surface tools like LEED, AES or photoemission. All SH results have been converted to functions of exposure or temperature but were obtained by monitoring the surface as continous functions of time during adsorption from gas pressures of

4×10^{-8} torr (i. e., 1 Langmuir in 25 sec), alkali metal doses at ~ 1 monolayer/min, and during thermal desorption processes where the sample temperature was ramped at ~ 5 K/sec.

The Rh(111) surface was cleaned with cycles of Ar+ sputtering, heating at 200°C in 2×10^{-7} torr of O_2, annealing at 900°C in vacuum, and then flash annealing to 1000°C. The cleanliness and order of the surface were checked with Auger Electron Spectroscopy (AES) and Low-Energy Electron Diffraction (LEED) and the sample was flash heated to 1000°C again just before gas or metal dosing experiments to remove CO adsorbed from the background and the C and O atoms deposited by the dissociation of CO during AES. Gas pressures were measured with an ionization gauge and O_2 and CO pressures have been corrected for ion gauge sensitivity relative to N_2. Na, K, and Cs SAES GETTERS sources were mounted so that SHG could be monitored during alkali dosing and the dosage rate could be detected simultaneously with a quadrupole mass spectrometer. Surface coverages of CO were measured by thermal desorption yield and calibrated by LEED.

B. O_2 and CO on Rh(111)

We first consider the adsorption of the acceptors O_2 and CO. In Fig. 1, we show how the SH signal from the Rh(111) surface at 315K varied as the surface was continuously exposed to O_2 gas. The SH dropped from the normalized bare metal value of 1.0 to a saturation value of 0.12 at about 1.8 Langmuirs of O_2 ($1L = 10^{-6}$ torr-sec). The sharp 2 X 2 LEED pattern of adsorbed oxygen,[3,4] was observed only when the exposure exceeded ~ 20 L.

The SH behavior in Fig. 1 can be explained by a model assuming that

oxygen adsorption obeys Langmuir kinetics and that all adsorption sites are equivalent and noninteracting. The former assumption has been confirmed experimentally by Yates et al.[5] The latter allows us to say that the surface nonlinear susceptibility with oxygen adsorption can be written as

$$\chi^{(2)} = A + B\theta/\theta_s \qquad (1)$$

where θ is the fractional surface coverage of oxygen with respect to Rh surface atoms, θ_s is the saturation value of θ, and A and B are constants. When the desorption rate is negligible, as in our case, the Langmuir adsorption kinetics dictates that the variation of θ with time follows

$$d\theta/dt = Kp(1 - \theta/\theta_s) \qquad (2)$$

where K is a constant accounting for the sticking coefficient and p is the oxygen pressure. Knowing that the SH signal is proportional to $|\chi^{(2)}|^2$, and taking B/A and K/θ_s as adjustable parameters, we can use the solution of Eqs. (1) and (2) to fit the experimental data as shown in Fig. 1. We find $B/A = 1.03\exp(i160°)$ and $K/\theta_s = 0.93/L$. This value of K/θ_s is in good agreement with the value of 0.78/L obtained by Yates et al. considering the typical accuracy of ionization gauges is 25%.[6] The sticking coefficient[7] for O2 to Rh(111) surface atoms is then determined to be ~ 0.5 if O atoms form a (2 × 2) overlayer ($\theta_s = 0.25$)[3] or ~ 1.0 if O atoms from 3 domains of (2 × 1) overlayers ($\theta_s = 0.5$).[4]

The SHG intensity from Rh(111) also decreased dramatically when it

was exposed to CO. This is seen in Fig. 2. The SH falls rapidly during the first Langmuir of exposure and the $(\sqrt{3} \times \sqrt{3})R30°$ LEED pattern corresponding to $\theta = 1/3$[8] appears at ~ 1.2L. The SH decreases less rapidly after 1.2L to a saturation level where the split (2 × 2) LEED pattern forms. The SH is reduced slightly more upon the formation of a sharp (2 × 2) pattern corresponding to the saturation coverage $\theta = \theta_s = 3/4$.[9] The (2 × 2) can only be formed at O_2 pressures higher than ~ 10^{-6} torr.

Previous studies have shown that CO can adsorb to two sites on Rh(111) with the carbon end down. For $\theta \leq 1/3$, CO bonds only to the top sites. For $1/3 < \theta < 3/4$, CO bonds to both the top sites and the bridge sites. The SHG data in Fig. 2 exhibit a rather sudden change in slope at $\theta \sim 1/3$. This suggests that CO bonded to a top site has a different nonlinear polarizability than CO bonded to a bridge site. We can see this effect even more clearly in Fig. 3 in which the SH intensity is plotted as a function of CO fractional surface coverage θ. Indeed, we can fit the data in Fig. 3 by assuming the surface nonlinear susceptibility has the form:

$$\chi^{(2)} = A + B\theta/\theta_s \text{ for } \theta \leq 1/3$$

$$= A + B/3\theta_s + C(\theta - 1/3)/\theta_s \text{ for } 1/3 < \theta < 3/4. \quad (3)$$

From the measured values of the phase and amplitude of the SH field at $\theta = 1/3$ and 3/4, we found $B/A = 1.36 \exp(i157°)$ and $C/A = 0.484\exp(i169°)$. The fit of the data to Eq. (3) is fairly good, as seen in Fig. 3. The result indicates that SHG is site-specific for CO on Rh(111).

Both CO and O_2 adsorption decrease the SH signal with respect to

that from the clean Rh(111) surface. This is presumably because the delocalized electrons of the metal surface which are largely responsible for the SHG are depleted through localization in the chemisorption bond. Contributions to the nonlinear response from CO electronic resonances are expected to be small for SH energies below the lowest-lying CO electronic resonance at ~ 6 eV (λ = 200 nm).[10] That the nonlinear response is dominated by the metal surface electrons, rather than by adsorbates or by localized electrons via charge-transfer resonances, is substantiated by both the similar magnitude of CO- and O-induced changes in SHG and there being almost no difference in the SH response to adsorption with 1.06 μm or 0.532 μm excitation. From these arguments one would expect SH to be as sensitive to other electron acceptors as it is to CO and O_2. In this first measurement we have quite easily obtained sensitivity to 5% of a monolayer.

C. Alkali Metals on Rh(111)

In Section B, we saw that SH decreased when acceptors adsorbed to the Rh metal surface. Here, we consider the complementary case of alkali metal atom adsorption in which electrons are donated to the Rh surface. Next to the adsorption of inert gases, the adsorption of alkali atoms is almost the ideal system for theoretical studies of adsorption. The adsorption of alkali metals on transition metals is also of great practical importance as well. The alkali are known to promote catalytic processes, in particular the dissociation of CO and NO for hydrocarbon and ammonia synthesis, respectively.[2]

In Fig. 4, we show the SH intensity as a function of Na, K, and Cs surface coverage on the Rh(111) at 210K with 1.06 μm excitation. The

coverage was inferred from the dosing rate as the sticking coefficient at such low temperatures is 1 even for several adlayers. For all three alkali, thermal desorption spectroscopy (TDS) showed that the atoms in the second adlayer desorb over a narrow (~ 50K) temperature range at a lower temperature than the atoms in the first layer.[11] The hexagonally close-packed (hcp) saturation monolayer coverage, θ_m, was calibrated by simply noting the SH intensity after the second layer had been removed by heating. The formation of sharp and sudden $(\sqrt{3} \times \sqrt{3})R30°$ and hcp LEED patterns at appropriate coverages indicated that the atoms in the first layer do not form clusters. The appearance of a third sharp TDS peak at coverages just above two monolayer equivalents indicated that at least the atoms in the second layer grow epitaxially. These LEED patterns also allowed us to determine that the saturation coverages are: $\theta_{Na} = 0.5$, $\theta_K = \theta_{Cs} = 0.35$, with respect to the density of Rh atoms ($1.6 \times 10^{15}/cm^2$). The corresponding nearest-neighbor distances for Na, K, and Cs on Rh(111) are 3.74 Å, 4.6 Å, and 4.6 Å, respectively, in agreement with 3.9 Å observed for Na on Ni(111),[11] 4.6 Å for K on Pt(111),[12] and 4.9 Å for Cs on polycrystalline W.[13] All alkali coverages from here on are quoted in units of saturation monolayers, i. e., $\theta = 1$ at saturation for all three alkali.

The rather complex SH behaviors in Fig. 4 naturally fall into 3 regimes: for $\theta < 0.5$ the SH for the three alkali metals are the same, for $0.5 < \theta < 2$ the SH for the three alkali are different but show resonance peaks at $\theta \sim 1$ for Na and K and at ~ 1.8 for Cs, and for $\theta > 2$ the SH for the three alkali are constant.

For $\theta < 0.5$, the SH signal increases presumably because Na atoms donate electrons to the Rh surface. This donation is known to saturate

around 0.5 from work function measurements on alkali metals adsorbed on other transition metals.[14,15] It is then reasonable that the SHG increases for all three alkali and that they also exhibit a saturation behavior at $\theta \sim 0.5$.

However, it is remarkable both that the SH increases so dramatically (10^2 ×) and by roughly the same amount for the three different alkali. If the SH were due only to the free-electron like response of the substrate conduction electrons, the alkali would have to increase the number of conduction electrons 10-fold. This is unlikely as Rh is as good a conductor as Na and must have a considerable number of conduction electrons. If on the other hand, the s-electrons modified the metallic bands and increased the transition probability for interband transitions in resonance with ω or 2ω then the SH[16] would increase faster than the square of the number of conduction electrons. While further work is necessary to resolve the dominant mechanism in this case, it is interesting to note that bulk Rh has such optically-active interband transitions:[17] one at 1.15 eV (near the excitation energy 1.17 eV) arising from the p-like L_6^- bands (band 4) just below the Fermi energy near point L in the Brillouin zone[18] to the unoccupied d-like L_6^+ and $L_4^+L_5^+$ bands (bands 5 and 6) and another at 2.65 eV (near the SH energy 2.33 eV) between bands 3 and 5 along direction Q in the Brillouin zone. The former may be the more important because the adsorbate would increase the p_z (in the (111) direction) character of the p-like L_6^- bulk band which might increase the overlap with the d-like final states[19] while the adsorbate would not greatly perturb states along Q (which extends from L to W and is perpendicular to (111)).

For $\theta < 0.5$, Electron Energy Loss Spectroscopy (EELS) shows a weak

loss peak that moves from a higher energy down to the ns-np transition of the alkali atoms. For Ni(100),[14] the peak moves from 3.5 to 2.3 eV for Na and from 3.5 to 1.5 eV for K where 2.3 and 1.5 eV are close to the Na 3s-3p transition at 2.1 eV and the K 4s-4p transition at 1.6 eV. The shift in energy is reasonable as the loss peak is probably due to transitions from the occupied alkali-transition metal s-d bonding bands and the unoccupied alkali non-bonding (p_x, p_y) bands. At low coverage the s-electron donation is strong and the occupied states in the s-d band are lower in energy than the s-electron of the pure alkali metal. As the s-electron donation saturates at $\theta \sim 0.5$, more electrons occupy states nearly degenerate with the ns level of the pure alkali. For Cs the 6s-6p transition is ~ 1.4 eV.[20] Because 2.3, 1.5, and 1.4 eV are quite different, this loss peak does not seem to affect the 1.06 μm SH response for $\theta < 0.5$.

For $\theta > 0.5$, plasmon studies indicate that the adsorbed alkali atoms begin to interact to form a metallic film.[21,22] Over the range $0.5 < \theta < 2$, the plasmon resonance frequency ω_p increases from one associated with the electron-enhanced transition metal surface to that of the pure alkali metal surface. In our SHG data, this is evidenced by the large change in signal for $\theta > 0.5$. As ω_p passes either the fundamental, ω, or the SH frequency, 2ω, the SH is expected to show some kind of resonance feature.[16] As a function of alkali coverage on Ni(100), U. Jostell[22] and coworkers found the loss energies in eV to be given by:

$$E = 3.0\ \theta^{0.4} \quad \text{for Na} \quad 0.5 < \theta < 2$$

$$E = 2.3\ \theta^{0.8} \quad \text{for K} \quad 0.53 < \theta < 1$$

$$E = 1.7\ \theta^{0.8} \quad \text{for Rb} \quad 0.69 < \theta < 1$$

Since the plasmon resonances are modes of the alkali film only, these energy values should also be valid for alkali on Rh(111). If we assume Cs is similar to Rb, then we expect a resonance between ω_p and 2ω (λ_{SH} = 532nm when $\theta_{Na} = 0.53$, $\theta_K = 1$, $\theta_{Cs} = 1.5$. The last two are in good agreement with the observed SH resonance peaks. The peak for Na may appear at $\theta = 0.9$ because both the plasmon excitation and the interband 3s-3p transition at 2.3 eV contribute to the SH resonance. That the SH resonance peaks have different shapes is reasonable as the linear response as given by the dielectric constant of the three alkali metals are also different near resonance due to interband transitions.[20]

For $\theta > 2.5$ and measured up to 10, the SH behavior with both 1.06 μm and 532 nm excitation changed less than 5%. The absence of change indicates that the SH signal from the alkali metal surface comes from the top 1 or 2 atomic layers. Since the surface plasmon energy does not saturate until ~ 2 monolayers, it is reasonable that the SH still changes until $\theta \sim 2$. The SH may originate from just the top layer of the alkali. This would be completely consistent with the SH being dipole-allowed from the surface region which is made asymmetric by the discontinuity in the incident field (i. e., the first few Thomas-Fermi screening lengths where $\lambda_{TF} \sim 0.7$ for the alkali) and the SH being dipole-forbidden in the lower layers of alkali which have the electronic properties of the centrosymmetric bulk. This clearly illustrates the surface specificity of SHG.

The SH behavior is much more complicated when the excitation wavelength is 532 nm, as shown in Fig. 5. Even for clean Rh the linear dielectric constant at the SH frequency has a large imaginary contribution due to interband transitions and the SH response should also be

effected by these interband transitions. Here, the SH response even for $\theta < 0.5$ is different for the three alkali. This difference is probably due to the differences in the ns-np interband transition energies. Photoemission studies indicate that the occupied Rh(111) d-band is 3.5 eV wide[18] and below the Fermi level which is 5.1 eV below the vacuum level.[23] The ionization energies[24] of Na, K, and Cs are 5.14, 4.34 and 3.89 eV respectively and the np levels should be at 3.04, 2.74 and 2.49 eV with respect to the vacuum. Assuming the s-d band for low alkali coverage is initially ~ 1 eV below the Fermi level then the d-ns $\rightarrow$ np transition energies should be 3.1, 3.4 and 3.6 eV. As θ increases to 0.5 one expects these values to move toward the energies in the pure alkali: 2.1, 1.6 and 1.4 eV respectively, causing a resonant enhancement in SH as they pass through the optical excitation energy 2.33 eV (λ_{exc} = 532 nm). One would expect resonance to be reached only at $\theta \sim 0.4$ for Na but around $\theta \sim 0.25$ for K and Cs. This is in fact what we see. The decrease in SH for K and Cs from $\theta \sim 0.25$ to $\theta \sim 0.5$ is probably due to the change in sign of the SH ploarizability as the interband transition energy changes from greater than to less than the excitation energy.

For $0.5 < \theta < 2$, the alkali film plasmon energies are expected to go through a resonance at the fundamental (λ = 532 nm) at $\theta_{Na} \sim 0.53$, $\theta_K \sim 1$ and $\theta_{Cs} \sim 1.5$ as discussed above. The sharp dip in the SH for Na at $\theta \sim 0.9$ exactly where the resonant enhancement occurs for the 1.06 μm excitation data indicates that the former is associated with a resonance at 532 nm which decreases the SH when the plasmon energy exceeds the fundamental. A slight feature at $\theta_K \sim 1$ is also probably due to a resonance at the fundamental. The increases in SH for $\theta_{Na} > 1$, $\theta_K > 1$ and $\theta_{Cs} > 0.5$ are all due to resonant enhancement as the plasmon energy

approaches but never gets to the SH energy. The resonant features at θ ~ 1.7 may be due to the second alkali layer absorbing SH photons generated from the underlying Rh-alkali interface. Since, in the 532 nm excitation case, the Rh SH field contribution is fairly considerable (1/3 that of K and ~ 1/10 that of Na and Cs), its absence may be detectable.

The dramatic changes in SHG for $\theta > 0.5$ are quite similar to those observed in an earlier study of SHG from Na on Ge.[25] The signals from the alkali metal surfaces are all much (between 10^2 and 10^4 times) larger than the signals from the clean Rh surface. This is reasonable because the alkali SH is resonantly enhanced by the plasmon excitations of the alkali film. A similar enhancement would be expected for the clean Rh surface signal if the SH energy were near 9 eV, the plasmon resonance for Rh. For $\theta > 0.5$, we can easily distinguish 1% of an alkali monolayer.

In the low coverage regime our 1.06 μm data shows that extremely small dosages of the alkali can perturb the band structure to enhance interband transitions, and that SH will be extremely sensitive to interband transitions near resonant with either the fundamental or SH frequencies. Similar sensitivity has been reported in a study of SH from Na dosed on a Cu film in UHV[26] in which a 35% increase in surface SH was observed with only 1% of an alkali monolayer.

D. O_2 and CO on Alkali-Metal-Covered Rh(111)

Calibration curves for the SH intensity vs. alkali coverage (Figs. 4 and 5) allowed us to prepare well-characterized and reproducible alkali layers on which to study the adsorption of O_2 and CO to alkali-covered

Rh(111). As mentioned before, adsorption to alkali-promoted catalytic surfaces is an active field of surface science research.[2]

In Fig. 6 we show the adsorption of O_2 to the Rh(111) surface predosed with enough Cs to make a sharp $(\sqrt{3} \times \sqrt{3})R30°$ LEED pattern (θ = 0.95, $n_{Cs} = 5.3 \times 10^{14}/cm^2$) at room temperature. We see the SH intensity decrease dramatically to zero at ~ 0.5 Langmuirs and approach saturation at 1.2 Langmuirs. In analogy to the analysis for O_2 adsorption on clean Rh(111) presented in Section B, we can fit the data quite well by assuming Langmuir kinetics and that the SH intensity is given by $|A + B\theta/\theta_s|^2$ where θ_s is the saturation coverage. Because the signal goes to zero, B/A is real and the SH saturation intensity at ~ 1.2 L dictates that B/A = -1.246. The best fit to the rest of the curve occurs for $K/\theta_s = 3.7 \pm 0.1$/Langmuir. We note that the data cannot be fit as well with a coverage determined with adsorption probability proportional to pairs of unoccupied sites, i.e.,

$$d(\theta)/dt = KP\ (1-\theta/\theta_s)^2.$$

Langmuir kinetics would then suggest that the O_2 molecule is dissociated at an unoccupied site leaving a stable Cs oxide and a mobile O atom that diffuses to an unoccupied adsorption site. As Cs_2O overlayers are most likely to form,[27] the sticking coefficient for O_2 molecules to adsorption sites with density 1/4 of the Cs monolayer density is ~ 0.75.

A similar adsorption curve was observed for 10 Langmuirs of O_2 exposure to Rh(111) with a $(\sqrt{3} \times \sqrt{3})R30°$ (θ = 0.95) K overlayer. Studies on Pt(111) indicate a stable K_2O layer is formed.[28] In addition we observed the SH during thermal desorption of O_2 or K_2O from the surface.

We observed the SH reverse back along the O_2 adsorption curve as the temperature was increased to 900K with rapid changes occuring between 400 and 500K and then again for T > 850K. This indicated that only O_2 desorbs below 900K and that at least two species of K_2O exist on the surface with one unstable at ~ 450K and another at ~ 850K. From 900K to 1070K the SH showed that both K and O desorb and the SH level indicative of the clean Rh sample was regained. The existence of several O_2 thermal desorption peaks at temperatures lower than the single K desorption peak has been observed for K_2O on Pt(111).[28]

We have also studied co-adsorption of CO and Na on Rh(111). Figure 7 shows the SHG during CO exposure to and thermal desorption from the Rh surface predeposited with θ ~ 0.6 of Na. The dosage curve in Fig. 7a has a nearly zero initial slope, in contrast to the cases of adsorption on clean Rh seen in Fig. 2. This suggests that the presence of Na must have significantly influenced the adsorption of CO. The fast drop in SHG from 1 to 2 L and the slow saturation after 2 L are similar to the SHG behavior observed for CO exposure to clean Rh. CO adsorption during the first Langmuir of exposure is different presumably because the Na layer can replenish the Rh surface charge that is withdrawn by low coverages of CO.

Electron Energy Loss Spectroscopy data indicates that CO binds initially to bridge sites and then to top sites on the alkali-promoted Rh(111) and Pt(111) surfaces.[12,29] We believe the kink in SH at 2 L is due to bridge-site adsorption saturating and top-site adsorption beginning. That the SH does not saturate until about 8 L indicates the adsorption at the proposed "top-sites" also does not saturate until 8 L. One would not expect such a dramatic kink for adsorption at one site

with continuously changing bonding strength.

After the CO coverage on Na/Rh(111) was allowed to saturate, the SHG was again used to monitor the subsequent thermal desorption at a rate (~ 15°C/s), as seen in Fig. 7b. The curve shows a desorption onset temperature of ~ 200°C, which is ~ 125°C higher than that for CO on clean Rh(111), indicating a stronger bonding of CO to the surface in the presence of Na. A similar increase in desorption onset temperature was observed for CO on K/Rh(111).[29] The SH increases rapidly from 400°C to 450°C indicating the desorption of bridge-site adsorbed CO. A distinguishable plateau (see arrow) appears between 450 and 520°C in the desorption curve followed by another rise in the the SH signal to a value consistent with only Na on Rh(111). This suggests the existence of another CO state on Rh which desorbs starting around 520°C. Similar adsorption states have been distinguished in other work on Rh(111),[29] Pt(111)[12], Fe(110)[30], and Ni(100)[31] surfaces. Preliminary evidence indicates that the CO molecules desorbed between 450 and 520°C had been dissociated on the Rh surface and that those desorbed below 400°C had not. This would indicate that this third CO state was one which dissociated CO either immediately on adsorption from the gas or upon heating. In addition, the SH signal displayed in Fig. 7b shows that a large number of Na atoms desorb simultaneously or immediately after the last CO molecules leave the surface. By retracing the SH level along the Na dosage curve (shown on a linear scale in Fig. 8), one finds that the Na coverage drops from θ = 0.6 to 0.26 by 575°C and decreases slowly to θ = 0 by ~ 800°C where the SHG returns to the level of the clean Rh surface. Na on Rh(111) usually desorbs in a broad peak between 100° and 900°C. It is clear that the CO molecules stabilize the Na atoms on the

surface and that once the CO leaves, all the Na that should have normally desorbed by ~ 550°C will desorb.

In another experiment, we found that with a Na coverage of θ ~ 1.0 on Rh(111), the CO adsorption on Na/Rh(111) was greatly reduced. The SH signal drops only 20% for 1200 L CO exposure as shown in Fig. 9. With a Na coverage of θ ~ 1.3, less than 2 % change in SHG could be observed for 600 L CO exposure. These results indicate that CO adsorption on Rh is effectively blocked by the Na film, and that the interaction of CO with Na must be very weak. Similar results have been observed on CO/K/Pt(111)[12] and CO/K/Rh(111)[29].

E. Benzene and Pyridine on Rh(111)

The bonding of aromatic hydrocarbons and their catalytic conversion to other organic molecules on transition metal surfaces are actively studied areas of surface science with obvious industrial applications.[2] EELS spectra of aromatic hydrocarbons adsorbed to Ag(111)[32] show relatively unshifted free molecule $\pi \rightarrow \pi^*$ excitations (~ 4 - 5 eV) as well as a band at lower-lying energy (~2 - 2.5 eV) corresponding to a new excitation of the metal-molecule system, the so-called charge- transfer (CT) state. The molecular $\pi \rightarrow \pi^*$ transitions are not always observed. Evidence indicates[10] the $\pi \rightarrow \pi^*$ transition of a molecule adsorbed flat against a metal surface may be broadened and its intensity reduced when the π or π^* levels interact strongly with the substrate. The CT band was not observed for benzene on Ag(111) but was observed for pyridine and pyrazine and was believed to come from transitions between the Ag (sp-band) to the unoccupied (π^*) levels of the aromatics.[32] The CT band could also come from transitions between the filled states of the

molecule and the unoccupied metallic states. On Ni(111)[19] benzene and pyridine induce a low-lying optical absorption at the surface at ~ 4.5 eV. However, because this same absorption peak is also seen for CO, O_2, and other adsorbates the absorption appears to be due to an adsorbate-induced increase in an interband transition of the metal substrate at ~ 4.5 eV.

From what we have seen for adsorbed alkali atoms, we expect SHG to be sensitive to the presence of adsorbates that change the probability of interband transitions nearly resonant with the fundamental excitation or SH frequencies. SH excited with 1.06 μm radiation with its SH photon energy at 2.33 eV should then be sensitive to CT states. The SH excited with 532 nm radiation with its SH photon energy at 4.66 eV should be sensitive to aromatic $\pi \rightarrow \pi^*$ excitations. SHG at either excitation wavelength should be sensitive to appropriate changes in the interband transitions of the substrate.

In Figs. 10 and 11 we show the SH intensity during the room temperature adsorption of benzene and pyridine on the Rh(111) surface using 1.06 μm and 532 nm excitation. The exposures have not been corrected for ionization gauge sensitivity. One notices immediately that the 1.06 μm and 532 nm excitation SH curves differ from each other. This difference is no doubt due to the different fundamental or SH frequencies probing different interband transitions.

For benzene, the 532 nm curve shows a distinct discontinuity in slope at ~ 0.68 L. The change in the 1.06 μm SH curve assures us that benzene adsorption has occured even though the 532 nm SH remains at the "clean Rh" level. After 0.68 L the 532 nm curve decreases smoothly while the 1.06 μm curve increases to a saturation value at the "clean

Rh" level. The discontinuity at ~ 0.68 L indicates the onset of binding at a second site. Both SH curves are saturated by 3.8 L suggesting the adsorption is saturated at this exposure.

The SH behavior under pyridine adsorption is oddly complementary to that of benzene. The 1.06 μm pyridine SH curve is similar to benzene's but the 532 nm curve has a smooth decreasing portion at low coverages (rather than at higher coverages as for benzene), and the SH saturates for exposures greater than ~ 3.5 L even though the 1.06 μm curve indicates additional pyridine adsorption occurs until 7 to 10 L. The existence of a portion of the 532 nm SH curve that is insensitive to adsorption indicates the onset of pyridine being bound to the surface in a second state at ~ 3.5 L.

HREELS data indeed indicates benzene is adsorbed on Rh(111) in two states. B. E. Koel[33] find that the second state commences adsorption after ~ 2 L, while we find the second state for benzene begins at 0.68 L. Perhaps SHG is more sensitive to the second state than is HREELS, thereby making the states onset more easily recognizable by SHG. Koel et al[33] find that the low coverage state is adsorbed flat either at the top or fcc hollow site (hollow site without a second-layer atom directly below center) while the second state of benzene is adsorbed flat at the hcp hollow site (hollow site with a second-layer atom directly below center. The absence of change in the 532 nm-excited SHG for the first site may be due to the strong benzene-metal bond broadening and reducing the $\pi \rightarrow \pi^*$ transition. The strength of adsorption at the first site is evidenced by thermal desorption studies in which benzene which is adsorbed at the first site is completely dehydrogenated when heated while some fraction of the benzene adsorbed at the second site may desorb

molecularly. The bonding to the second site is less strong and a change in SH due to increased $\pi \rightarrow \pi^*$ transition probability is observed.

Preliminary HREELS results on pyridine adsorbed to Rh(111)[34] also indicate there are two adsorption states. The pyridine molecule appears to be adsorbed with it ring parallel to the surface as for benzene but the first low coverage adsorption site is the hcp hollow site and the second adsorption site is either the fcc hollow or top site (opposite to the case for benzene). The 532 nm-excitation SHG is indeed consistent with the two adsorption states commencing in the opposite order for pyridine than for benzene and for adsorption at the first site causing the increased SH sensitivity to the $\pi \rightarrow \pi^*$ transition. For both benzene and pyridine, the $\pi \rightarrow \pi^*$ assignment to the rapidly decreasing portion of the SH curve would require measurements of SH at more frequencies to identify the location of the resonance. It could be due to a molecule-enhanced Rh interband transition rather than a molecule resonance.

The interpretation of the 1.06 μm-excitation SHG curves is not clear at this time. The similarity in the benzene and pyridine curves despite the two different adsorption site preferences, suggest that the SH dip to ~ 0.8 the level of the clean surface may be due to adsorbate-induced changes in a Rh interband transition probability where the transition is nearly resonant with either the fundamental or SH frequency. A resonance with the SH (i. e., 2.33 eV) is unlikely because a corresponding resonance in the 532 nm-excited SH curve is not observed. Evidence for adsorbate-induced modification of a Rh interband transition probability near 1.17 eV has already been presented to explain the effect of alkali adsorption on the 1.17 eV-excited SH from Rh (Section C).

In Fig. 12 we show the SH from the Rh(111) surface predosed with 30

L of benzene as we thermally-induced the dehydrogenation of the benzene. Previous studies[33] have shown that for a 30 L (saturation monolayer) overlayer, approximately 18% of the benzene desorbs molecularly around 395K with a width of 70K. The benzene ring is broken to hydrocarbon fragments at 473K with a width of 50K. H_2 is slowly evolved from the hydrocarbon fragments as the temperature is increased to 750K. At 750K only a carbon layer remains on the surface. We see in Fig. 12 that as the temperature is increased past 400K the SH remains constant. This indicates that the benzene that is molecularly-desorbed is initially bound in a way that does not affect the SH. Around 500K, we see a rise in SH level corresponding to the breaking of the aromatic ring into hydrocarbon fragments. From 500K to 700K, when H_2 evolves from the surface, the SH remains constant indicating that these hydrocarbon fragments have the same nonlinear response on the Rh surface as adsorbed carbon alone. This is reasonable as calculations on carbon atoms adsorbed to Rh(111)[35] indicate that the metal-carbon bonding orbitals are 3-fold combinations of C2s, $C2p_{x,y}$, and Rh orbitals which are independent of whether or not the nonbonding $C2p_z$ orbital is unoccupied or is bonded with hydrogen. Thus, the SH response which is determined by the metal-C bonding is independent of the carbon coordination to hydrogen. The presence of C-atoms like the presence of O-atoms (considered in Section B) lowers the SH from the Rh by localizing metal orbitals in the chemisorption bond. The rapid increase in SH in Fig. 12 between 800 and 1000K is due to the carbon atoms diffusing into the bulk of the Rh sample. By 1500K, the Rh(111) surface is clean and the SH level for clean Rh is regained.

F. Summary

We have demonstrated that the results of surface SHG studies correlate very well with those obtained with conventional surface probes by studying a variety of well-characterized, catalytically interesting surface systems. SHG had several unique features which made it a useful complement to existing surface tools. Because of SHG's fast time response, all experiments were performed during continuous processes on the order of 1 minute. Because laser radiation at appropriate intensities is non-destructive, SHG can be used to great advantage when electron probes tend to dissociate adsorbates on the surface. In addition, the surface sensitivity of SHG allows it to be used even during high pressure doses of gas (10^{-4} torr) when the operation of electron guns and filaments could be detrimental to the equipment and to the experimental results.

We have found that SHG is extremely sensitive to adsorbates that perturb the electronic properties of the surface -- either electron acceptors, electron donors, or adsorbates that alter the band structure of the substrate surface. We have used SHG to distinguish adsorption at different sites and to even monitor changes in surface composition during thermal desorption and dehydrogenation processes. This work clears the way for the successful application of SHG to other systesm of interest in surface science and catalysis.

References

1. T. F. Heinz, C. K. Chen, D. Ricard, and Y. R. Shen, Phys. Rev. Lett. 48, 478 (1981).
2. See, for example, G. A. Somorjai, Chemistry in Two Dimensions: Surfaces (Cornell Univ. Press, Ithaca, NY, 1981).
3. D. G. Castner, B. A. Sexton, and G. A. Somorjai, Surf. Sci. 71, 519 (1978).
4. D. G. Castner and G. A. Somorjai, Appl. Surf. Sci. 6, 29 (1980).
5. J. T. Yates, P. A. Thiel, and W. H. Weinberg, Surf. Sci. 82, 45 (1979).
6. J. F. O'Hanlon, A User's Guide to Vacuum Technology, (J. Wiley and Sons, New York, 1980), p. 71.
7. The sticking coefficient α is given by $K = (\alpha/n_s)(RT/2\pi M_g)^{1/2} n_g$, where n_s is the surface density of adsorption sites, R is the gas constant, T is the temperature in K, M_g is the molecular weight of the gas, and n_g is the density of the gas.
8. L. H. Dubois and G. A. Somorjai, Surf. Sci. 91, 514 (1980).
9. M. A. Van Hove, R. J. Koestner, and G. A. Somorjai, Phys. Rev. Lett. 50, 903 (1982) and references therein.
10. Ph. Avouris and J. Demuth, "Electron Energy Loss Spectroscopy in the Study of Surfaces," to appear in Annual Reviews of Physical Chemistry, Vol. 35, 1984.
11. R. L. Gerlach and T. N. Rhodin, Surf. Sci. 19, 403 (1970).
12. J. E. Crowell, E. L. Garfunkel, and G. A. Somorjai, Surf. Sci. 121, 303 (1982).
13. J. B. Taylor and I. Langmuir, Phys. Rev. 44, 423 (1933).

14. S. A. Andersson and U. Jostell, Surf. Sci. 46, 625 (1974).

15. G. Broden and H. P. Bonzel, Surf. Sci. 84, 106 (1979).

16. J. R. Bower, Phys. Rev. B14, 2427 (1976).

17. J. H. Weaver, C. G. Olson, and D. W. Lynch, Phys. Rev. B15, 4115 (1977).

18. For Rh band structure: B. Borstel, W. Braun, M. Neumann, and G. Seitz, Phys. Stat. Solidi B 95, 453 (1979).

19. In analogy with the model proposed for adsorption on Ni(111): H. J. Robota, R. M. Whitmore, and C. B. Harris, J. Chem. Phys. 76, 1692 (1982).

20. For Cs: N. V. Smith, Phys. Rev. B2, 2840 (1970); for Na and K: N. V. Smith, Phys. Rev. 183, 634 (1969).

21. S. A. Lindgren and L. Walldén, Phys. Rev. B 22, 5969 (1980).

22. U. Jostell, Surf. Sci. 82, 333 (1979).

23. W. Braun, M. Neumann, M. Iwan, and E. E. Koch, Phys. Stat. Solidi B 90, 525 (1978).

24. C. Kittel, Introduction to Solid State Physics, 5th Edition (J. Wiley, New York, 1976), p. 75.

25. J. M. Chen, J. R. Bower, C. S. Wang, and C. H. Lee, Optics Comm. 9, 132 (1973).

26. J. M. Chen, J. R. Bower, and C. S. Wang, Jpn. J. Appl. Phys. Suppl. 2, Pt. 2, 711 (1974). This conference proceeding is not easy to get. For summary see ref. 16.

27. C. A. Papageorgopoulos and J.-L. Desplat, Surf. Sci. 92, 119 (1980).

28. E. L. Garfunkel and G. A. Somorjai, Surf. Sci. 115, 441 (1982).

29. study of CO/K/Rh(111): J. E. Crowell, E. L. Garfunkel, and G. A.

Somorjai, to be published.

30. G. Broden, G. Gafner, and H. P. Bonzel, Surf. Sci. 84, 295 (1979).

31. M. P. Kiskinova, Surf. Sci. 111, 584 (1981).

32. Ph. Avouris and J. E. Demuth, J. Chem. Phys. 75, 4783 (1981).

33. B. E. Koel, J. E. Crowell, C. M. Mate, and G. A. Somorjai, "An HREELS Study of the Surface Structure of Benzene Adsorbed on the Rh(111) Crystal Face," submitted to J. Phys. Chem.

34. C. M. Mate, Dept. of Chemistry, U. C. Berkeley, private communication.

35. P. J. Feibelman, Phys. Rev. B26, 5347 (1982).

Figure Captions

Fig. 1 Second harmonic signal from the Rh(111) surface during O_2 exposure. (___), experimental result; (---), theoretical fit.

Fig. 2 SH intensity from the Rh(111) surface as a function of CO exposure. LEED patterns were observed at the exposures noted.

Fig. 3 Second harmonic output from the Rh(111) surface versus CO fractional coverage, θ. (o), experimental points; (___), theoreti-

Fig. 4 SH intensity vs. alkali coverage for Na, K, and Cs deposited on the Rh(111) surface using an excitation wavelength of 1.06 μm. Note the SH is plotted on a log scale.

Fig. 5 Same as in Fig. 4 except the excitation wavelength was 532 nm.

Fig. 6 SH intensity from a Rh(111) surface prodosed with 0.95 of a saturation monolayer of Cs vs. O_2 exposure.

Fig. 7 SH intensity from Rh(111) surface predeposited with 0.6 monolayer of Na, a) as the surface was exposed to CO and (b) the thermal desorption process from the Na/Rh(111) sample in (a) after 15 L of CO exposure.

Fig. 8 Detail of the SH intensity vs. Na coverage using 532 nm excitation. During thermal desorption of Na in Fig. 7b, the SH retraces the curve as indicated by the temperature noted.

Fig. 9 SH intensity from Rh(111) surface predeposited with 1.0 monolayer of Na as the surface was exposed to CO.

Fig. 10 SH intensity from Rh(111) surface vs. benzene exposure for 1.06 μm and 532 nm excitation. Smooth curve has been drawn as a guide to the eye.

Fig. 11 Same as in Fig. 10 but vs. pyridine exposure.

Fig. 12 SH intensity from Rh(111) surface predeposited with 30 Langmuir of benzene as the sample is heated and the benzene is dehydrogenated.

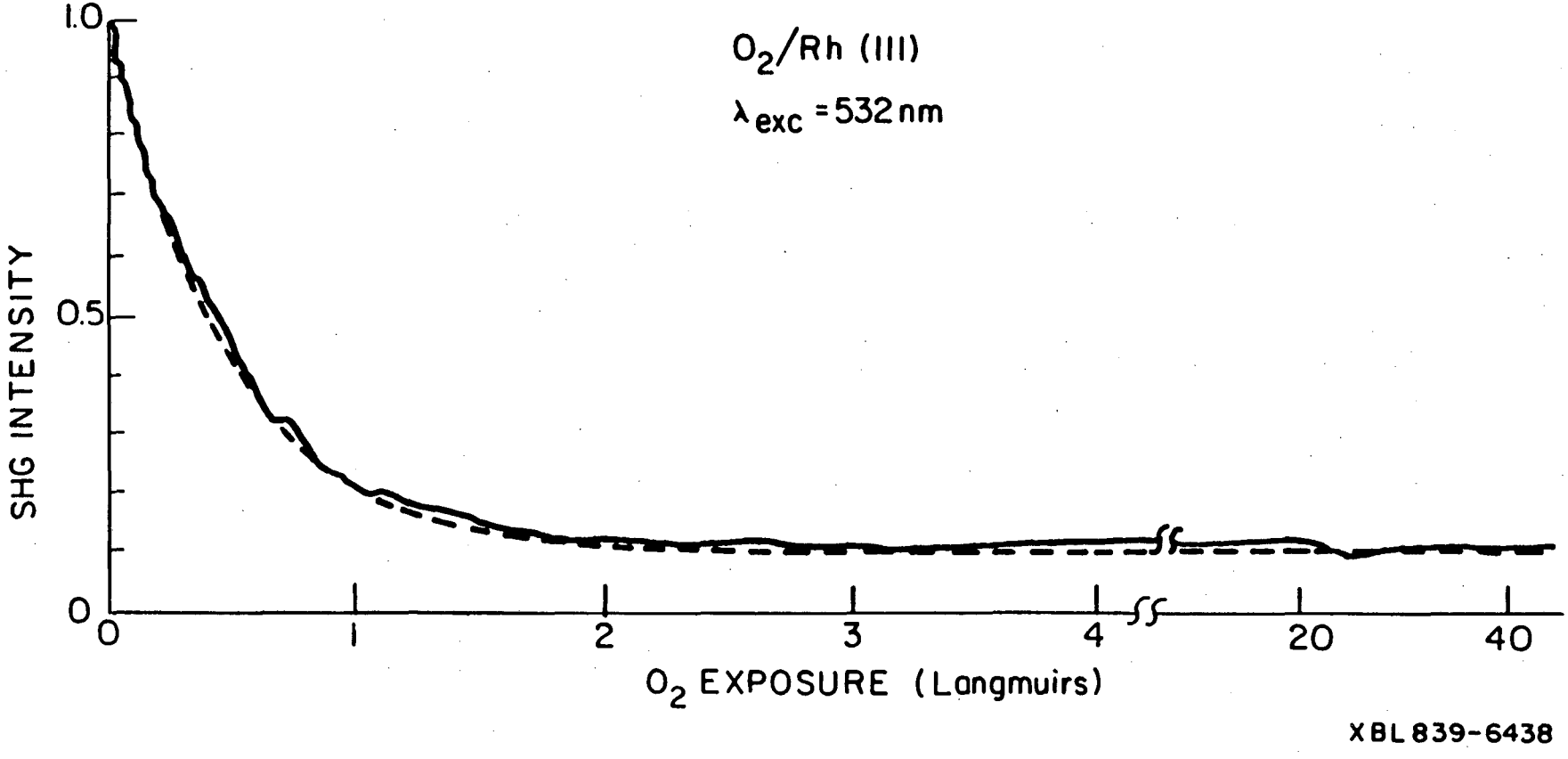
1.0
0.5
0
SHG INTENSITY
O_2/Rh (111)
λ_{exc} = 532 nm
0
1
2
3
4
20
40
O_2 EXPOSURE (Langmuirs)
XBL 839-6438

Fig. 1

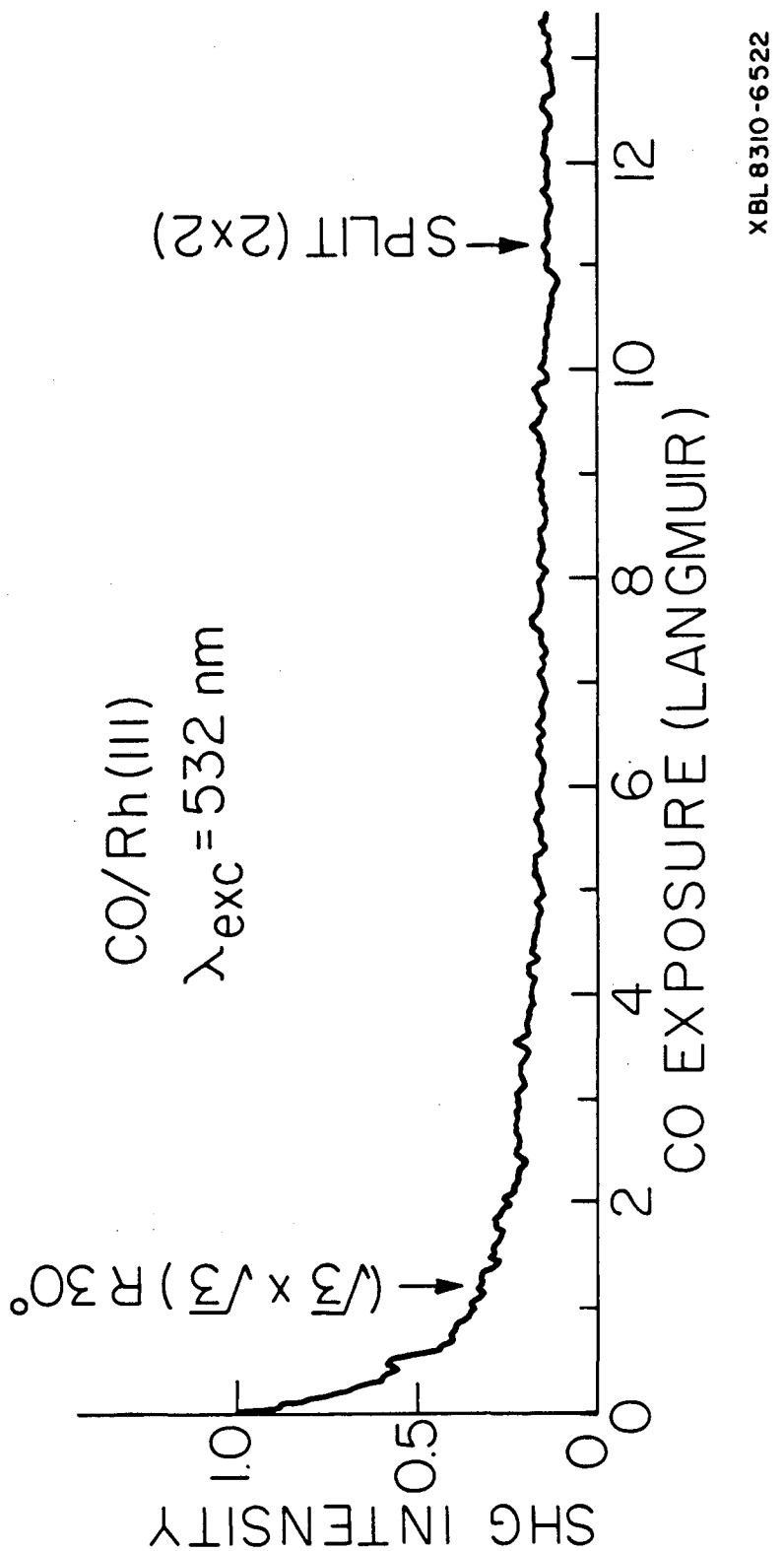
SHG INTENSITY
0.0
0.5
1.0
0
2
4
6
8
10
12
CO EXPOSURE (LANGMUIR)
CO/Rh(111)
λ_{exc} = 532 nm
(√3 x √3) R 30°
SPLIT (2x2)
XBL 8310-6522

Fig. 2

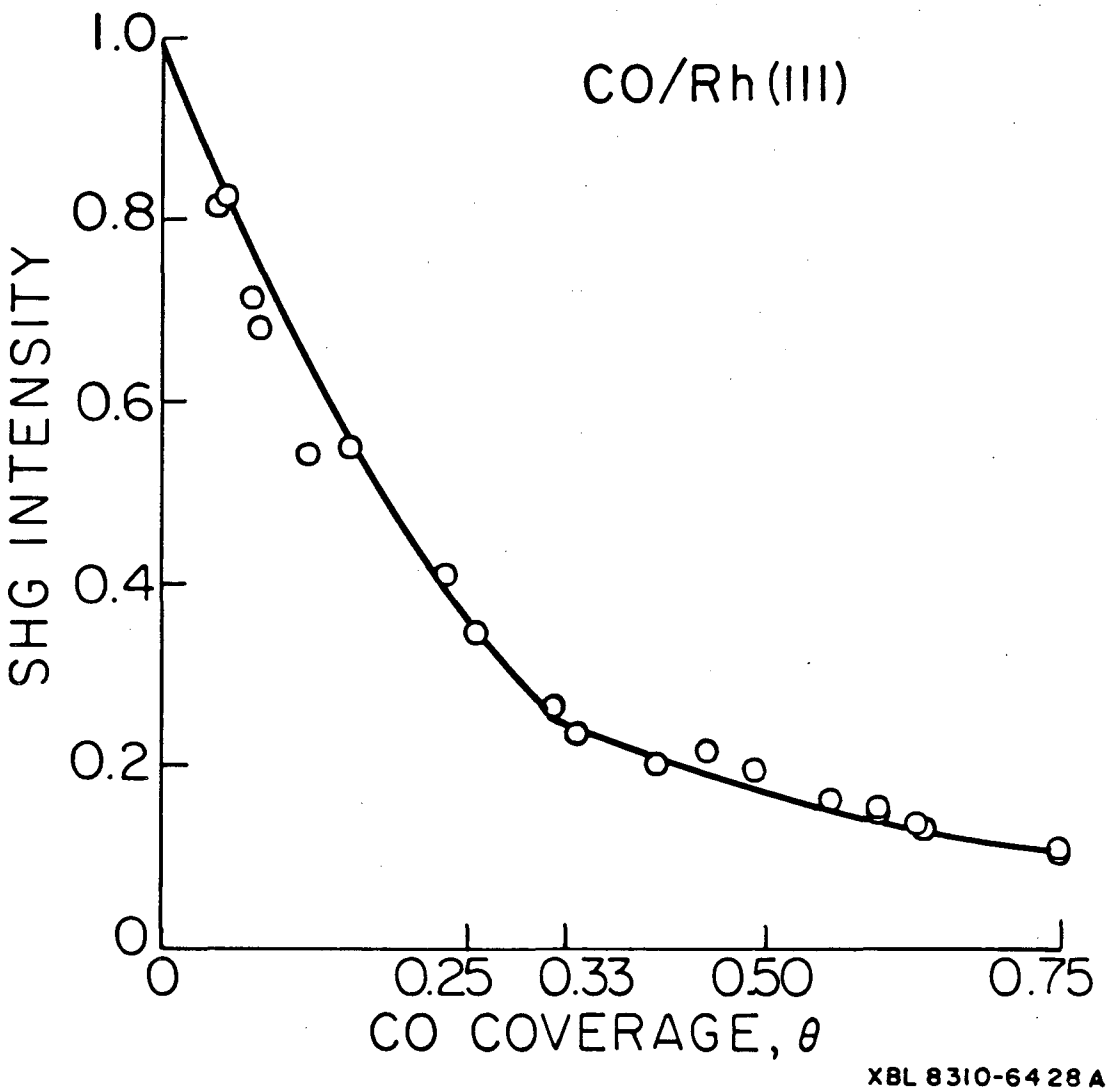
CO/Rh(111)
SHG INTENSITY
1.0
0.8
0.6
0.4
0.2
0
0
0.25
0.33
0.50
0.75
CO COVERAGE, θ
XBL 8310-6428A

Fig. 3

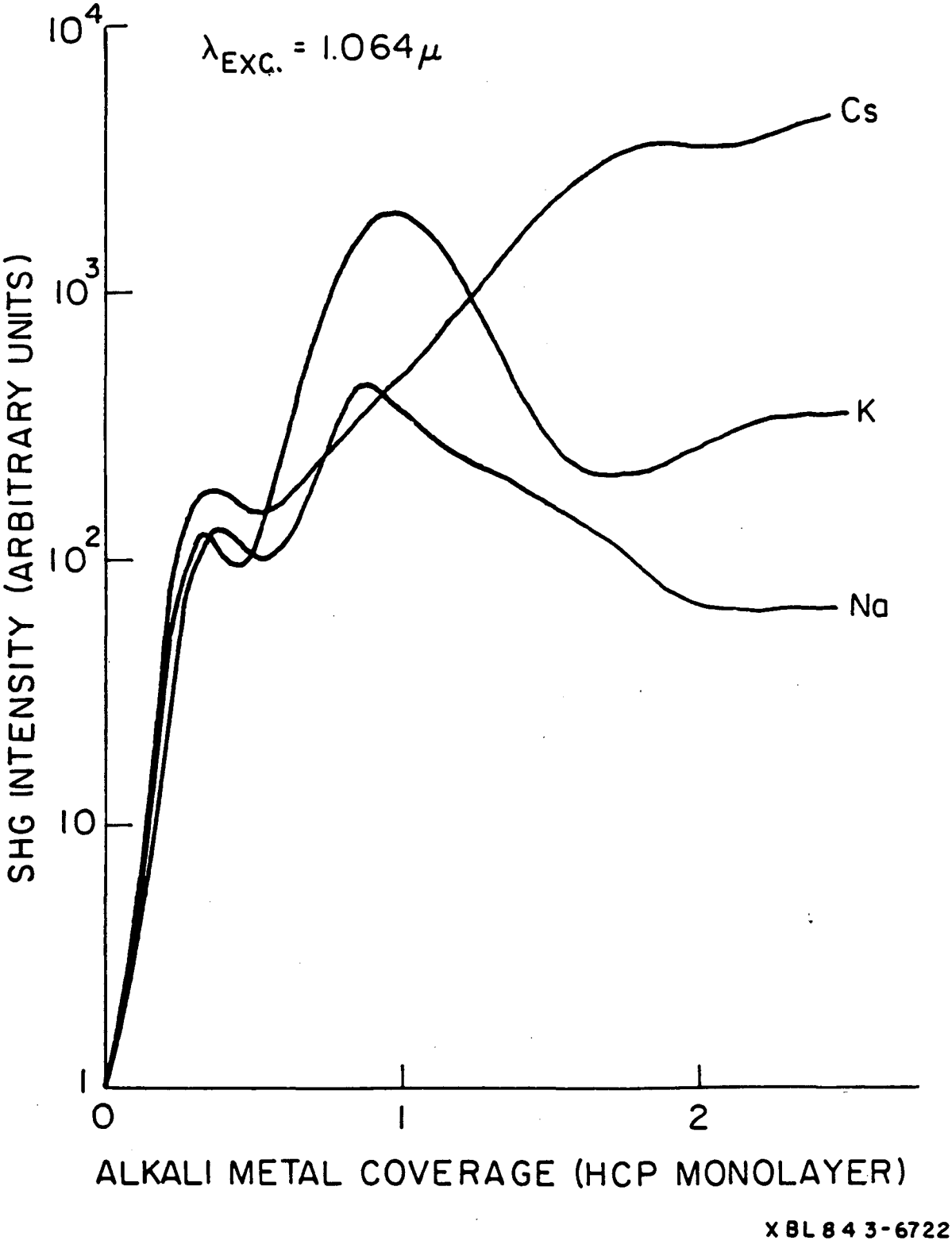
10^4
$\lambda_{EXC.} = 1.064\mu$
Cs
K
Na
10^3
10^2
10
1
SHG INTENSITY (ARBITRARY UNITS)
0
1
2
ALKALI METAL COVERAGE (HCP MONOLAYER)
XBL843-6722

Fig. 4

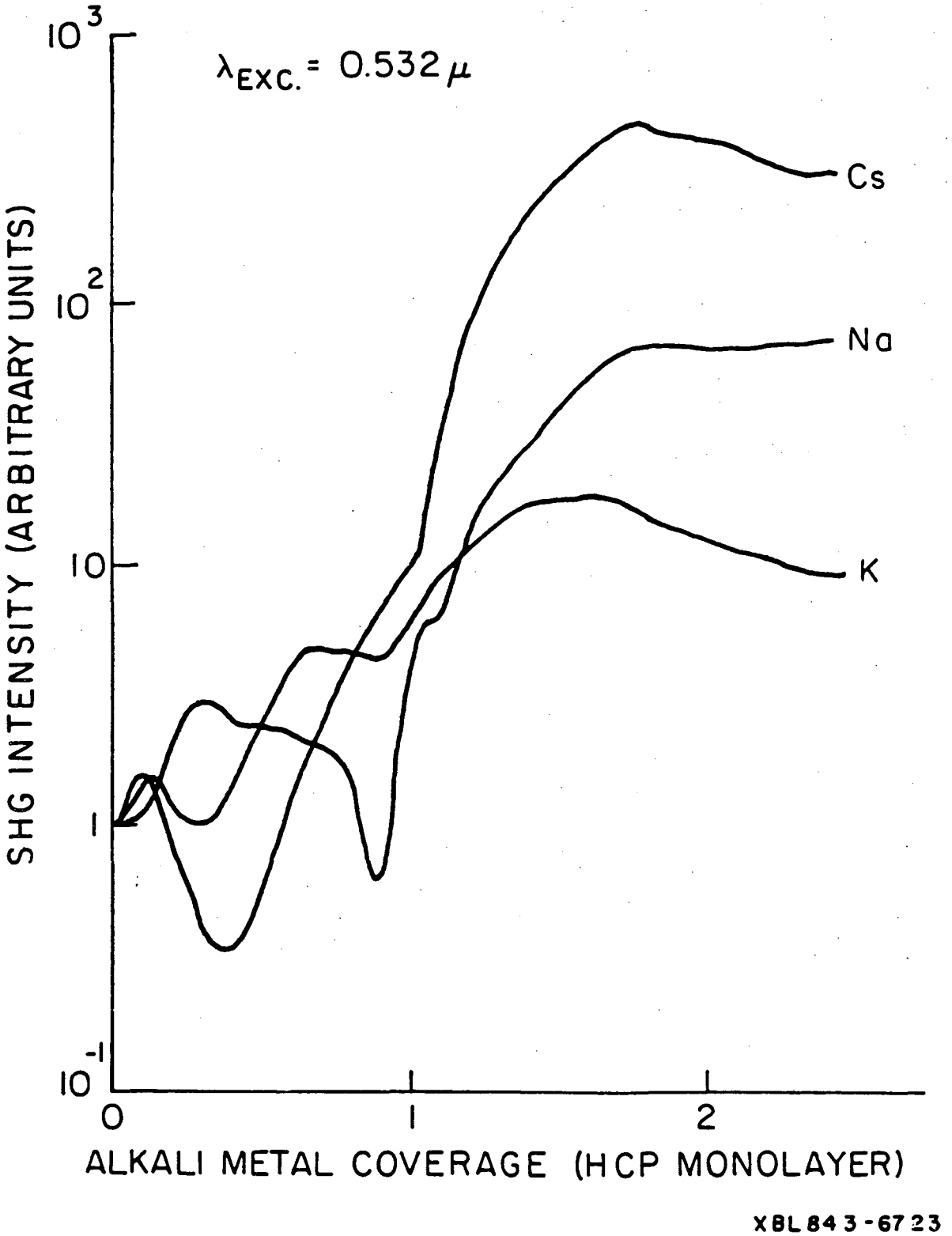
$\lambda_{EXC.} = 0.532\,\mu$
Cs
Na
K
SHG INTENSITY (ARBITRARY UNITS)
10^3
10^2
10
1
10^{-1}
0
1
2
ALKALI METAL COVERAGE (HCP MONOLAYER)
XBL843-6723

Fig. 5

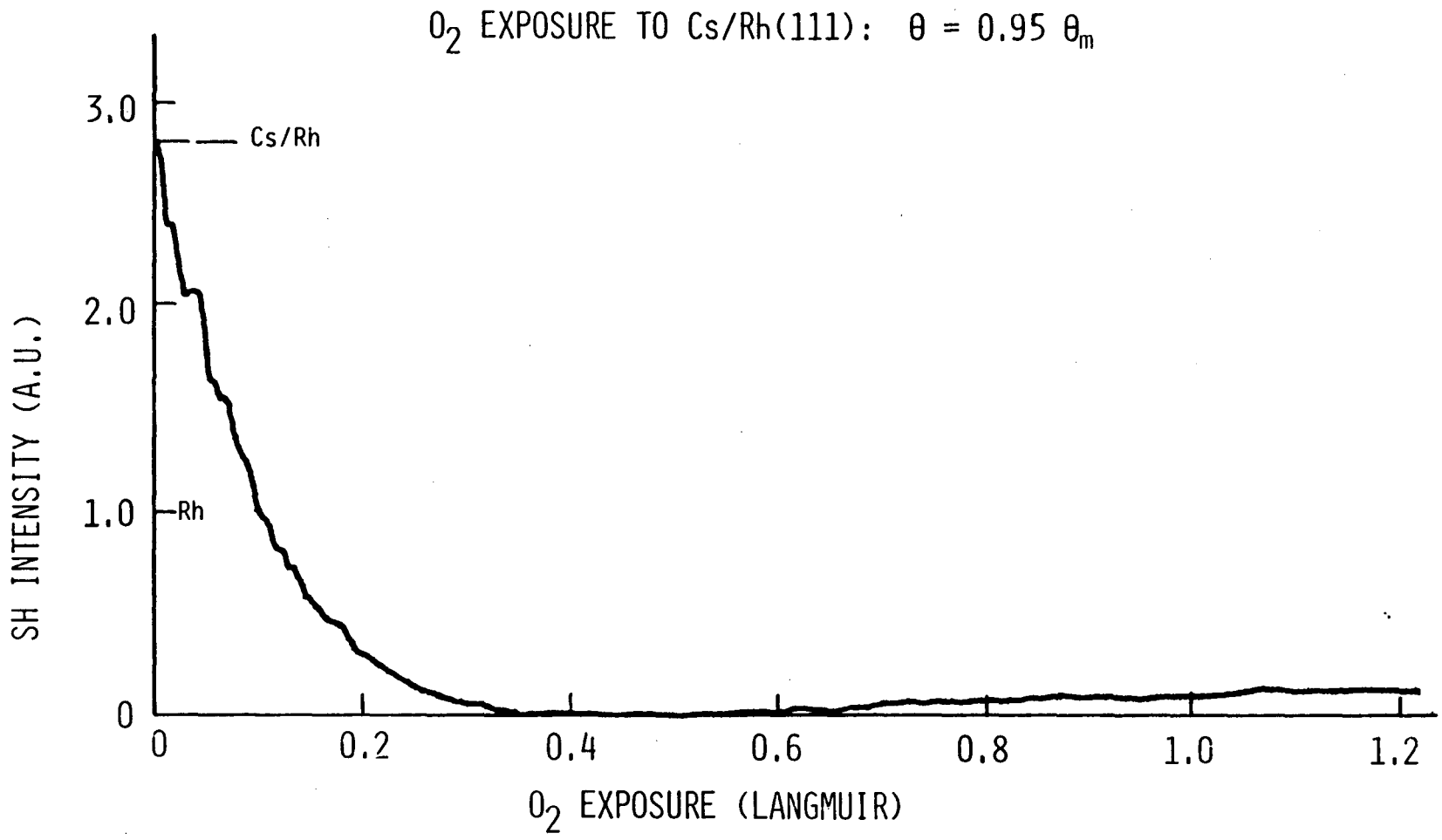

XBL 844-6871

Fig. 6

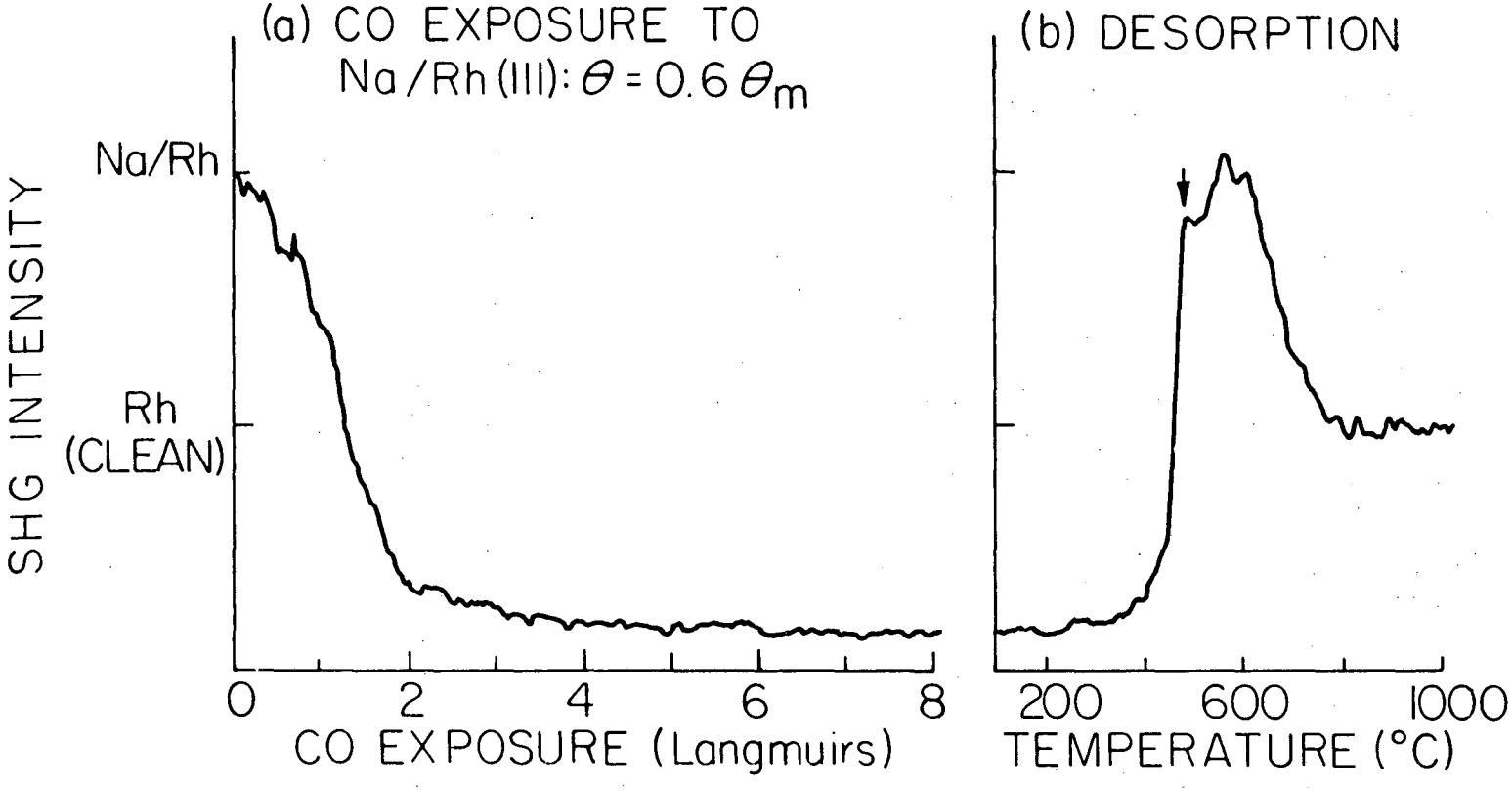

XBL 8310-6427A

Fig. 7

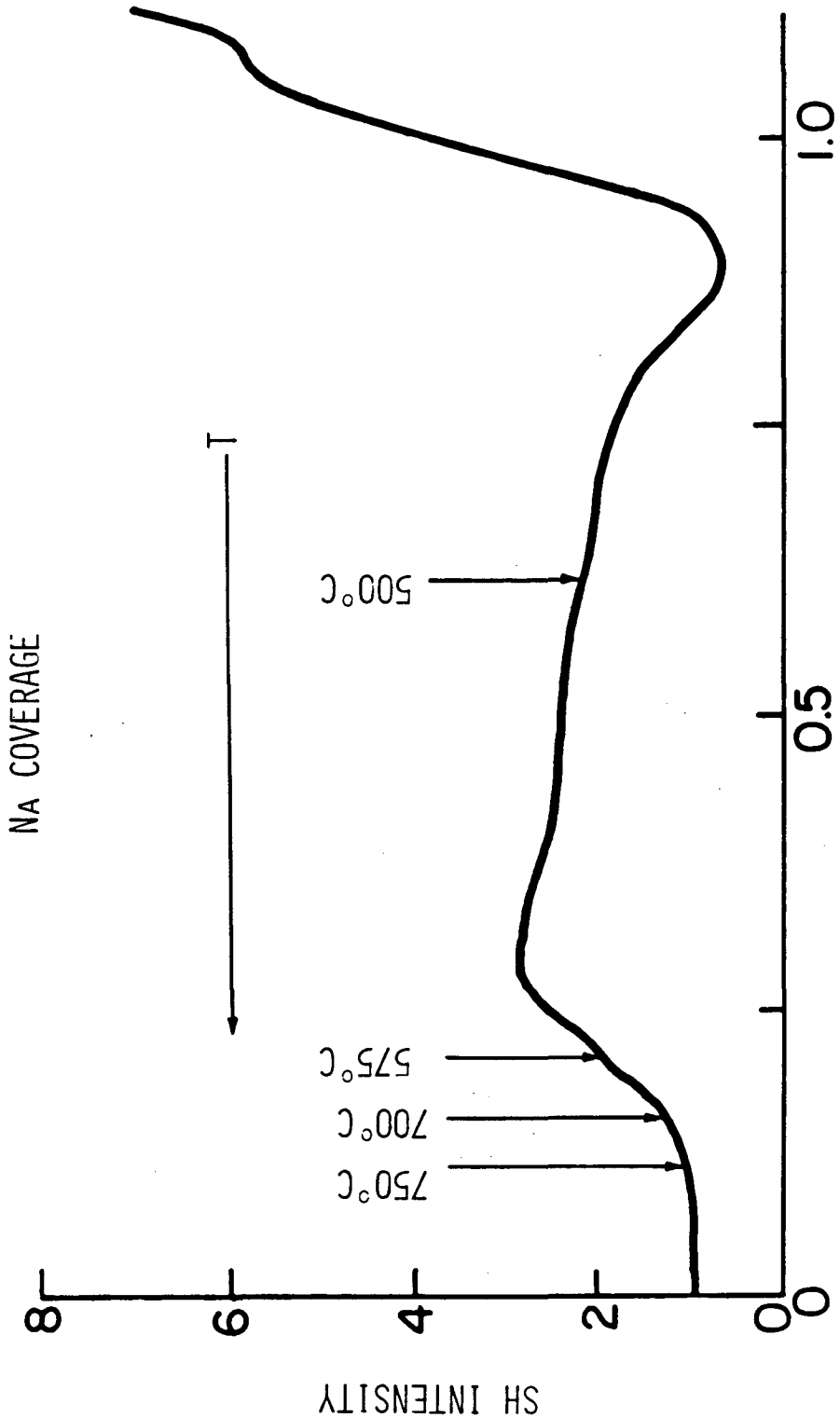

XBL 839-11890

Fig. 8

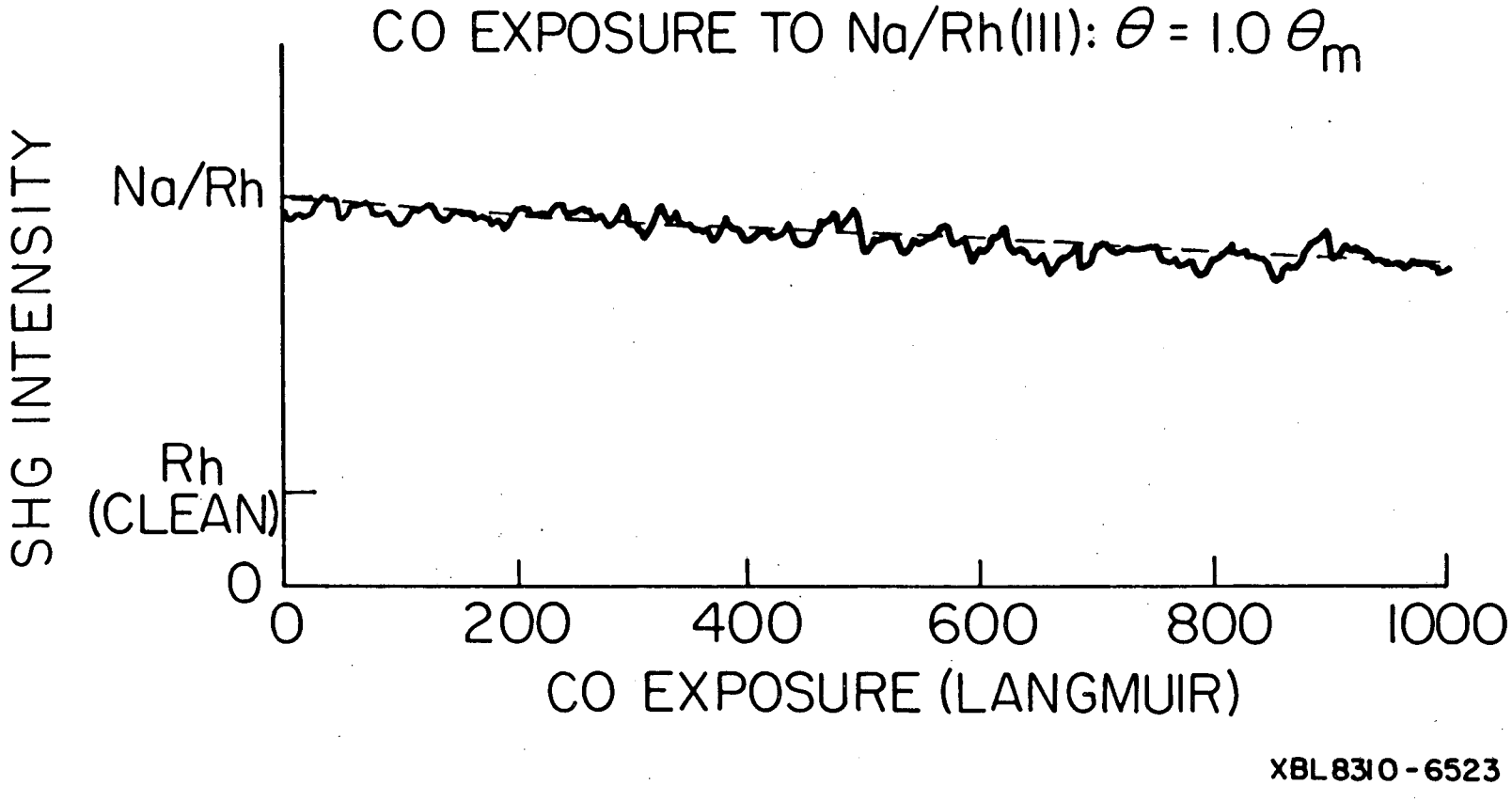
CO EXPOSURE TO Na/Rh(111): θ = 1.0 θm
SHG INTENSITY
Na/Rh
Rh
(CLEAN)
0
0
200
400
600
800
1000
CO EXPOSURE (LANGMUIR)
XBL8310-6523

Fig. 9

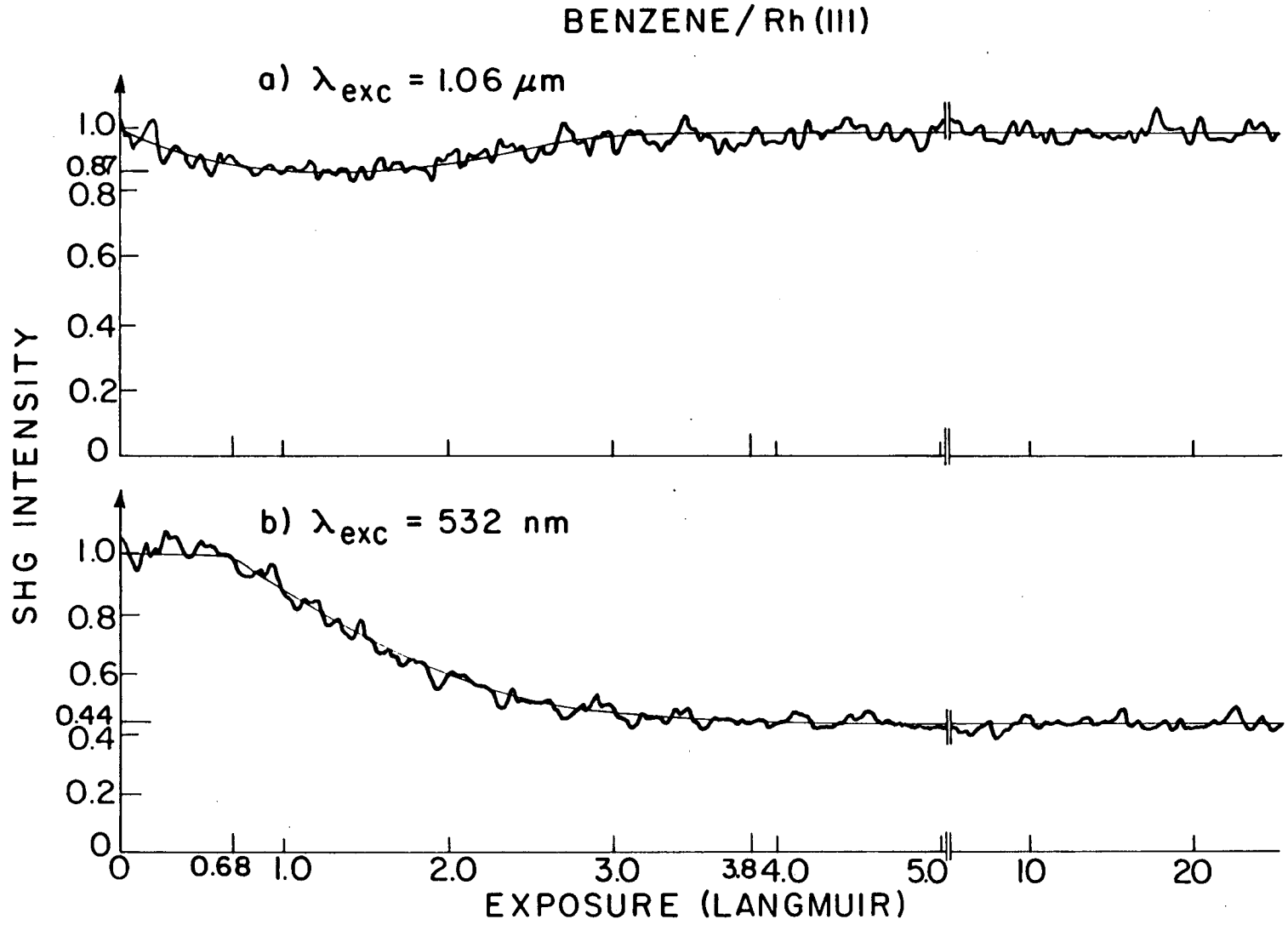

XBL 8311-6569

Fig. 10

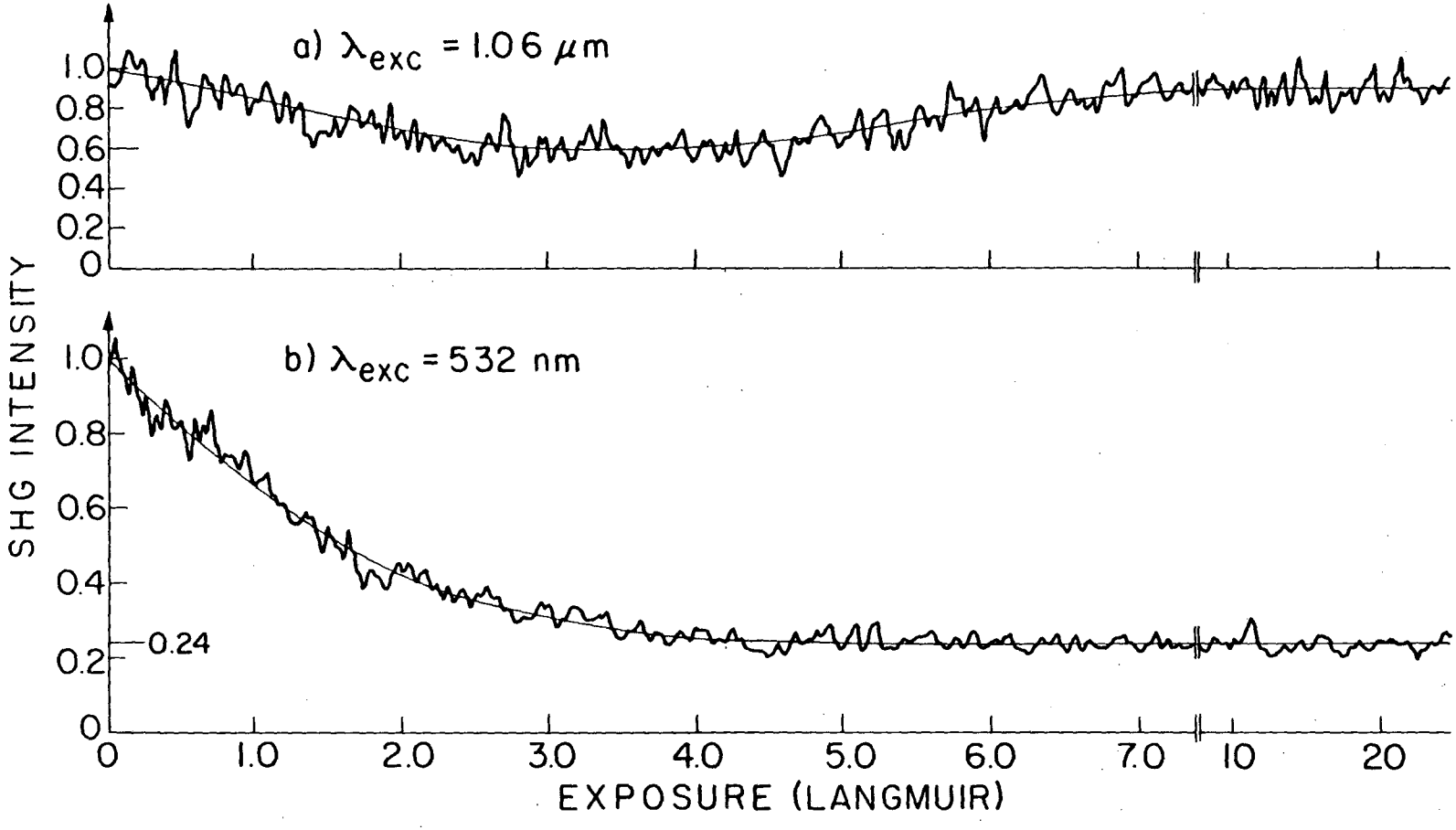
PYRIDINE / Rh(III)
a) λ_{exc} = 1.06 μm
b) λ_{exc} = 532 nm
SHG INTENSITY
1.0
0.8
0.6
0.4
0.2
0
0.24
0
1.0
2.0
3.0
4.0
5.0
6.0
7.0
10
20
EXPOSURE (LANGMUIR)
XBL8311-6570

Fig. 11

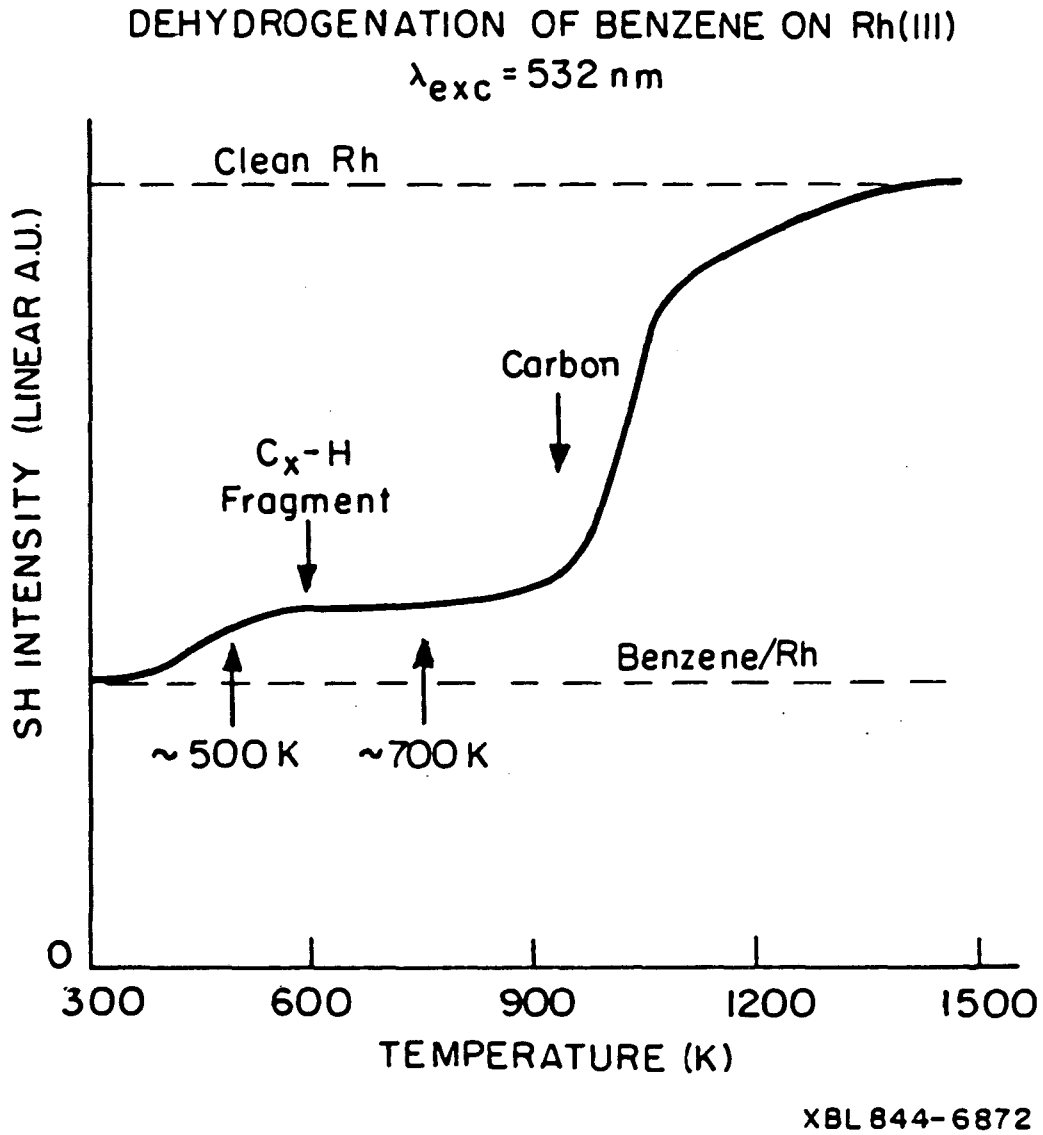
DEHYDROGENATION OF BENZENE ON Rh(111)
λ_{exc} = 532 nm
Clean Rh
Carbon
C_x-H
Fragment
Benzene/Rh
~500 K
~700 K
SH INTENSITY (LINEAR A.U.)
0
300
600
900
1200
1500
TEMPERATURE (K)
XBL 844-6872

Fig. 12

VII. CONCLUSION

The experiments described here have helped to demonstrate the kinds of information accessible with SHG and SFG. The major advantage of these probes is the extreme surface sensitivity. As shown for insulator, semiconductor, and metal substrates, the background signals from the centrosymmetric bulk media are the same order of magnitude or less than the nonlinear response of the interface and thus may be subtracted out or neglected. The intensity, polarization properties, and frequency dependence of the SHG or SFG from the interface can be used to measure coverage, orientation and the electronic properties of adsorbed molecules or the structural symmetry and electronic properties of clean surfaces. The extremely fast time response and the non-destructive nature of the probes make them useful supplements to the surface probes available to the surface scientist.

Certainly a major weakness of SHG is the lack of species specificity and the use of SFG to obtain vibrational spectra should be developed further to alleviate this problem. Another problem with nonlinear optical probes is the possibility of damaging the surfaces with the high field intensities required to generate an observable response. So far, all systems studied have given adequate signals well below the threshold for optical damage or laser-induced desorption. In using SHG or SFG as a probe of electronic transitions of the surface, an adequate microscopic theory is needed to relate the resonance enhancements observed to the electronic structure. Such a theory is still lacking, even though the qualitative aspects, i. e., enhancement of SH when interband transitions are resonant at the fundamental or SH frequency, are clearly reasonable

and have been observed (Ch. VI).

While useful in ultrahigh vacuum environments (UHV), both SHG and SFG probes are more unique at interfaces between dense media where few other surface probes are available. Applications of these techniques at solid/solid (heterostructures), liquid/solid (electrochemical cells, adhesion, crystal growth), and gas/liquid interfaces hold great promise. SHG may also be used to probe two-dimensional layers such as polymers, membranes or suspended surfactants. The most exciting use of these laser techniques, however, is probably their use to follow the time-evolution of surfaces and their adsorbates during laser-induced structural phase transitions or chemical processes. In this regard, the prospect for observing and understanding new physics and chemistry through SHG and SFG studies is most bright.

APPENDIX I

Anisotropic Term of the SH Polarization In Cubic Media For (100) and (111) Surfaces

Here we consider the form of the bulk nonlinear polarization of the form $P_{B,i}^{axis}(2\omega) = \zeta E_i(\omega)\nabla_i E_i(\omega)$ where the i-directions are along the principal axes of the cubic crystal. The results are most easily derived taking the following coordinate transformations. Let the unit vectors along the principle {100} axes be designated (e_1, e_2, e_3). In order to relate these vectors to the lab frame, let the projection of $\hat{e}_1$ onto the surface lie along the unit vector $\hat{x}'$ and let $\hat{z}'$ be normal to the surface directed into the bulk. For the (100) face

$$\hat{e}_1 = \hat{x}'$$

$$\hat{e}_2 = \hat{y}'$$

$$\hat{e}_3 = \hat{z}'.$$

For the (111) face

$$\hat{e}_1 = 6^{-1/2}(2\hat{x}' + \sqrt{2}\,\hat{z}')$$

$$\hat{e}_2 = 6^{-1/2}(-\hat{x}' + \sqrt{3}\,\hat{y}' + \sqrt{2}\,\hat{z}')$$

$$\hat{e}_3 = 6^{-1/2}(-\hat{x}' - \sqrt{3}\,\hat{y}' + \sqrt{2}\,\hat{z}').$$

Now the sample rotation about the surface normal $\hat{z}'$ can be easily incorporated by letting coordinates (x', y', z') be rotated angle ψ from the fixed lab frame coordinates (x, y, z) where $\hat{z} = \hat{z}'$ is normal to the surface and the $\hat{x}$-$\hat{z}$ plane is the plane of incidence. Then

$$\hat{x}' = \cos\psi\hat{x} + \sin\psi\hat{y}$$

$$\hat{y}' = -\sin\psi\hat{x} + \cos\psi\hat{y}.$$

To find $\vec{P}_B^{axis}$ one simply adds $P_{B,i}^{axis}$ over $i = 1, 2, 3$. The incident electric field $\vec{E}(\omega)$ is taken to be a single plane wave in the nonlinear medium 2 with wavevector $\vec{k}(\omega) = k_x(\omega)\hat{x} + k_z(\omega)\hat{z}$. It is convenient to write $\vec{E}(\omega) = -(k_z(\omega)/k(\omega))E_p\,\hat{x} + E_s\,\hat{y} + (k_x(\omega)/k(\omega))E_p\,\hat{z}$ where $k(\omega)$ is the magnitude of $\vec{k}(\omega)$ and E_p and E_s are the $\hat{p}$- and $\hat{s}$-polarized components of $\vec{E}(\omega)$ in medium 2. $E_i(\omega) = \hat{e}_i \cdot \vec{E}(\omega)$ while $\nabla_i = i\hat{e}_i \cdot \vec{k}(\omega)$.

One then finds for the (100) face:

$$P_{B,x}^{anis} = i\zeta k_x(\omega)\{(k_z(\omega)/k(\omega))^2E_p{}^2(\cos^4\psi + \sin^4\psi) + E_s{}^2(\sin^2 2\psi)/2 - (k_z(\omega)/k(\omega))E_pE_s(\sin 4\psi)/2\}$$

$$P_{B,y}^{anis} = i\zeta k_x(\omega)\{\left((k_z(\omega)/k(\omega))^2E_p{}^2 - E_s{}^2\right)(\sin 4\psi)/4 - (k_z(\omega)/k(\omega))E_pE_s\sin^2 2\psi\}$$

$$P_{B,z}^{anis} = i\zeta k_z(\omega)(k_x(\omega)/k(\omega))^2E_p{}^2 \qquad (*)$$

For the (111) face:

$$P^{anis}_{B,x} = i\zeta(18)^{-1/2}\{\ k_z(\omega)[((k_z^2(\omega) - 2k_x^2(\omega))/k^2(\omega))E_p{}^2 - E_s{}^2]$$
$$\times (\cos^3\psi - 3\sin^2\psi\cos\ \psi)$$
$$+((k_z^2(\omega) - k_x^2(\omega))/k(\omega))2E_pE_s \times (\sin^3\psi - 3\cos^2\psi\sin\psi)$$
$$-(2)^{-1/2}k_x(\omega)[((k_z^2(\omega) - 2k_x^2(\omega))/k^2(\omega))E_p^2 - E_s^2]\ \}\quad (*)$$

$$P^{anis}_{B,y} = i\zeta(18)^{-1/2}\{\ k_z(\omega)[((k_z^2(\omega) - 2k_x^2(\omega))/k^2(\omega))E_p^2 - E_s^2]$$
$$\times (3\cos^2\psi\sin\psi - \sin^3\psi)$$
$$+((k_z^2(\omega) - k_x^2(\omega))/k(\omega))2E_pE_s \times (\cos^3\psi - 3\sin^2\psi\cos\psi)$$
$$+\sqrt{2}\ (k_z(\omega)k_x(\omega)/k(\omega))E_pE_s\ \}\qquad (*)$$

$$P^{anis}_{B,z} = i\zeta(18)^{-1/2}\{\ k_x(\omega)[(k_x^2(\omega)/k^2(\omega))E_p^2 - E_s^2]$$
$$\times (\cos^3\psi - 3\sin^2\psi\cos\psi)$$
$$+2k_x(\omega)(k_z(\omega)/k(\omega))E_pE_s \times (\sin^3\psi - 3\cos^2\psi\sin\psi)$$
$$+\sqrt{2}\ k_z(\omega)[((k_z^2(\omega) - k_x^2(\omega))/k^2(\omega))E_p^2 + E_s^2]\ \}\qquad (*)$$

We note that the angular functions that appear in $\vec{P}^{B}_{anis}$ are 4-fold symmetric for the (100) face and 3-fold symmetric for the (111) face as expected. There are also angularly-independent terms noted by the (*) on the right margin that will contribute to the isotropic part of the total SHG (see text).

TECHNICAL INFORMATION DEPARTMENT
LAWRENCE BERKELEY LABORATORY
UNIVERSITY OF CALIFORNIA
BERKELEY, CALIFORNIA 94720